The Effect of Delays on Wide-Area Damping Control of Electromechanical Oscillations

Ristomatti Karppanen

School of Electrical Engineering

Thesis submitted for examination for the degree of Master of Science in Technology.

Espoo 10.03.2016

Thesis supervisor:

Docent, D.Sc. (Tech.) Kai Zenger

Thesis advisors:

M.Sc. (Tech.) Otso Mäki

D.Sc. (Tech.) Jukka Turunen

Aalto University
School of Electrical Engineering

AALTO UNIVERSITY
SCHOOL OF ELECTRICAL ENGINEERING

ABSTRACT OF THE
MASTER'S THESIS

Author: Ristomatti Karppanen

Title: The Effect of Delays on Wide-Area Damping Control of Electromechanical Oscillations

Date: 10.03.2016 Language: English Number of pages: 7+93

Department of Electrical Engineering and Automation

Professorship: AS-74 Control Engineering

Supervisor: Docent, D.Sc. (Tech.) Kai Zenger

Advisors: M.Sc. (Tech.) Otso Mäki, D.Sc. (Tech.) Jukka Turunen

In this thesis the effects of delays on the wide-area damping control of electromechanical oscillations were studied. The research goals were two fold: to identify and define the delay sources in phasor measurement based (PMU) wide-area measurement systems for power systems, and to study the effects of delays on wide-area damping control using power system simulations as a research tool. The implementation the delays into a pre-existing power system simulation program as also a part of this work.

The thesis shows and identifies the delays components and their properties in the wide-area measurement systems. It gives a survey on the reports of real delays observed in wide-area measurement systems worldwide. The simulation results show that delay has an impact on the damping control. Power system have a delay margin they are able to tolerate before turning unstable. Additionally, latency changes the properties of the electromechanical oscillations.

Keywords: electromechanical oscillations, wide-area control, wide-area measurement, damping, delay, latency

AALTO-YLIOPISTO
SÄHKÖTEKNIIKAN KORKEAKOULU

DIPLOMITYÖN
TIIVISTELMÄ

Tekijä: Ristomatti Karppanen

Työn nimi: Viiveiden vaikutus sähkömekaanisten heilahtelujen laajan alueen vaimennussäätöön

Päivämäärä: 10.03.2016 Kieli: Englanti Sivumäärä: 7+93

Sähkötekniikan ja automaation laitos

Professuuri: AS-74 Systeemitekniikka

Työn valvoja: Dosentti, TkT Kai Zenger

Työn ohjaajat: DI Otso Mäki, TkT Jukka Turunen

Tässä diplomityössä tutkittiin viiveiden vaikutusta sähkömekaanisten heilahtelujen vaimennussäätöön. Työ oli karkeasti jaettavissa kahteen erilliseen osaan. Ensimmäinen osa oli voimajärjestelmien PMU-pohjaisten laajan alueen mittaus- ja ohjausjärjestelmien viivelähteiden löytäminen, tunnistaminen ja luokittelu. Toinen osa oli viiveiden vaikutusten tutkiminen laajan alueen heilahtelusäätöön käyttäen voimajärjestelmäsimulointia tutkimuksen työkaluna. Työn toteutus sisälsi viiveellisten mittauksien ja ohjauksien toteuttamisen valmiina olevaan simulaatio-ohjelmaan. Työ näyttää laajan alueen mittaus- ja ohjausjärjestelmien viivekomponentittien ominaisuudet ja vaikutuksen viiveketjuun sekä millaisia lukemia on raportoitu käytössä olevista järjestelmistä ympäri maailman. Työn viivesimulaatiot osoittavat, että viiveillä on merkitys sähkömekaanisten heilahtelujen vaimennussäätöön. Viiveellinen säätö muuttaa sähkömekaanisten heilahtelujen ominaisuuksia ja osoittaa, että voimajärjestelmillä on niille ominainen viiveen sietokyky.

Avainsanat: Sähkömekaaniset heilahtelut, vaimennussäätö, viiveet

Preface

I'd like to thank my thesis advisors and supervisor for their contributions, and extend my thanks also to Liisa Haarla and Janne Seppänen for their interest and contributions to the thesis.

Otaniemi, 10.03.2016

Ristomatti Karppanen

Contents

Symbols and abbreviations

Symbols

τ	delay [s]
f	frequency [Hz]
μ	mean
σ	standard deviation

Operators

$\sum_i$	sum over index i

Abbreviations

DNP3	Distributed Network Protocol
EMS	Energy Management System
FACTS	Flexible AC Transmission System
GPS	Global Positioning System
HVDC	High-Voltage Direct Current
IP	Internet Protocol
ITSE	Integral Time Multiplied Squared Error
LAN	Local Area Network
LOM	Loss of Mains
MPC	Model Predictive Control
PDC	Phasor Data Concentrator
PMU	Phasor Measurement Unit
PSS	Power System Stabilizer
SCADA	Supervisory Control And Data Acquisition
SPSS	Supervisory Power System Stabilizer
SVC	Static VAR Compensator
TCP	Transmission Control Protocol
TCSC	Thyristor Controlled Series Capacitor
UDP	User Datagram Protocol
WAMC	Wide-Area Monitoring and Control System
WAMS	Wide-Area Measurement System
WAN	Wide-Area Network

1 Introduction

This Master's thesis is a required fulfillment towards the degree of Master of Science (Tech.) in Automation and Systems Engineering at Aalto University School of Electrical Engineering. This thesis was made at the Department of Electrical Engineering and Automation at Aalto University as a part of the Nordic energy research project, STRONGrid, which aims to research and develop wide-area monitoring and control applications, and to implement them in a common platform. The STRONGrid partner was Fingrid, the Finnish national electricity transmission grid operator.

The topic of the thesis was to study the effects of delays on the wide-area damping control of electromechanical oscillations in power systems. The introductory part of the thesis gives a brief overview on the topic, describes the research goals and scope of the Master's thesis in detail, and finally outlines the structure of this thesis in the last section.

1.1 Background

Power system stability is an important topic for power system operation, and electromechanical oscillations in power systems are one of the major challenges for power engineers and researchers [1].

The increasing size and electricity consumption in power systems have made electromechanical oscillations, particularly at interarea frequencies, a serious problem which threatens power system stability. Poorly damped oscillations in power systems can result in partial or widespread blackouts, or cause countermeasures which limit the power flow between power system areas. [1],[2]

Electromechanical oscillations, risen from the constantly changing imbalance between generated and demanded electricity, can lead to instabilities without sufficient damping. The different loads in power systems, such as simple resistive loads or more complex loads with control systems, and other factors add complexity and nonlinearity into the systems. The complex nonlinear nature of a power system means that the power systems risk instability at various operating points. The power system stability has three main categories which are voltage stability, angle stability and frequency stability. [1],[3]

The transient instability problem, which falls under the phase angle stability, has been one of the hardest to prevent. The crucial point is the power system's ability to maintain synchronism under large disturbances, such as large load increases, the loss of tie lines or loss of generating units. It requires constant speed control on generators by speeding them up and slowing them down in order to maintain the constant synchronous speed among the generators. [1],[3]

The traditional approaches of damping oscillations by local power system stabilizers (PSS) or other damping controllers have solved this problem locally but may risk achieving limited success when there is a need to damp oscillations over a wider area. [1],[4],[5]

With the steady increase of various wide-area measurement systems (WAMS), which collect measurements over large physical distance in the power system, new

solutions have emerged to solve these wide-area problems. However, the need to measure and transmit data over long distances has made time delays something new to consider in such systems. Unlike in the traditional power system stability control methods, which have generally used only the local information with very small measuring delays, in wide-area measurement systems new kinds of time delays exist in the power system. [5],[6]

Although, the subject of time delays is well studied and analyzed in traditional control processes, time delays have often been ignored almost completely in power system control. Despite the fact that the understanding of delays has a wide range of engineering applications in signal processing, fiber-optics research and circuit design. [2],[7]

In this thesis the delays that could be experienced in wide-area monitoring and control (WAMC) systems and in wide-area measurement systems are investigated, and the relevant parameters and properties, such as time-out and the number of measurement units, are identified and defined. In the next section, a detailed description of research goals and scope is given.

1.2 Research Goals and Scope

The main objective of the thesis is to study the effects of delays on the wide-area damping control of electromechanical oscillations. The objective had two different research goals which required different research methods. The main avenues to accomplish the research goals were literature review and the power system simulations with delay implementations.

The first research goal is to identify the typical sources for latency in wide-area measurement systems and to define their magnitudes and to report on any latency measurements studied in real world systems. The interest in particular is on the phasor measurement unit -based wide-area measurement systems. The second research goal is to study the effects of delays on wide-area damping control of electromechanical oscillations. The purpose is to determine using power system simulations whether the delays have no impact, have some impact or are crucial for the damping control of electromechanical oscillations. The two research goals complement each other. The information gathered in the first part is utilized in the setup and evaluation of the second part.

The focus is on wide-area damping control only and complementing wide-area damping with local damping methods is not a part of the thesis. Other parameters left out of the scope are the effects of signal noise, data corruption, data loss, missing measurements or measurement errors. Additionally, the effects of delay compensation are not in the scope of the thesis.

The power system simulation environment chosen for the thesis is MATLAB and Power System Toolbox [8]. The simulation program did not have an existing delay implementation, and therefore the implementation of delayed measurements and control into the simulation program was an integral part of the thesis. The delays were to be implemented in such a way that they were realistic. The studied power system was decided to be a two-area four generator power system model [9].

1.3 Structure

The thesis is divided into six chapters. Each of them is a clearly defined and contained package divided further into sections for improved clarity. The first chapter is the introduction explaining the background, research goals and scope of the thesis and its structure. The second chapter is a presentation on electromechanical oscillations and on wide-area measurement systems, and their typical system components. This chapter forms the basis for the rest of the thesis which concentrates on the research goals. The third chapter defines, identifies and reports the various delays associated with wide-area measurement systems as required by the research goals. The fourth chapter introduces the simulation environment, the simulated power system models, the damping controller, and most importantly it presents the delay implementation for the power system simulation. In addition, it describes the methods used later to evaluate the damping control performance. The fifth chapter contains the simulation results and reviews their validity and discusses them. The sixth chapter presents the results made from the research as defined by the requirements of the research goals. The last chapter is the conclusion which summarizes the results of the thesis.

2 Power Systems and Electromechanical Oscillations

In this chapter, the concepts of electromechanical oscillations, wide-area measurement systems or wide-area monitoring and control systems (WAMC) and the components of such systems are explained. They are covered from the viewpoint of the thesis.

The first section provides a short general overview of electromechanical oscillations. The second section gives an overview of wide-area measurement systems and the last section covers the typical components of such systems.

2.1 Electromechanical Oscillations in Power Systems

Power systems are under continuous changes, and due to the dynamic nature of power systems, each of these changes leads to an oscillatory response from the power system. The changes causing electromechanical oscillations in power systems are from a number of different sources, such as varying power demands and power generation in the system, connections and disconnections of transmission lines, the power system network's properties, fast exciters or negative interaction from controllers. [3],[10]

The power system oscillations are observable in most of the system variables which can be measured, including variables like bus voltages, transmission line currents and generator speed deviations. There are several modes of oscillation concurrently present at all times in power systems. An example of an oscillation mode is shown in Figure 1. Some oscillations modes are more dominant than others, and can be observed in most of the system variables over wide areas while others are contained within limited areas. Although, electromechanical oscillations exist in all power systems, and are an inseparable part of them, they can lead into partial or full blackouts in some cases, if not properly controlled or damped. [3],[10]

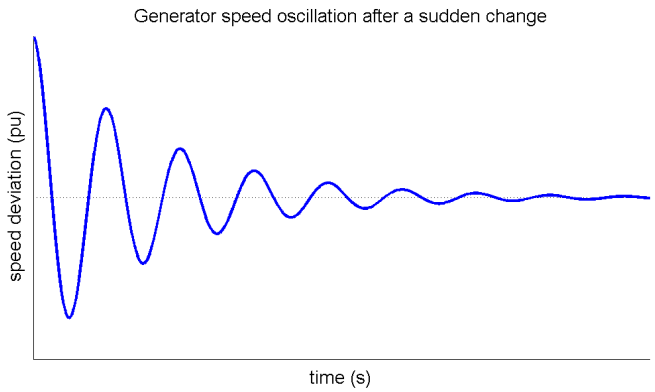

Figure 1: An example of decaying oscillation mode.

A core concept of power systems oscillations is small signal stability, which is a part of the phase angle instability problem. Small signal stability describes the capability of the interconnected power system's synchronous generators to remain in synchronism under various disturbances. It is the power system's ability to maintain balance between electromechanical and mechanical torques in each of the synchronous

machines in the system. This electromagnetic torque is the result of two components, synchronizing torque and damping torque, which are in phase with rotor angle and speed deviation respectively. Insufficient damping torque causes low frequency oscillations in power systems. [3]

In general, four oscillation properties are the most relevant when electromechanical oscillations are measured. The properties are frequency, decay time, amplitude and phase. They are illustrated in Figure 2. [11]

The frequency of oscillations, or alternatively the period of the oscillation cycle, is a core property of all oscillations. The amplitude of oscillation is also of interest since it determines the initial and overall impact of that oscillation mode on the system. Oscillations with lower amplitudes are less relevant than those with higher ones. [3]

The third property is the oscillation mode's decay time which is the time it takes for the oscillations to decay away from their peak value. When damping control is applied to the power system, it is better to use the term damping rather than decaying since the oscillations are in the case of damping forced to decay rather than allowed to naturally oscillate. The mode shape of the oscillation is relevant when two or more oscillation modes oscillate against or in synchronization with each other. [11],[12]

The damping and frequency of electromechanical oscillations can be modified in various ways. Although the oscillations can not be entirely removed, a good damping for them is sufficient. The frequency and damping of existing modes may change or new modes may emerge, as changes are introduced into the system through damping control. [12]

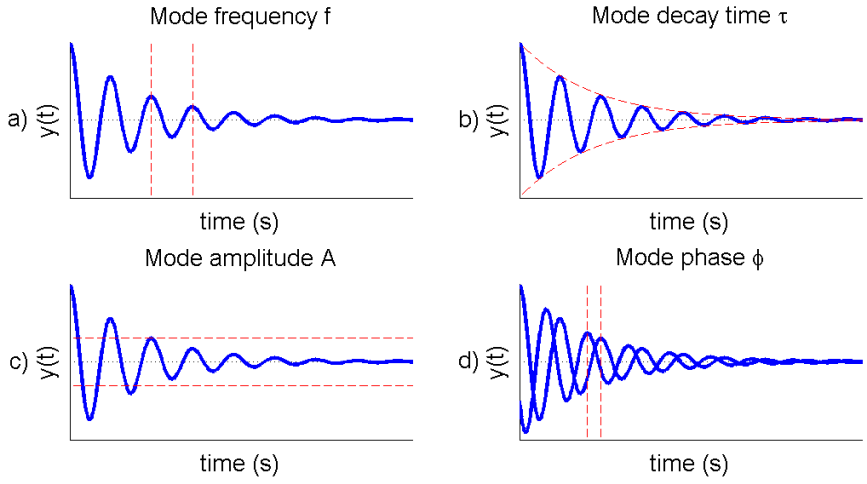

Figure 2: The four main oscillation mode properties: a) mode frequency, b) mode decay time, c) mode amplitude and d) mode phase. [11]

Electromechanical oscillations are classified into five main types of oscillations by their interaction characteristics. The five types of oscillation are local mode oscillations, interarea mode oscillations, intraplant mode oscillations, torsional modes

between rotating plants and control mode oscillations. [12] ,[13]

2.1.1 Local Oscillation Modes

In local mode, one generator or small group of generators oscillates against the rest of the system at natural frequencies typically between around 1.0 to 2.0 Hz. The impact of the oscillations is localized to the generator and the line connecting it to the grid. Local mode oscillation problems are the ones most commonly encountered and are often caused by high response exciters or other controls. The characteristics of local mode oscillations are well understood and they can be reliably and locally damped by power system stabilizers (PSS). [3],[10],[12],[13]

2.1.2 Interarea Oscillation Modes

Interarea modes are associated with generators in one area of the system oscillating against generators in other areas of the system and their characteristics are more complex than those of the local modes. Interarea mode is associated with long weak transmission lines and heavy power transfer in the power system, and it is observed over a large part of the power system network. The natural oscillation frequencies of interarea modes are often in the range of 0.1 to 1.0 Hz. The damping of interarea mode oscillations involves controlling more than one electronic utility and often requires the cooperation of all associated machines to arrive at the most effective and economical solution. [10],[12],[13],[14]

2.1.3 Other Oscillation Modes

The third type of oscillations is the intraplant mode where the synchronous generators on the same generation site oscillate against each other. The typical intraplant mode oscillations have higher frequencies of 1.5 to 3.0 Hz depending on the local configurations of the system, the rest of the power system is generally unaffected by intraplant mode oscillations. [10],[13],[14]

The fourth type of oscillations is torsional mode oscillations which are associated with rotational mechanical components. They can happen at series capacitor compensated power systems when the capacitor interacts at the natural frequency of the network, and the frequencies are typically at the sub-synchronous frequency range. [3],[12],[13]

The last type of oscillations are control mode oscillations which are mainly associated with generators and their poorly tuned exciters, and other equipment and controllers such as turbine governors, HVDC converters or SVC controls. Additionally, different loads and excitation systems can interact through control modes. The observability of the control modes largely depends on the equipment they originate and vary from local observability to wide-area observability. Control mode oscillations, typically around 1.5 to 3.0 Hz, are hard to damp in such a way that adequate damping is achieved for all control modes. [10],[12],[13]

2.2 Wide-Area Measurement Systems

The prominence of wide-area measurement and control systems for power systems has risen from the need to combat the stability and security challenges of large interconnected power systems which have been threatened by electromechanical oscillations in the past. [2],[5]

The traditional methods for damping electromechanical oscillations, such as power systems stabilizers or other local damping controllers can not be entirely trusted to handle interarea oscillations reliably in an effective way at all times, since these methods lack the coordination and observability of the power system over a wider area. A continuous wide-area monitoring and control brings observability and other control advantages which the traditional methods lack, and therefore a substantial amount of research and development has gone into the application of wide-area signals for monitoring and controlling power system stability. [2],[4],[5]

The advancements done in wide-area measurement systems (WAMS) and wide-area monitoring and control systems (WAMCs) allow the remote measuring of many power system signals over a wide-area at the various substations of the power system. A great advantage of wide-area measurement is the capability to monitor the dynamics of the power system centrally, and with the support of a good communication infrastructure the monitoring can be done in real time. This has opened new possibilities in power system design, automation and control, and enabled the deployment of solutions which are effective against system-wide disturbances. [2],[5]

One of the many advancements in the field of the wide-area measurement of power systems is the development of phasor measurement units (PMUs) which are used for measuring power system signals. A PMU is a digital device which extracts current and voltage measurements, referred sometimes as synchrophasors, based on a synchronized reference time signal. In PMU-based wide-area measurement systems, the phasor measurements are taken from the various locations of the power system for a wide coverage and the time synchronized signals enable them to be collected at centralized control centers for further processing and power system control. [15],[16],[17],[18]

Although wide-area measurement systems and control schemes have solved some previous problems, they have also raised a new set of challenges for power system monitoring and control. The communication between remote locations and over long distances has introduced data loss, corruption and latency into the monitoring and control systems. The first two of these problems can be adequately mitigated through state estimation and various data reconstruction techniques, but the use of these techniques further contributes to the third challenge, latency, due to the increased data processing and transmission requirements. Furthermore, the data propagation of signals through communication networks with variable congestion levels and complexities alone amounts to an increased latency in the control and monitoring systems. [2],[5],[19]

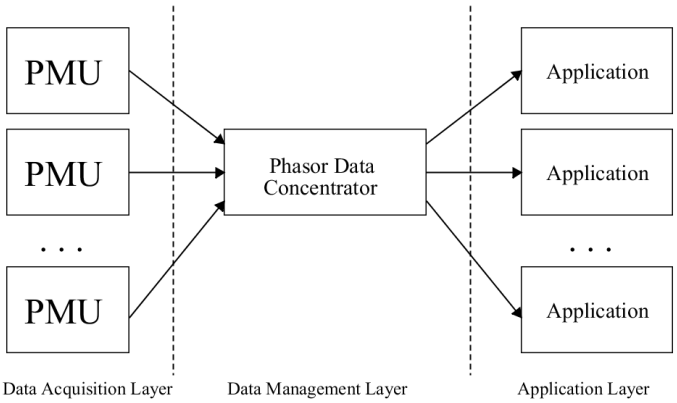

Figure 3: The functional layers of wide-area measurement systems. [20]

The phasor measurement units are used to add synchrophasor measurements into many electricity utilities worldwide. They provide additional data from important substations on the power system to entire power systems critically depending on the PMU measurements. The functional layers of a wide-area measurement system are shown in Figure 3. The first layer is where PMUs are located and where the measurements are taken from the power system substations or from the power lines. In the data management layer the PMU measurements are collected and sorted into a time synchronized data set through varying levels of concentration. The third layer presents the applications which use the time synchronized measurements provided by the data management layer. The communication network used in data transmission impacts between the layer interfaces. [21],[22]

The phasor measurements are used by various applications and the four main applications in monitoring and control systems are state estimation and monitoring, instability prediction, adaptive relaying and improved control of the power system. [15],[16],[21]

State estimation and monitoring is one of the most crucial parts of wide-area measurement systems. It relies on the capability of PMUs to relay continuous data to control and monitoring center at high rates. This data can be then used for monitoring and the calculation of power system dynamics. [19]

The online prediction of instabilities is also possible in real time with the help of synchrophasors. Additionally, adaptive relaying can be done dynamically through the use of PMUs making the responses to power swings in the system better than other solutions, such as simulation-based contingencies. [19]

Lastly, the phasor measurements can be used to provide direct feedback from a wide-area to the various controllers improving the dynamic control of the power system. The usage of wide-area information removes the need for relying solely on local feedback and on power system models which do not necessarily correlate to the actual conditions of the power system. [19],[16],[17]

As stated earlier, the data from phasor measurements units is transmitted and collected at local level, and then further transmitted into data concentration points. A typical data concentration hierarchy of a PMU-based measuring system is shown in Figure 4, and there are often either one or two levels of data concentration before

any applications. The devices at the next levels of the hierarchy above PMUs are known as phasor data concentrators (PDCs). [15],[19],[23]

The phasor data concentrators gather data from several PMUs, reject bad or invalid data, synchronize it based on timestamps and create a coherent record of simultaneously measured data of the power system. The synchronized timestamped set is then forwarded by the PDCs to the next level of data concentration or to the applications using the data. [17],[21]

In addition to PMUs and PDCs, other components typically considered part of these monitoring and control systems are the applications themselves (generators, exciters, compensators etc.) and the communication network. [21],[22]

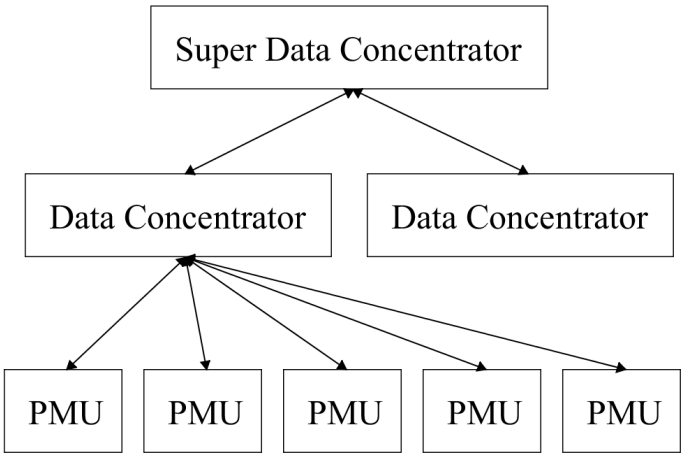

Figure 4: The hierarchy of the phasor measurement units (PMUs) and phasor data concentrators (PDCs). [17]

The response requirements of real time use and the propagation of data over wide-areas highlight not only the importance of the performance of each individual device or application in the power system but also the importance of the communication infrastructure. Therefore, the importance of the communication network and its role as a possible bottleneck in the architecture of wide-area measurement systems is significant. The delays in the system information and the quality of the remote data from PMUs depends on the communication infrastructure's capabilities and its architecture. [22]

The operating principles and roles of each of these components is further expanded in the upcoming subsections.

2.3 Wide-Area Measurement System Components

This chapter covers the four main components present wide-area measurement systems. The first section covers a generic phasor measurement unit and its operating principles, the second section gives an overview of a phasor data concentrator and its operating principles.

The third section covers typical applications or instruments used in wide-area measurement systems. The last section gives an overview of various communication networks and protocols used in wide-area measurement systems.

2.3.1 Generic PMU

The PMUs available differ from each other in many ways depending on the manufacturer and the compliance to the feature levels defined in the synchrophasor standard, and thus it is not feasible to discuss and describe a PMU hardware configuration that would apply to each device. Therefore, a generic PMU and its main components and functionalities are described here which is sufficient to give an overview of the subject. The main standard for phasor measurement units and their applications is IEEE C37.118. The main components of a PMU are illustrated in Figure 5. [17],[24]

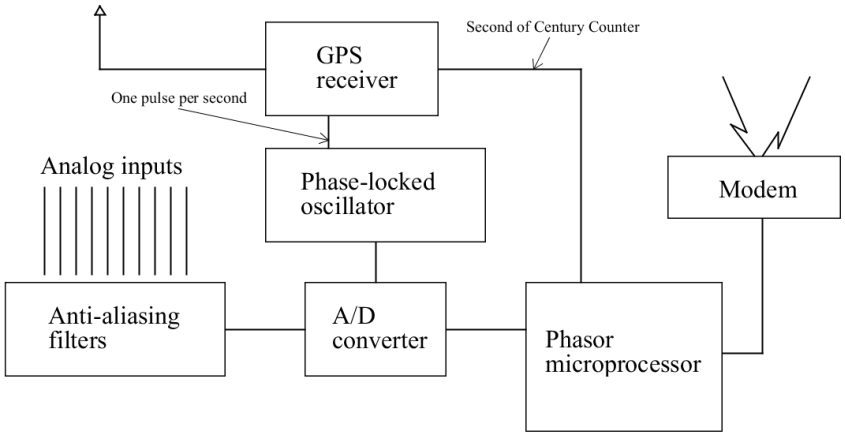

Figure 5: The main components of the phasor measurement unit (PMU). [17]

The main function of a phasor measurement unit is the measurement of synchrophasors. A phasor is a complex number that represents both the magnitude and phase angle of voltage and current sinusoidal waveforms at a specific point in time. The sinusoidal waveform and phasor representation is shown in Figure 6. The PMUs measure voltage, current, and frequency phasors using the discrete Fourier transform (DFT), and can detect transients or surges within milliseconds of their occurrence. They can additionally determine other analogue and digital measurements such as frequency, the rate of change of frequency or circuit breaker status. [16],[17]

One of the most significant features of the phasor measurements units are their high precision timestamps which are recorded at the source. The use of timestamps allows the PMU data to be later synchronized, sorted and compared despite coming in at different times. The Global Positioning System (GPS) is widely used to provide the timestamp for the phasor measurements. [17],[18]

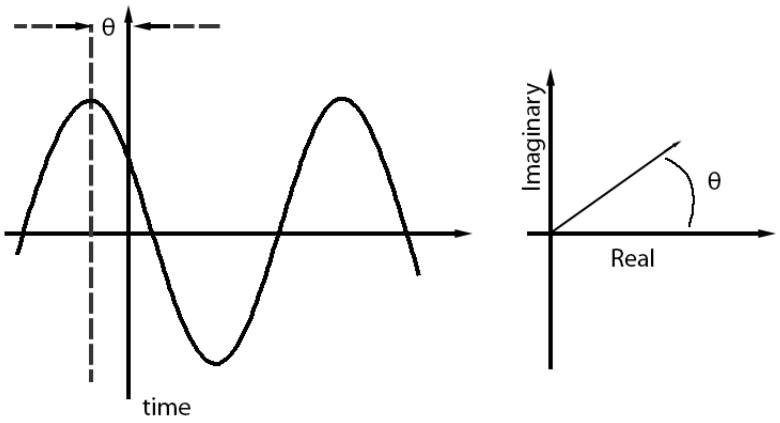

Figure 6: The sinusoidal waveform and the correlation to its phasor, or complex form. [18]

A phasor measurement unit obtains voltage and current as analog inputs from the secondary windings of the current and voltage transformers. The output is the corresponding positive sequence current or voltage phasor. The current and voltage signals are converted to voltages that match the requirements of the analog-to-digital converters and the sampling rate of the sampling process determines the frequency response of the anti-aliasing filters. [16],[17]

Typically, these analog filters have a cut-off frequency that satisfies the Nyquist criterion, less than half of the sampling frequency. The phasor measurements have a small uncertainty, as the magnitude and angle are affected by the noise in the analog input signal caused by the electronic equipment of the power system. [16],[17]

Because of this uncertainty, higher sampling rates are desirable since they correlate to more accurate estimations and are used to minimize measurements errors. Longer data windows also reduce errors. Sampling rates have steadily increased over the years and modern PMUs have high sampling rates. [16],[17],[18]

The sampling clock is a phase-locked oscillator with the GPS clock pulse and the phasor microprocessor in a PMU handles the calculations of the signals, creates the timestamp from two of the time signals originating from the GPS receiver and forms the PMU data file to be sent through the modem to a central location. [17]

Phasors are dependent on the number of samples, and data windowing and filtering is used to smoothen the spectrum of frequency and reduce time domain discontinuation caused overshoot of the signal. Positive-sequence measurements are carried out from all three-phase currents and voltages and a PMU can have several different feeders originating in the substation or voltages from various buses in the substation. [16],[17]

There are two types of PMUs defined by the synchrophasor standard, the P-class and the M-class, based on the intended applications of the PMUs. The P-class PMUs are aimed for support applications which require responding to dynamic changes with minimal delay. The M-class PMUs avoid signal aliasing, have longer latency and are intended for support applications able to withstand longer delays but being

affected by signal aliasing. [24]

The synchrophasor standard defines four file types for the phasor measurement units. Header files, configuration files and data files are generated by the PMUs, and the last one, command file, is used for communicating with higher level infrastructure such as a PDC. The first bytes in a PMU data frame are used to synchronize the data transfer and the last part is a check sum which marks the end of the data transmission. The frame size defines the size of the whole data structure and the following blocks are used for unique id which identifies the unit, and provides the correct timestamp for the reported data. The structure of the synchrophasor format is further illustrated in Table 1. The length of the data section is defined in the PMU configuration. These data files contain the phasor measurements and any other related measurements, such as frequency or the rate of change of frequency. [17],[25]

Table 1: Phasor packet components and data length. [25]

Component	**Bytes**
Header	16
Phasors	32
Frequency	4
Frequency Deviation	4
Discrete Values	2
Checksum	2
Total	60

The computed synchrophasors are transmitted through a communication medium to a higher level of application hierarchy often at a rate of 10 – 60 Hz depending on the frequency of the power system. The synchrophasor standard IEEE C37.118 requires all PMUs to operate at frequencies which are divisors of the frequency of the power system, as shown in Table 2. [24]

Table 2: Required PMU operating frequencies defined in the IEEE C37.118 standard. [24]

Rates for a 50 Hz power system (Hz)				
10		25		50
Rates for a 60 Hz power system (Hz)				
10	12	20	30	60

The receiving device is often a phasor data concentrator responsible for collecting and handling several PMU signals since the synchrophasors are rarely used locally but are transmitted from remote locations. [18]

2.3.2 Generic PDC

The phasor data concentrator (PDC) receives the synchrophasor measurements from the phasor measurement units. A PDC can be a software solution running on a

general computer or a specific hardware solution. The main function of a PDC is to filter out erroneous measurements, sort the measurements based on the timestamp on their frame and downsample or upsample them, and then store the sorted data set and forward it to other applications, such as power system control. [17],[26],[27]

The PDC works by receiving the incoming phasor measurements, sorting them on their arrival and waiting for the rest of the measurements of that timestamp to arrive before storing and forwarding them. The sorting algorithm for PDCs is not specified by any standard and most vendors consider the details of the algorithms as confidential. [17],[26]

The incoming measurements are stored in the input buffer while the PDC waits to receive the rest of them. The input buffer determines the time the measurements are stored and it has a maximum size or wait time. The input buffer typically contains the measurements for the past $1 - 4$ seconds after which the measurements are discarded. Additionally, the PDC has a time-out parameter which is applied individually for each timestamp once the PDC receives the first measurement of that particular timestamp. The time-out determines the maximum wait time between the first and the last measurement of a given timestamp. The data flows of a PDC are illustrated in Figure 7. [17],[26],[27]

Sorting the data without the time-out parameter is possible but it has the drawback of waiting for the buffer to be full. This works reasonably well when network delay is minimal or no significant packet loss occurs, but in practice this is not feasible. [20],[21],[22]

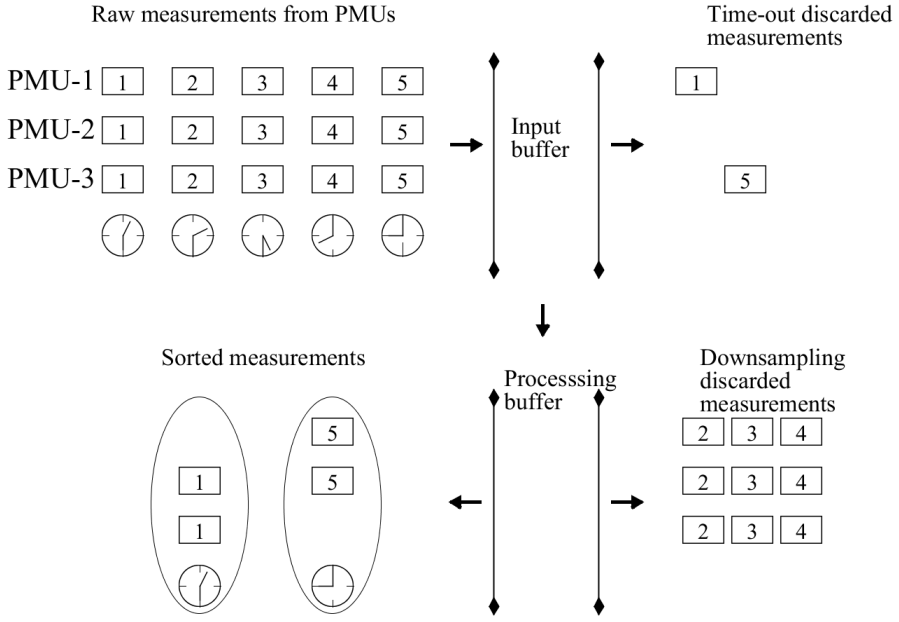

Figure 7: The data flows of a phasor data concentrator (PDC). [26]

The purpose for assigning a time-out for each arriving timestamped PMU measurement is to solve the problem of irregular network propagation delays. The real time application of wide-area monitoring and control systems is hurt by waiting for an

excessive amount of time for each measurement. The selection of the time-out parameter has many consequences on the monitoring and control system. The advantage of a time-out is a ceiling for the waiting time and to detect when the waiting time exceeds the time-out parameter. A too small time-out parameter can increase the data incompleteness of the system as the PDC might forward the data as incomplete since all measurements have not had enough time to arrive. [20],[21],[22],[26]

On the opposite side, a too long waiting time adds more delay to the measurement propagation but can improve the data completeness of the system since the phasor data concentrator waits longer for incoming measurements. In the case of a time-out, the PDC sends the data set incomplete, complements the missing data with previous values, or disregards the data set altogether based on the configuration of the PDC. [20],[22],[26]

The PDC has also the option to downsample the measurement data by systematically discarding data from the processing buffer. The downsampling of synchrophasor frames to a lower rate of frames is used to add flexibility or scalability for the benefit of other applications in wide-area measurement systems. The output options for phasor data concentrators are numerous, such as direct interfaces to a SCADA, EMS systems, some control systems or another PDC on a higher level of data concentration hierarchy. [18],[26]

2.3.3 Applications

Many different applications can utilize PMU-based measuring systems and the main focus in the past has been in the development of applications intended for measuring or assessing power systems dynamics, along with adding control to the power systems. Applications for power system state estimation, protection and instability prediction, already previously mentioned in Section 2.2, are some of the main purposes of wide-area measurement systems. The phasor measurement units have replaced and more often augmented the older measurement systems and allowed the development of entirely new monitoring and control schemes not previously possible for various reasons, such as low sampling rates or lack of time synchronization. [23],[28]

Some examples of more specific PMU-based applications are various fault event monitoring systems, fault location and detecting systems or Loss of Mains (LOM) systems dealing with generator disconnections within the power system. Other applications include harmonic estimation applications and power system load modeling which uses synchrophasors for power system state estimation. [23],[28],[29]

In the case of wide-area monitoring and control systems the use of synchrophasors allows for smart control centers which coordinate the damping control in the power system, and devices such as breakers, excitation systems and compensators can be controlled more intelligently. Additionally, the data inputs of various control devices, such as static VAR compensator (SVC) damping controllers or thyristor controlled series capacitor (TCSC) damping controllers, high voltage DC (HVDC) controllers or flexible AC transmission systems (FACTS), can be complemented with synchrophasor data. [1],[30]

In addition, there are various generic power system controllers or stabilizers using

PMU-measurements for wide-area damping control. Global power system stabilizers use remote feedback control in addition to the local control schemes, and supervisory power system stabilizers (SPSS) apply information gathered from many substations to improve the cooperation between local power system stabilizers. [7]

2.3.4 Communication Network

The components of the communication network are significant factors in determining the overall performance and capabilities of wide-area measurement systems. The potentially long transmission distances and demands for data completeness in PMU-based measuring systems, and the real time requirements of these systems set quite high demands and restrictions for the communication network. In the basic communication model the PMUs are connected through local area networks (LAN) into wide-area networks (WAN) responsible for data transmission over the power system, shown in Figure 8. This section mainly concentrates on the WAN aspects of the communication network since their total contribution generally has more impact when compared to local connections. [22],[31]

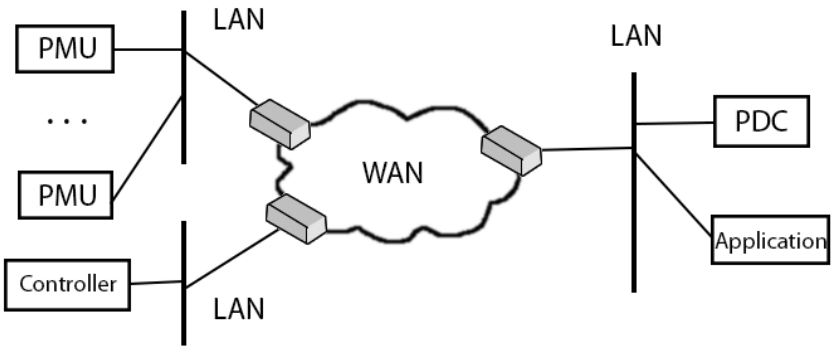

Figure 8: A typical wide-area communication model showing LAN and WAN connections between local and control centers. [31]

The type of communication link and the complexity of the communication network can be the largest contributors to the total performance of the network. The available communication methods for transmitting phasor measurement data used are numerous, and both wireless and wired mediums are utilized. However, wired options are more common and generally better over longer distances in terms of latency, packet loss and data corruption. [16],[17]

The two most important aspects of data transfer for synchrophasors are channel capacity and latency. Communication latency is one of the key factors determining the performance of a wide area monitoring and control system. In addition, network protocol and network congestion levels determine the communication delay between each data transmission interface. Generally, the wide-area measurement systems involve small amounts of data but at high transmission rates. While modern communication links should not have problems with data transmission capacity, this is

not the case with some older transmission methods. However, these older methods often suffer already from latency issues due to their low data transmission speeds. [16],[17],[22]

Telephone lines, fiber optics or power line communication lines are commonly used wired options, and the wireless options are mainly limited to communication links based on satellites when long distances are concerned. The communication links have each their own channel capacities and topologies which further affect the network performance and result in different latencies. [17],[16]

In addition to the communication links and the topology of the communication network, other significant factors affecting the performance of the communication network are the various network transfer protocols which are used for data encapsulation and transmission. Several communication protocols are also possible, including but not limited to Transmission Control Protocol (TCP), User Datagram Protocol (UDP) and Distributed Network Protocol (DNP3). Additionally, the communication network's performance depends on the complexity and congestion of the network through signal routing. Furthermore, the data transmission network architectures can be divided into two main categories which are dedicated networks and shared networks. [22],[32]

Dedicated networks are networks with direct communication links, point-to-point connections, dedicated to the sole use of the wide-area measurement systems. They are reliable, secure and provide high speed for data transmission, and thus minimize the effects of delays and congestions in the network. [16],[22]

Shared networks are not only dedicated to the use of wide-area measurement systems but share it with other applications, systems and users. They are wide-area networks which often use TCP/IP -protocol for data transmission, and can have issues with routing, congestion and packet loss, unlike dedicated networks. [16],[22]

In general, the preferred communication medium for PMU-based measurement systems are fiber-optic data links. Fiber-optics have high channel capacity and high data rates, and are immune to electromagnetic interference contributing to decreased signal noise. Fiber-optics are also cost effective with low operating cost and without any licensing fees. [17],[22]

3 Delays in Wide-Area Measurement Systems

In this chapter the delays in wide-area measurement systems are researched and identified for a power system with a single wide-area damping controller. The sources for latency are covered and their overall impact on the power system as a whole is evaluated. The results and conclusions are applied to the power system simulations covered later in Chapter 4.

First, a general overview of delays in wide-area measurement systems is provided, followed by a more detailed coverage on the individually identifiable sources for latency. In the detailed coverage some general values for delay are provided for the sake of clarity but they are further expanded in the last section about previous research done into wide-area measurement delays.

3.1 Overview of Delays

The strict time requirements of real time wide-area monitoring and control systems were already already previously briefly highlighted in Chapter 2. For a proper understanding about the capabilities of a wide-area measurement system, the delays and time requirements have to be identified, analyzed and responses to emergency phenomena in the power system under certain time limits have to be known. [5]

A common challenge in the deployment of synchrophasor control applications is the possibility of the inadequate performance of the supporting information communication infrastructure. However, there are many other sources for delays in wide-area monitoring and control systems, and they can be traced to the various processes and components in the system architecture. Figure 9 gives an overview of both the common system components and the various delays associated with PMU-based wide-area measurement systems. [20],[26]

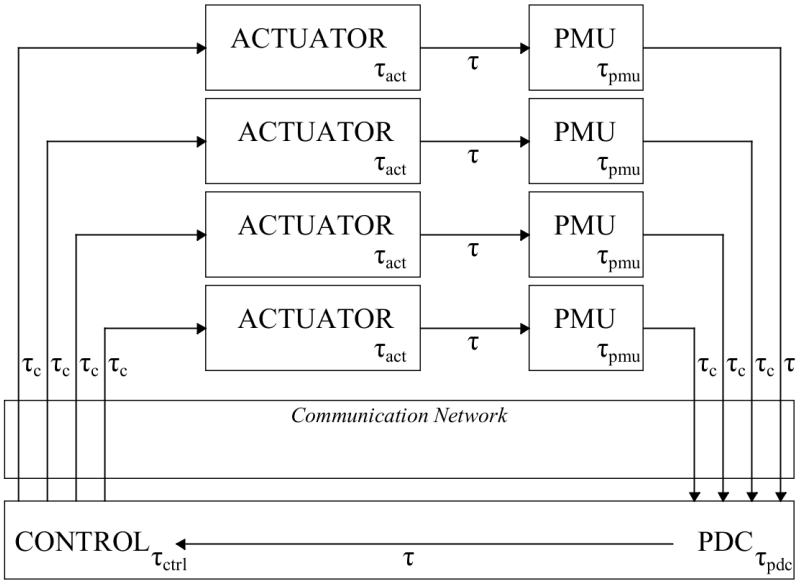

Figure 9: Illustration of PMU-based wide-area measurement system and its associated delays. [20]

Some clearly identifiable sources for delay are the processing and execution times of the various devices, such as the PMU measurement and processing delay, the PDC sorting and processing delay, the control calculation and control actuation time. [20]

The communication network is a crucial part of a wide area control system and can be a possible bottleneck in the architecture of these systems. The communication protocols, communication load, transmission distance and channels are among the key factors in determining the communication delay. Depending on the specifics of the power system, data transmission and communication delays over the network between the various components and the actuator related delays usually accumulate several times since the measurement, control calculation and execution take place at physically different locations. [2],[20]

If non-dedicated communication channels are used in these systems, they often add further delays due to their associated complexities, levels of congestion and data transmission limitations compared with those communication networks which are dedicated to the power system use only. [2],[21]

In order to describe the total chain of delays, a concept of end-to-end delay has to be introduced. The end-to-end delay describes the total delay for a particular variable from the moment of its measurement to the time when control actuation based on its value has an impact on the power system. Therefore, the total end-to-end delay of a phasor measurement signal from the time of sampling to the moment it has impact on the power system through damping control is the following:

$$\tau_{ete} = \tau_{pmu} + \tau_{c_1} + \tau_{pdc} + \tau_{c_2} + \tau_{ctrl} + \tau_{c_3} + \tau_{act} \tag{1}$$

where τ_{pmu} is the PMU measuring and processing delay, τ_{c_i} are the data transmission delays, τ_{pdc} is the PDC processing and waiting delay, τ_{ctrl} is the time taken to compute

control action and τ_{act} the time it takes for the particular actuator to apply the control.

The following subsections cover each of these delays, shown in equation (1), in more detail and describe their causes and magnitudes on the overall delay structure.

3.1.1 Phasor Measurement and Processing Delays

The PMU delay is the total time it takes for the sensor to perform synchronized sampling, phasor calculation and data encapsulation. The delay is primarily caused by transducers, Discrete Fourier Transform (DFT) window size and processing time, the data size of the PMU output, and multiplexing and transitions. Typically, the most time consuming process is the calculation of the frequency from positive sequence three phase signals. [4],[16],[33]

Transducer delays are caused by the voltage transducers and current transducers that are used to measure the voltages and currents at sampling time. The window size of the DFT is the number of samples required to compute the phasors using DFT and the processing time is the time it takes to convert the transducer data into phasor information using Discrete Fourier Transform. The correlation between latency, the assigned timestamp, the phasor estimation window and processing time is illustrated in Figure 10. [16],[24]

The total delay for a PMU is the following:

$$\tau_{pmu} = \tau_{mea} + \tau_{proc} \tag{2}$$

where τ_{mea} is the measuring latency mainly caused by the sampling window and τ_{proc} is the processing delay of phasor calculation. [24]

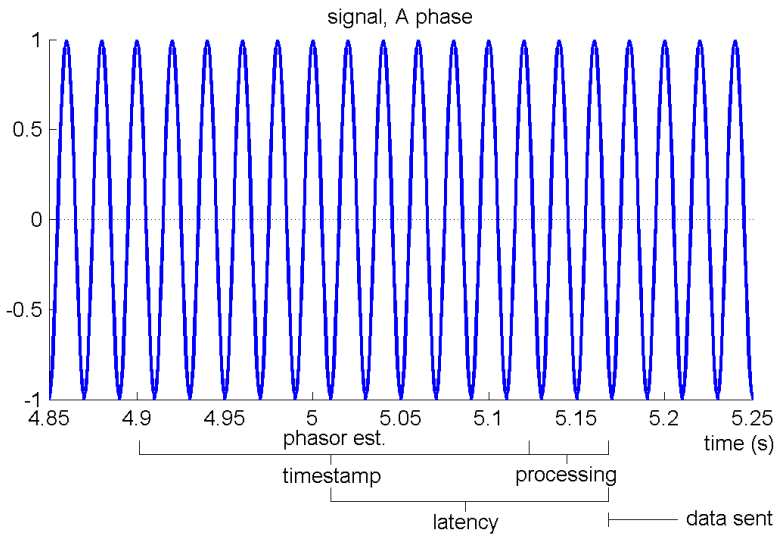

Figure 10: The structure of PMU latency consisting of phasor estimation and processing time. [34]

While the PMU delay is somewhat hardware and settings bound, it is possible to determine the maximum latency for any PMU that fulfills the requirements of

the synchrophasor standard C37.118.1. This standard defines a maximum reporting latency for P-class and M-class PMUs based on their sampling frequency. Equation (3) applies for P-class PMUs and (4) applies for M-class PMUs. The reporting latency is the time it takes for the timestamped measurement to become available at the PMU output. [24]

$$\tau_{P_{max}} = \frac{2}{f} \tag{3}$$

and

$$\tau_{M_{max}} = \frac{7}{f} \tag{4}$$

where f is the reporting frequency of the particular PMU.

As an example, a common PMU operating frequency of 50 Hz would allow a maximum delay of 40 ms for each phasor measurement in the case of a P-class PMU. In addition, the floor value for delay between two consecutive measurements is dependent on the PMU sampling frequency. An operating frequency of 50 Hz would result in a minimal delay of 20 ms between two consecutive measurements regardless of other delays in the system. [24],[34]

However, it should be noted that occasional processing spikes may occur causing random delay jitter regardless of the compliance to the synchrophasor standard. The delay introduced to the system by a PMU can be considered a fixed delay for most cases since the time required to measure and calculate the phasors remains relatively constant. The delay caused by PMUs sets a floor value for the overall latency of the wide-area measurement system. [19],[24],[34]

3.1.2 PDC Processing and Waiting Delays

The delay of a PDC depends mainly on the processing time of the sorting algorithm and the PDC waiting time spent waiting for a full set of PMU measurements. The PDC delay is affected by the number of PMUs, the time-out parameter and the maximum transmission time from the PMUs. [17],[18]

Downsampling and upsampling have their own unique effects on the delay. Additionally, dedicated PDC hardware generally achieves lower processing times than software based solutions. Many PDC devices allow large amounts of PMU connections, without any performance penalties. [22],[27]

A phasor data sorting algorithm will group the measurements from the same timestamp to form a data set while the measurements are arriving to the PDC. These data sets will be forwarded to the other applications once the timestamped buffer is full or the timeout parameter is exceeded. This process was illustrated in Figure 7 in Subsection 2.3.2. [21],[22]

The PDC processing delay is thus the following:

$$\tau_{pdc} = \tau_{proc} + T_w \tag{5}$$

where τ_{proc} is the delay associated with the PDC processing and sorting of the timestamped data, and T_w is the PDC waiting time. [27]

The PDC latency contributes towards the absolute latency of the PMU measurements from the moment they were measured based on their timestamp. The PDC waiting time consists of waiting for all the measurements to arrive, or alternatively from the time-out parameter. This structure is shown through an example in Figure 11, where all the measurements have arrived before the assigned time-out parameter expired. [27]

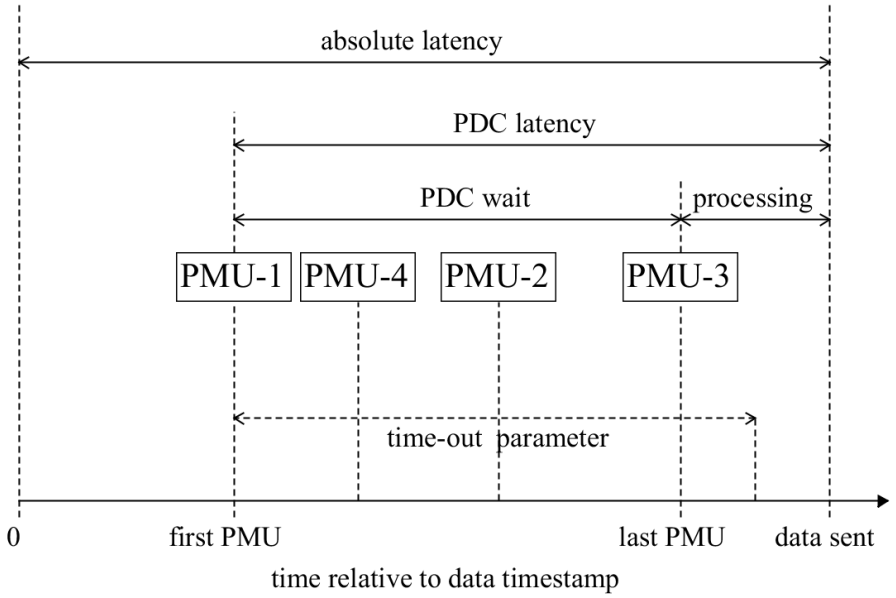

Figure 11: The structure of PDC latency in a system with four PMUs. [27]

The PDC waiting time is dependent on the delays caused by data transmission and PMUs, and the processing delay is unknown without knowledge of the particular PDC. It would be possible to derive a general processing time estimate for a synchronization algorithm from the requirements of the sorting and synchronization tasks even if the specifics of the algorithm are not known. [17],[20],[21]

The PDC acts as a bottleneck since it waits for all PMU measurements to arrive before it forwards all the measurements from the timestamped buffer. If the network experiences significant delays or packet loss, there is no way to determine the waiting time for the data in the buffer. In phasor data concentrators the PMU packet with the longest transmission and processing time determines the maximum waiting time T_w. [21],[22]

$$T_w = max(\tau_{pmu_i}) \quad i = 1...N \tag{6}$$

where N is the number of PMUs connected to the PDC and τ_{pmu_i} is the data transmission and processing time for each PMU.

The use of time-out parameter mitigates the problem of excessive waiting. The total PDC delay in addition to the processing time is the function of time-out

parameters and the time it takes for data to arrive at the PDC. Finally, this gives the complete general PDC delay τ_{pdc} which consists of the processing time and either the time-out parameter or the maximum waiting time.

$$\tau_{pdc} = \tau_{proc} + min(T_w|T_{to}) \tag{7}$$

where τ_{proc} is the time it takes to process and sort the data, T_w is the waiting time and T_{to} is the time-out parameter. [20],[21]

Tests [27] show that the equation (8) applies for many hardware PDC solutions and the general mean PDC processing latency is tied to the operating rate of the device.

$$\tau_{proc} \leq \frac{2}{3f} \tag{8}$$

where f is the reporting rate of the PDC. [27]

The PDC processing time is sometimes not considered at all since in most cases $\tau_{proc} << min(T_w|T_{to})$ applies and in many applications the PDC processing delay, typically 10 to 20 ms, has little impact on the overall end-to-end delay. [20],[21]

The selection of the timeout parameter T_{to} has significant effect on the delay added by the phasor data concentrator. Discarded data set, incomplete data or packet loss can be interpreted as a delay from the point of view of the applications. A PDC operating at 50 Hz causes a complete or partial delay of 20 ms at minimum when a data set is discarded or forwarded as incomplete since the applications have to operate with measurements from previous cycles. [26]

The effect of the timeout parameter on delay and how to decide it has been researched and some methods [26] have been suggested. Generally lower latency is favored over data completeness. [21],[26]

3.1.3 Control and Actuator Delays

There is no universal way to determine the processing times for control calculation or control command execution time. Literature review into reports and research done on many power system control systems suggests a wide range of different values depending on the properties of each system. In many distributed control systems, the time delays on local level control applications are usually less than 10 ms. [7]

Wide-area control application delays vary from the order of milliseconds for simple controllers to the order of tens of milliseconds in the case of more complicated computation applications, and even up to 100 ms in some critical decision applications, or protective safety applications. Several wide-area controller systems which have seen use, suggest control action computation delays of 40 – 50 ms for certain devices and systems. [4],[23],[35],[36]

3.1.4 Communication Delays

Data transmission delays are entirely dependent on the amounts of data transmitted, and the properties of the communication network. Data transmission latency is a

subject of great interest and study, and the effects of various networks types and configuration have been widely studied. For actual values for typical communication delays, consult the later Section 3.2. This subsection provides a general overview to the composition of communication delays. [7],[37],[17]

The common types of delay that occur in communication systems are serial delays, in-between packet delays, routing delays and propagation delays. Serial delays are caused by having to send one bit of data after another. Serial delays occur also between packets denoting the time between consecutive packets being sent. Routing delays are the time required for data to be sent through a router and resent to another location. One routing phenomenon is congestion, which occurs when large amount of signals are to be routed through a single router. Congestion results in additional latency and increases the variability and uncertainty of the latency. Propagation delays are the time it takes to transmit data over the communication medium. Figure 12 illustrates the communication delays associated with data transmission from a phasor measurement unit to a phasor data concentrator. [7],[37]

In wide-area measurement systems the phasor data is typically transmitted in the form of packets. The packets are formatted as a block of information according to the phasor data structure explained in Subsection 2.3.1. [17],[37]

Therefore, a typical transmission packet delay would represented as

$$\tau_c = \tau_s + \tau_b + \tau_p + \tau_r + \theta \tag{9}$$

where τ_s is the serial delay, τ_b is the delay between two consecutive packets, τ_p is the propagation delay which occurs in the transmission of data over the communication medium and τ_r stands for routing delay which is introduced by the routers while forwarding the data. Lastly, the random delay jitter is represented by θ. [16],[22],[37]

The serial delay can be defined as the delay between two consecutive bits as

$$\tau_s = \frac{P_s}{D_r} \tag{10}$$

where P_s is the size of the packet (bits/packet) and D_r is the data rate of the network. [22],[37]

The propagation delay is dependent on the length of the communication link and the velocity of data transmission as

$$\tau_p = \frac{L}{V} \tag{11}$$

where L is the link length and V is the velocity of data transmission. They are dependent on the physical distances involved in the communication network and the types of communication links used. [22],[37]

Lastly, routers are an important part of the communication infrastructure in wide-area measurement systems, especially in systems using shared communication networks. Their contribution to the communication delay depends on many factors, such as level of traffic, hardware properties, network complexity and protocols. Several methods for approximation of routing delays exist in telecommunication and computer engineering. [37]

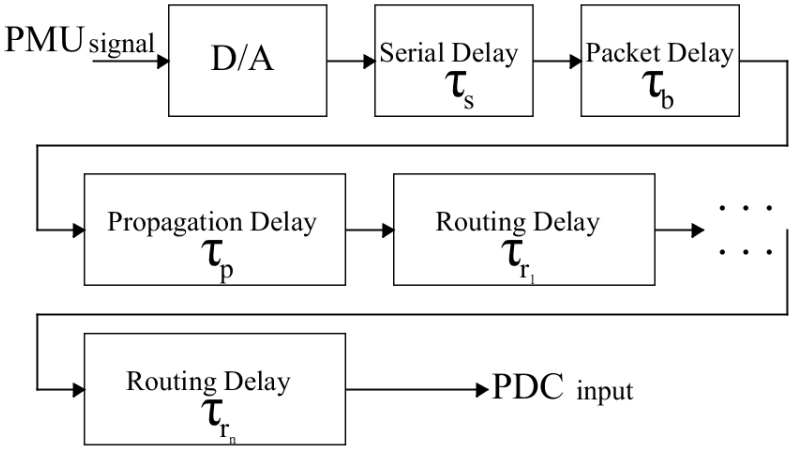

Figure 12: Communication delays associated with data transfer between a PMU and a PDC. [22]

3.2 Reports on Delays in Wide-Area Measurement Systems

General system design principles assume the phasor measurement time delay for a power system to be in the scope of 100 ms [2]. This degree of latency has notable impact on feedback control in many time sensitive applications. Furthermore, a mean delay of 200 ms is typically seen as a tolerable general margin for most wide-area measurement systems. [1],[5],[11]

It has been approximated that individual delay contributions are on average in the range of 20 to 50 ms over each component in the system. Research into communication delays shows that they vary from tens to several hundred milliseconds. These approximation do not include packet loss, corruption or disconnections in communication network. [2],[5]

The chain of WAMS latency is illustrated in Figure 13 and the possible impact of the various phases of the chain is reflected by the relative sizes of those latencies. The dominance of the phasor computation window and the potential effects of transmission delay can be seen clearly from the illustration. [11]

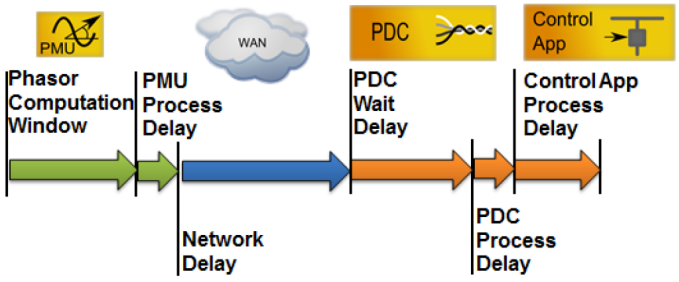

Figure 13: The relative impact of various delays on one way delay depending on circumstance. [11]

A general consequence of latency is the introduction of phase lag into the damping

system before any control action is taken. In addition, phase lag contributes towards slower control responses contributing further to instabilities. For these reasons alone the effects of delays should be considered in damping control design. [16],[38]

PMU processing delay research [19] estimates the delays to be about 75 ms on the hardware used at time of the research. Other studies and sources suggest a PMU processing and measuring delay of 30 to 40 ms on newer hardware [4]. Research [39] at Hydro-Quebec in Canada estimated the one way latency values, shown in Table 3, for that PMU-based system to be around 110 ms.

Table 3: The one way PMU data latency at Hydro-Quebec Power System. [19],[39]

Source	**Latency**
PMU processing time	73 ms
Local data concentration	16 ms
Central data concentration	10 ms
2000 km in optical fiber	10 ms
Total estimated latency	109 ms

In a protective WAMC system [36], research and estimations suggested latency values presented in Table 4 for a PMU system on a shared IP-based wide-area network using fiber optics and optimized connections. However, the information on the specifics and configurations of the devices involved are limited in these aforementioned studies.

Table 4: The data latency in IP-based shared network in a certain protective WAMC system. [36]

Source	**Latency**
Sensor processing time	5 ms
Transmission time of information	10 ms
Processing incoming message queue	10 ms
Computing time for decision	100 ms
Transmission of control signal	10 ms
Operating time of local device	50 ms
Total estimated latency	185 ms

Implementations and experiences of a wide-area HVDC damping control done in China Southern Power Grid [4] found out a total delay in their WAMS to be around 110 ms. It was a PMU-based system where several PMUs and HVDC damping controllers were connected to a control center through a high speed optic-fiber network. The findings are shown in Table 5 in more detail. [4]

Table 5: The latencies of a wide-area measurement system in China Southern Power Grid. [4]

Source	**Latency**
PMU data processing	40 ms
Fiber optic communication	$<$ 15 ms
Data processing and waiting	15 ms
Control execution	40 ms
Total estimated latency	110 ms

Research into communication delays suggests that fiber-optic delays are largely independent of the distances due to their high data rate but other methods for communication are dependent on distances and other factors. Several studies done into the use of fiber optics in wide-area measurement systems have reported delays under 15 ms. [4],[16],[26]

Further research [26] also shows that fiber-optic communication delays in certain TCP/IP networks can be modeled as bi-modal distributions and in fiber optic communication systems the mean delays are in range of 9 – 15 ms. The effect of excessive delays and spikes contributes to the deviation σ of the distribution more than to the mean delay μ. The observed parameters for unprocessed PMU data are shown in Table 6. [16],[26]

Table 6: Empirical results for unprocessed PMU data latency distribution in a fiber-optic TCP/IP network. [26]

Bi-modal distribution parameters	
μ_1= 7.5 – 13 ms	σ_1= 0.5 – 2.5 ms
μ_2= 16 – 18 ms	σ_2= 1.6 – 4.0 ms

Some typical propagation delays associated with various communication links are shown in Table 7 based on [16], and the results have been augmented with previous findings on communication delays.

Table 7: Associated one way delays with various communication links. [16]

Communication link	**Associated delay**
Fiber optic cables	10 – 15 ms
Digital microwave links	25 – 75 ms
Power line	75 – 275 ms
Telephone lines	125 – 225 ms
Satellite link	425 – 625 ms

4 Simulation of Delays

This chapter covers the power system model and its power system simulation implementation with time delays in the measurement system. First, a general overview of the studied power system and the simulation methods is provided, and then three different power system simulation models with different properties are presented. Finally, the delay implementation which was added to the power system simulation is described and the methods to be used to analyze the results later in Chapter 5 are discussed.

4.1 Power System Simulation

The studied power system is a two-area four generator system [9] which has two load areas and two generation areas. The diagram of the system is shown in Figure 14. Generators G1 and G2 represent the main cluster of machines in Area 1, and generators G3 and G4 the machine cluster in Area 2. The two areas are connected by two transmission lines at bus 101. The constant system loads in the model are at buses 4 and 14 for both areas. The original power system model did not contain the phasor measurement units but were added next to each of the four generators at the buses 1, 2, 11 and 12.

In total, three different power systems based on the same template were used to study the effects of delays on oscillation damping control. The three power systems have slightly different properties resulting in different behavior and natural oscillation modes. The goal of using three different systems was to use them to find common behavior or patters when delays were introduced into the systems. The properties of the simulation models and their natural oscillation modes are presented in Section 4.1.

The wide-area damping was done by a model predictive control (MPC) damping controller which had been previously developed [40]. A summary of the controller can be found in Subsection 4.1.2. The wide-area monitoring and control scheme used in these simulations is illustrated in Figure 15.

The measurements travel through the wide-area network from the PMUs to the phasor data concentrator and continue to an imagined control center from which they are sent to each of the generation sites. The controller applies its control signal to the generator exciters which adjust the generator speeds.

The simulated power systems do not contain any local power system stabilizers (PSS) since the goal was to study the effects of delays on the wide-area damping control alone. It was assumed that on a simple two-area four generator system the local damping would be otherwise sufficient to damp the oscillations alone or at the very least would obfuscate the results.

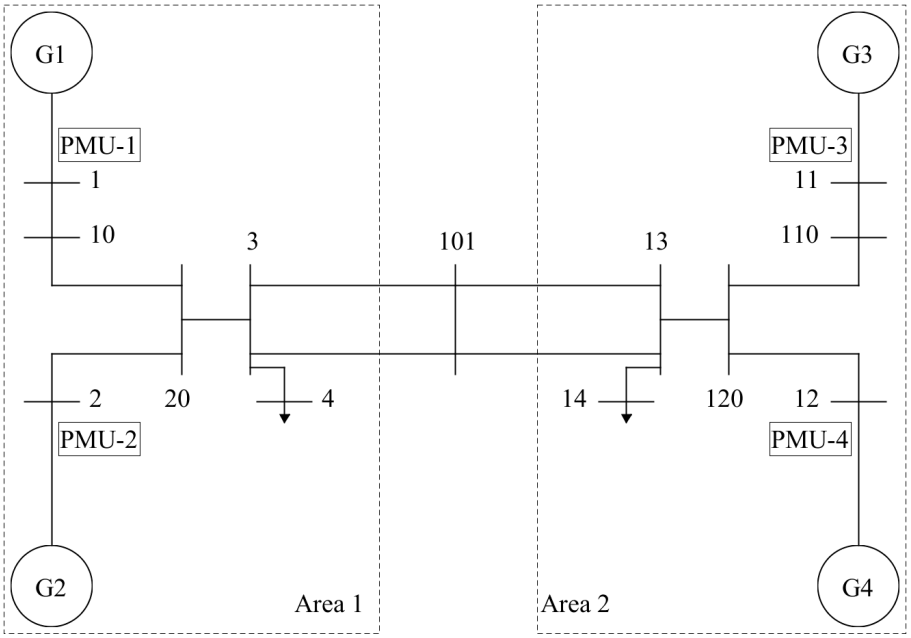

Figure 14: The diagram of the two-area four generator system and the placement of PMUs used in the simulations. It is modified from [9].

The effect of delays on the wide-area damping control of electromechanical oscillations was studied using MATLAB and the Power System Toolbox (PST-Toolbox). The simulations were done using the Power System Toolbox's nonlinear subtransient power simulation which uses a detailed generator model with 11 states. The simulation model did not have any latency related functionality regarding measurements, data transmission or control action. This functionality was added into the simulation program as a part of this thesis in order to be able to study the effects of the simulations. A detailed explanation of the delay implementation is given in Section 4.2.

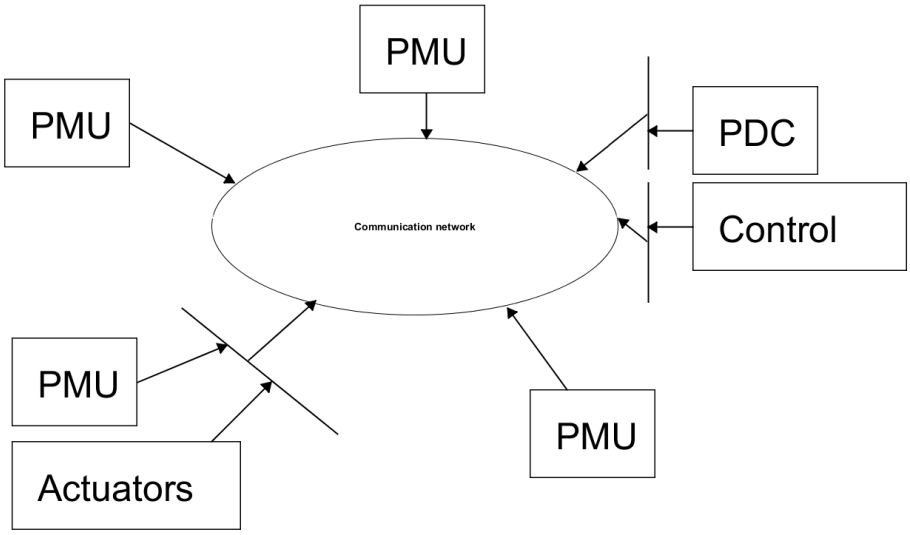

Figure 15: The wide-area measurement and control scheme used in the simulations.

4.1.1 Power System Models

The three different power systems used in the simulations have slightly different properties. The power systems will be referred as power systems A, B and C for the rest of the thesis. The different power system configurations have an effect on the dynamics of the power system and how it will behave when the fault is applied.

Each of the power systems is different and their configurations are described in Tables 8, 9 and 10 for power systems A, B and C respectively.

Table 8: Power system A properties.

Properties
Reference system
G1 & G2 inertia constant H = 6.5 s
G3 & G4 inertia constant H = 6.15 s
Bus 4 load = 9.76 pu
Bus 14 load = 17.65 pu

The model for power system A is the reference system. The two other system properties were deviated from the properties of power system A.

Table 9: Power system B properties

Properties
Inertia constants for generators increased
G1 & G2 inertia constant H = 15.5 s
G3 & G4 inertia constant H = 15.15 s

The model for power system B was created by increasing he inertia constants of the generators. The model for power system C was created by altering the loads for the areas.

Table 10: Power system C properties

Properties
Decreased load for Area 1
Increased load for Area 2
Bus 4 load = 8.26 pu
Bus 14 load = 19.15 pu

The natural oscillation modes for each of the power systems without any control are important for the rest of this work. Identifying the local and interarea modes prior is helpful later when the results are examined. The mode properties are shown in Tables 11, 12, and 13. The values were obtained using the PST-Toolbox's numerical eigenanalysis method which perturbates the power system in order to calculate its properties. [41]

This numerical method, based on the small changes in the power system, is not as accurate as a classical mathematical modal analysis would be but should be sufficient for the purposes of the simulations presented in this thesis [41]. The mode interactions are assumptions of the interaction based on the respective frequencies. Interarea modes are the most important followed by the local modes for the purposes of the thesis.

Table 11: The oscillation modes of power system A. Interarea and local modes are emphasized.

	Mode	**Freq (Hz)**	**Damping ratio** $\zeta(\%)$
1	$-0.253 \pm 0.654i$	0.10	36.00%
2	$0.063 \pm 4.239i$	**0.67**	**-1.48%**
3	$-0.518 \pm 7.386i$	**1.18**	**7.00%**
4	$-0.515 \pm 7.595i$	**1.21**	**6.76%**
5	$-8.296 \pm 9.259i$	1.47	66.73%
6	$-8.191 \pm 9.510i$	1.51	65.26%
7	$-5.607 \pm 14.842i$	2.36	35.34%
8	$-3.789 \pm 17.442i$	2.78	21.23%

The power system A has eight modes as shown in Table 11. The interarea mode is 0.67 Hz and is unstable as can be seen from the eigenvalue's positive real part or from the negative damping value. More information on the damping ratio is provided in Section 4.4 where the evaluation criteria is presented. The local modes are the modes 3 and 4, both around 1.2 Hz with a sufficient damping ratio. The rest of the modes are various other modes, such as intraplant modes.

Table 12: The oscillations modes of power system B. Interarea and local modes are emphasized.

	Mode	**Freq (Hz)**	**Damping ratio** $\zeta(\%)$
1	$-0.162 \pm 0.389i$	0.06	38.56%
2	$-0.011 \pm 2.687i$	**0.43**	**0.40%**
3	$-0.560 \pm 4.505i$	**0.72**	**13.19%**
4	$-0.616 \pm 4.574i$	**0.73**	**13.55%**
5	$-7.887 \pm 9.306i$	1.48	64.65%
6	$-7.813 \pm 9.572i$	1.52	63.23%
7	$-5.509 \pm 14.892i$	2.37	34.69%
8	$-3.794 \pm 17.440i$	2.78	21.25%

The power system B has no unstable modes, although the interarea mode at 0.43 Hz is very poorly damped. The effects of the slower generators can be seen in this system clearly. The local mode of oscillations are low local modes slightly above 0.70 Hz. The rest of the modes are other oscillations types.

Table 13: The oscillations modes of power system C. Interarea and local modes are emphasized.

	Mode	**Freq (Hz)**	**Damping ratio** $\zeta(\%)$
1	$-0.252 \pm 0.653i$	0.10	35.99%
3	$0.050 \pm 3.868i$	**0.62**	**-1.29%**
4	$-0.523 \pm 7.331i$	**1.17**	**7.12%**
5	$-0.576 \pm 7.491i$	**1.19**	**7.67%**
6	$-8.128 \pm 9.837i$	1.57	63.69%
7	$-8.057 \pm 10.098i$	1.61	62.37%
8	$-5.486 \pm 16.420i$	2.45	33.52%
9	$-4.008 \pm 17.649i$	2.81	22.15%

The power system C has one unstable mode which is the interarea mode at 0.62 Hz. The effect of different loads with otherwise same properties as system A show very similar properties. The local modes 4 and 5 are slightly below 1.20 Hz.

4.1.2 Wide-Area Damping Controller

The power system simulations have a MPC-based wide-area damping controller developed separately [40] earlier. It has been applied for the power system models used in the simulations. In general, model predictive control is characterized by certain features, such as the explicit use of system models to predict future states, the calculation of control responses based on objective functions to be minimized, and by the use of control and prediction horizons. [42],[43]

The MPC damping controller in the simulations receives four simultaneous measurements from the phasor data concentrator as its input. The measurements

are essentially the generator rotor angles from the four generation sites where the PMUs are located, more on the measurements in Subsection 4.2.1 about the PMU. In addition to the measurements, the controller uses the power system model and the previous control output to determine its new control output. The output signals are the exciter control signals for each of the four generators used to control the generator speeds. The MPC is executed at every time step of the simulation. Both the prediction and control horizons used across all the simulations have 40 steps.

The wide-area damping controller is completely delay unaware. It does not take into account the measurement delays and control actuation delays before or after control command calculation.

4.2 Delay Implementation

The delays were implemented into the PST-Toolbox simulation program by changing the existing implementation using MATLAB's scripting language. As previously stated, the simulation program did not have any functionality regarding measurement and control latencies. The delays and measurements were implemented into the system based on the architecture and delay structure presented in Section 4.1. For practical reasons, the delay structure was further abstracted while retaining the same basic functionality. The abstracted delay chain implemented in the simulation program is shown in Figure 16. Each block is a component in the system which adds some delay to the signal and similarly the transmission lines contribute communication delay. Four signal converge into PDC and through control block diverge again into the actuators.

The delay implementation was done by adding the components of a wide-area measurement and control system into the simulation program. It should be understood that none of the components are simulations of any of the actual components but rather abstractions which have the same basic functionalities as the real actual components would have. Therefore, the functionalities of phasor measurement units, a phasor data concentrator, control calculation and execution are mimicked from the perspective of how they add latency into the system. In addition, signal noise, data loss and measurement errors were out of the scope of this thesis, as outlined in the introduction, and the simulation does not contain these features.

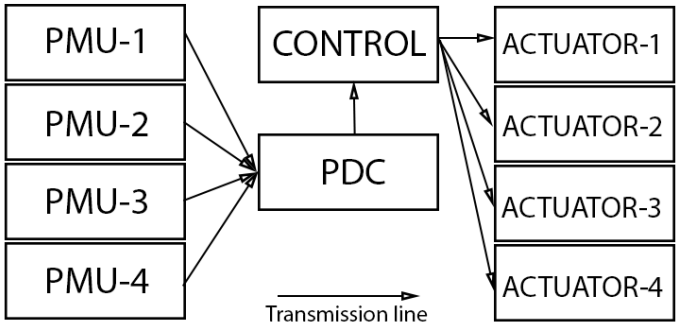

Figure 16: The delay chain implemented in the simulation program. Each block and line contributes to the delay.

In the implementation of the new features to the simulation, the first step was to create several different data arrays to handle the data latency functionality. One measurement array, one control array and four actuation arrays were created. The lengths of the arrays were equal to the duration of the simulation in time steps. Therefore, the indices of the array items corresponded to that particular moment of the simulation in timesteps.

The next phase was to set up the measurement system by reading values from buses 1, 2, 11 and 12, as indicated by Figure 14. These measurements were read by the four PMUs which forwarded their measurements to the measurement array. The measurements were forwarded as a data set identified the timestamp of the measurements. Additionally, each PMU added their own processing and communication delays into the measurements as additional data. The PMU with least latency determined where the data set was placed on the measurement array.

The phasor data concentrator read the measurement array and processed the measurements by forwarding them into the control array, if the timestamp of the measurements was newer than the previous one processed by the PDC. In addition, the PDC handled the total latency based on the varying delays of each of the four measurements. This setup ensured that only the most current data which arrived on time was forwarded and data sets arriving too late were discarded. The PDC added further communication latency to the data set.

The control system read the control array and performed control action calculations for the actuators, if the measurements had newer timestamp than the previous one. The control commands went into the corresponding actuator arrays for each of the generators with an added delay consisting of processing, communication and actuator action latency. Control was applied constantly and if there were no new commands, the previous control was applied until new command arrived. This delay structure can be expressed as

$$\tau_{ete} = \tau_{pmu} + \tau_{pdc} + \tau_{ctrl} \tag{12}$$

The delays and their values are described in more detail in the subsections below. The delays, their implementation and values are based on the previous sections covering the wide-area measurement and control delays.

4.2.1 Abstract PMU

The abstract phasor measurement unit implemented into the system did not compute real phasors from the three phase voltage, but instead it measured the generator terminal voltage angle and sent it to the phasor data concentrator. In the absence of real phasor measurements, the terminal voltage angle represents sufficiently the generator rotor angle when the variation pattern is important [44].

The operating frequency is the only property of the abstracted PMU. The operating frequency is set at 50 Hz in the simulations. Hence, the PMU forwards the terminal voltage angle measurement at 20 ms intervals, or every fourth simulation step since the timestep is 0.005 seconds.

All the PMUs in the simulation are worst-case PMUs and operate at the maximum reporting latency allowed by the standard for a P-class PMU. Therefore, the PMUs have a base latency of 40 ms given their operating frequency. Additional processing delays are drawn from a probability distribution based on [34]. The components of reporting delay are shown in Table 14.

Table 14: The components of PMU reporting delay in the simulations.

Source	**Delay (ms)**
PMU reporting delay	40
PMU processing spikes	P(89%) = 0, P(10%) = 20 or P(1%) = 200

The PMU sends its measurements forward by drawing a transmission delay from a wide-area network delay distribution, described later in Subsection 4.2.4. The four PMUs in the simulation send their measurements as one package based on the timestamp. Their placement in the measurement array is determined by the PMU with the lowest communication delay, i.e. the first measurement of that timestamp to arrive at PDC.

Therefore, the PMU delay is the following:

$$\tau_{pmu} = (40\,ms + P(X)) + \tau_c \tag{13}$$

where τ_{pmu} is the PMU's associated delay consisting of reporting latency, $P(X)$ processing spikes latency and communication delay τ_c for abstract P-class PMU operating at 50 Hz.

4.2.2 Abstract PDC

The abstracted phasor data concentrator operates at the same operating frequency as the PMUs, and therefore no downsampling or upsampling is required. The PDC's function in the simulations is to read the synchrophasor packages based on the arrival of the first measurement, calculate when all the measurements would have arrived and forward them into the control array if they arrive within the time limits. The PDC discards delayed measurements which arrive later than newer ones by not forwarding them.

Although, the abstracted PDC has a time-out functionality implemented it was turned off in the simulations. Frequent or consecutive reliance on the time-out functionality is essentially a form of data loss and thus outside of the scope of the thesis. Furthermore, the focus was on the effects of delays instead of tuning the time-out parameter in an artificial environment.

The PDC operates at a constant operating latency according to its operating frequency of 50 Hz, based on the information provided in Subsection 2.3.2. In addition, it draws a communication delay value from the wide-area network latency distribution, see Subsection 4.2.4.

Therefore, the PDC delay is the following:

$$\tau_{pdc} = 10\,ms + \tau_c \tag{14}$$

where the PDC delay τ_{pdc} consists of constant processing and sorting delay and communication delay τ_c.

4.2.3 Abstract Control and Actuation

The wide-area damping controller reads the control array which contains the delayed measurements. The controller runs at the simulation timestep and new control is calculated at every time step. A short explanation of the wide-area damping control was given in Subsection 4.1.2. The delay of the control and actuation consists of calculation delay, communication delay and actuator execution delay.

The value for the actuator's execution of the control signal was chosen to be a constant 10 ms. The communication delay is drawn from the wide-area network delay distribution, see Subsection 4.2.4. Finally, the control calculation delay was a set of precalculated values based on a normal distribution with a median value of 30 ms with a small standard deviation.

Table 15: The components of the control and actuation delay.

Source	**Delay (ms)**
Control command calculation	Normal distribution P, $\mu = 30$ and $\sigma = 5$
Actuator execution	10

Table 15 shows the components for the control and actuation parts, and the mathematical form of the delay is shown below.

$$\tau_{ctrl} = P(X) + t_c + 10\,ms \tag{15}$$

where the total control and actuation delay τ_{ctrl} consists of control command delay $P(X)$, communication latency t_c and the constant latency for the actuator's execution of the control command.

4.2.4 Wide-Area Network

The data in the simulation is transmitted through a wide-area network, as shown in Figure 15. The wide-area network, like other components in the simulation, is an abstract construct which does not simulate real communication links, communication protocols, routers or network topology. The transmission of data adds latency whenever data travels between components in the simulation.

The various different simulation cases were achieved by altering the communication delay properties, as it was the most convenient way to do it and under real circumstances also the one with most variance. The delay distributions used in the simulations are shown in Table 16.

Table 16: Communication delay distributions used in the simulations.

Delay distribution	**Properties (ms)**
Bi-modal distribution	$\mu_1 = 10.25, \mu_2 = 17, \sigma_1 = 1.5, \sigma_2 = 2.8$
Poisson distributions	$\mu_n = 10n, \sigma = 15.00$ (n = 2,3,4, ...)

The bi-modal distribution, based on values shown in Table 6, is an abstraction of a dedicated fiber-optic network, which was the preferred communication medium for wide-area measurement systems, see Subsection 2.3.4. The Poisson distributions were used to simulate generic wide-area networks with varying but increasing levels of latency. The Poisson distributions have different mean values but the same deviation since data loss was defined outside of the scope for the thesis and all measurements are thus expected to arrive within a reasonable deviation.

Poisson distributions were chosen over normal distributions since data arrival rates have been shown to follow Poisson process [45] and for the purposes of the simulation they provide sufficient stochasticity for the communication delay. It should also be noted that each of the delay values from the distribution were quantized to the nearest value divisible by 5 ms, a limit set by the timestep of the simulation.

The setup of the wide-area network properties allowed different simulation cases with increasing delay, yet the cases were clearly identifiable from each other and still within the other requirements.

4.3 Simulation Cases

All the simulations done for this thesis have the same rundown on the stages of the simulation. Five events determine each of the simulations runs. The start and stop events which begin and end the simulation, and three events for an impulse trigger. The first event starts the simulation at $t = 0.0$ s, and the simulation is started at a linearized balance point where no oscillations occur and no damping control is required initially.

The simulation is allowed to run for a while and then at $t = 4.0$ s a fault is applied into the system. The fault acts as a disturbance which triggers the system and causes the power system to oscillate. The trigger is a three-phase fault at bus 3. The near end of the line from bus 3 to bus 101 is cleared 0.1s after the fault, and the remote end is cleared after a further 0.005s at $t = 4.105$ s.

This event causes a transient in many of the system variables and the simulation is run a further 30 seconds which is common practice and should be sufficient to study the effects. The active load in the system is assumed to be static. The simulation time and load configuration has been found sufficient in most cases to study transient stability. [41]

The simulation uses a fixed discrete timestep of 0.005 s to run and this timestep also naturally limits the smallest window of time that can be studied to the same length. A power system simulation which runs for 35 seconds has 7000 discrete steps in total with the chosen timestep. The length of the simulation and the timestep

were considered from the perspectives of sufficient accuracy, required duration and reasonable computation times.

For each of the various power systems the simulations were done using various communication delays. The communication delays were chosen to be the one changing variable between the simulations contributing to the different total end-to-end mean delays between the simulation runs. It was the most convenient way to do it and most closely resembling real conditions where the communication network is the most varied component.

The different simulation cases run for each of the power systems A, B and C are shown in Table 17. A no delay case was run for each of the power systems for a reference performance without any delays. The fiber-optic case was chosen for fiber-optic being a preferred communication method for wide-area systems. In the rest of the simulations a variable amount of increasing Poisson delays was used until the systems became unstable. The intention was to study the effects of delays and to stop doing the simulations when the delay margin for the last stable case was found. PMU sampling delay contains only the PMU measurement delay and no communication delay between data transmissions.

Table 17: The simulation cases for each of the three power systems.

Simulation case	**Purpose**
No delay	Reference case
PMU sampling delay	Effect of delays
No communication delay	Effect of delays
Fiber-optic wide-area network	Typical case
Increasing Poisson delays	Effect of delays
...	
Until the system becomes unstable	Delay margin

4.4 Evaluation Methods

In order to study the effects of delays on the wide-area damping control of electromechanical oscillations, several criteria were chosen to evaluate and compare the results. The system variables chosen for observation are mainly the speed deviations for each of the four generators.

The Integral of Time Multiplied Squared Error (ITSE) was chosen to simply evaluate the overall damping response and provide a comparison value for the simulations among each system. The Prony analysis is used to extract oscillation modes, their frequencies, damping ratios and phase angles. In addition, a side-product of Prony analysis is the frequency spectrum of the oscillations which was also used for study purposes. These two previous methods are applied to the generators speed deviations, which are also compared to each other. Additionally, the MPC generator speed predictions are reviewed in addition to the control signal output.

The following subsection cover in detail the main criteria: ITSE and damping ratio. Additionally, the methods of Prony analysis are covered.

4.4.1 Integral of Time Multiplied Squared Error

The Integral of Time Multiplied Squared Error (ITSE) is an integral criteria used to evaluate control performance. It emphasizes larger errors, difference between desired and actual value and weights them with time, putting less weight for early deviations and more weight for later deviations. It is a common performance criteria used in controller design and control performance evaluation. [46]

$$ITSE = \int_0^\infty e^2(t)t\,dt \tag{16}$$

where $e(t)$ is the difference between the measured and reference value at time t.

It is common practice to choose a suitable time period where the ITSE is applied [46]. In these simulations, the ITSE is calculated for 30 seconds after the fault is introduced into the power system.

The ITSE criteria was chosen in order to avoid the initial transient in the simulations dominating the error calculation, since ITSE criteria weighs later values more, but the effects of the transient were still wanted to include in the value.

The ITSE values were calculated for each generators separately. The sum of the generator pair values is the ITSE value for each area and the sum of the area values is the total ITSE value for the system. The purpose of using ITSE criteria is to evaluate the overall step response of the damping control excluding any consideration for oscillations modes. The values can be used only as comparative values between varying delays within the same power system.

4.4.2 Prony Analysis

Prony analysis was the chosen method in the thesis was to evaluate the generator speed deviation response to the introduced fault. It was used to evaluate the subsequent transients and oscillations. The Prony analysis was done on the generator responses using MATLAB with the aid of the Prony Toolbox [47].

The Prony analysis is a method which estimates the parameters of an oscillating signal $y(t)$ by fitting a sum of complex damped sinusoids in time domain. The Prony analysis can obtain the amplitude, phase, frequency and damping of each of the signal components. Each of the components corresponds to an oscillation mode of the power system. Equation (17) shows the sinusoid fitted representation of the original signal.

$$\hat{y}(t) = \sum_{i=1}^{L} A_i e^{\sigma_i t} cos(2\pi f_i t + \phi_i) \tag{17}$$

where L is the number of components, or the model order, and i indicates a single component. For each component: A_i is amplitude, σ_i is damping coefficient, ϕ_i is its phase and f_i the frequency of the component.

In addition to the previous properties, the eigenvalue representation of each oscillation mode was obtained. The eigenvalue is required to calculate the damping

ratio described later in Subsection 4.4.3. The eigenvalue presentation is shown in (18) and one exists for each Prony component. They are derived from Euler's formula not presented here.

$$\lambda_i = \alpha_i \pm j\omega_i \tag{18}$$

where the real part α_i is the attenuation and the imaginary part ω_i is the oscillation part.

The connection between oscillation frequency f_i and the imaginary part is the following:

$$f_i = \frac{\omega_i}{2\pi} \tag{19}$$

Prony analysis is a powerful signal analysis technique which is widely used in many applications including the analysis of electromechanical oscillations in power systems. However, it has some downsides such as poor behavior under noise, inconsistency between results and the reliance on properly chosen parameters. [47] The simulations in the thesis do not have any noise but the parameters for the analysis, such as sampling frequency, window length and model order, were carefully considered.

Sampling frequency for the Prony analysis is critical for accurate results. One requirement is that the sampling is uniform [48]. Otherwise, it has to fulfill the requirements of Nyquist's sampling theorem which states that the sampling needs to be at least two times the highest frequency in a signal. In addition, a too high sampling frequency has also been shown to result in poor accuracy when using the Prony analysis. A sampling frequency of two or three times higher than the highest frequency oscillation is considered to produce accurate results. [48]

Another important parameter for Prony analysis is the window length which is the period where the Prony analysis is performed. The window has a specific starting point in addition to its length. The length of the window should be at least one and a half times the period time of the lowest frequency signal. However, a too long window increases the risk of breaking actual oscillation modes into several components. [48]

The model order for Prony analysis is another important parameter. Initially it has to estimated for each Prony analysis since there is no way to know the properties of the signal. A good starting value for the model order is a value less than a third of the data length. A too high order breaks real oscillations into multiple component representations of actual oscillation modes. However, a model order less than the number of oscillation modes is not an accurate approximation. A practical approach first estimates an initial model order and adjusts it according to some parameter, such as the root mean square error (RMSE), until a suitable model order is found. [48]

For these reasons, the sampling frequency was chosen to be 8 Hz which required downsampling by a decimation factor of 20 in time domain for the original signals. A sufficient sampling frequency for detecting oscillation modes up to 4 Hz. The initial analysis of the power systems in Subsection 4.4.1 shows that the lowest expected frequencies are in the range of 0.06 to 0.1 Hz, and the highest frequencies less than 3 Hz. The Prony window was chosen to be 15 seconds. This length risks loosing the

lowest of oscillation frequencies but is more robust against actual oscillations modes breaking into multiple components. It is sufficient for the interarea and local modes which are most important for the topic of the thesis.

In addition, the Prony window was chosen to start 1.75 seconds after the transient has been introduced to the systems in order to reduce possible interference from strong control action expected to take place instantly after the transient. The initial model order was chosen to be 12 and was only increased if RMSE was larger than $5 * 10^{-8}$. However, the model was not allowed to exceed the value of 48 which was one third of the Prony data length. Overview of the Prony analysis parameters is shown in Table 18 for a quick reference.

Table 18: The key parameters used for Prony analysis.

Parameter	**Value**
Sampling frequency	8 Hz
Window start	5.75 s
Window length	15 s
Model order	$12 \leq L \leq 48$
max(RMSE)	$5 * 10^{-8}$

4.4.3 Damping Ratio

The damping ratio ζ for any oscillation mode can be calculated from its eigenvalues using equation (21). Positive damping ratio indicates that the oscillation decays eventually while a negative value indicates an unstable oscillation with an increasing amplitude. A damping ratio which is zero describes an oscillation that does not decay or increase but remains stable. [49],[41]

$$\zeta = \frac{-\alpha}{\sqrt{\alpha^2 + \omega^2}} \tag{20}$$

where α is the real part is the attenuation and ω is the imaginary part indicating the frequency of the oscillation mode, from the eigenvalue form $\lambda = \alpha \pm \omega i$.

The eigenvalues for oscillation modes in this thesis were obtained using Prony analysis, or the Power System Toolbox in the case of initial power system analysis.

For decaying oscillations there are three different cases of damping depending on the value of the damping ratio. These are the over-damped case, the critically damped case and the under-damped case [50], and they are illustrated in the Figure 17.

The case where $\zeta > 1$ applies for the damping ratio, is called the over-damped case. It has only two real and distinct eigenvalues resulting in a decaying exponential with no oscillation. A critically damped case, $\zeta = 1$, has multiple and real eigenvalues and is the border case between over-damped and under-damped cases. [50]

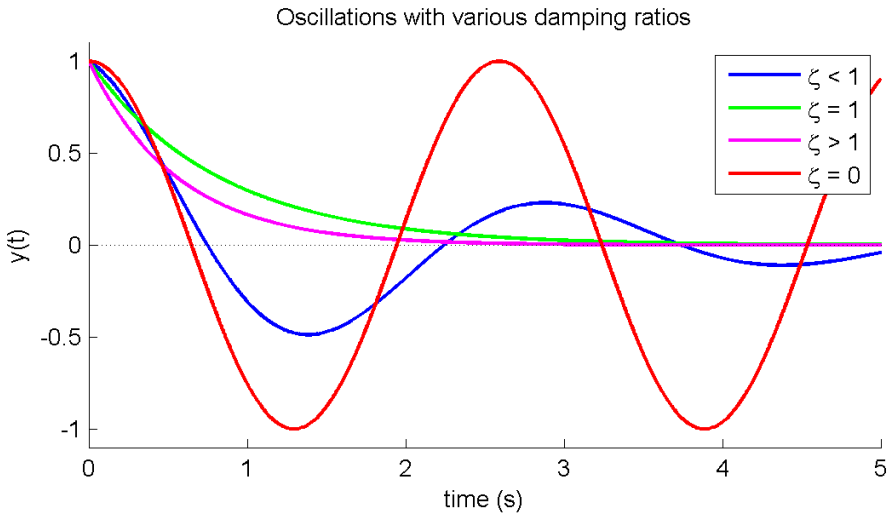

Figure 17: Examples of under-damped $\zeta < 1$, critically damped $\zeta = 1$, over-damped $\zeta > 1$ and non-damped $\zeta = 0$ oscillations. [50]

The under-damped case is the most important one and the most common in control system applications. The eigenvalue of an under-damped oscillation is a pair of complex conjugates. [50]

Electromechanical oscillations where $\zeta > 0.05$ applies are considered satisfactory under most circumstances. While lower damping ratios, such as $\zeta > 0.03$, are acceptable under certain conditions, the value of 0.05 for damping ratio should be a minimum target for any damping control performance [41].

Damping ratio can be expressed also in percentage form [49], and for the sake of clarity will be expressed as such in the rest of the thesis. For example, a damping ratio of 0.03 corresponds to 3% damping.

4.4.4 Other Criteria

In addition to the previous criteria, other information will be used to evaluate the effects of delays. These methods include frequency spectrums which are obtained as a side-product of performing Prony analysis, comparisons of damping controllers' prediction states and real generator speed values, and comparisons of generator speed deviation behavior.

5 Simulation Results

In the first part of this chapter, the simulation results for each of the simulated power systems are presented, examined and compared. For each of the systems, a few cases are picked and examined in more detail. In addition, the results of several delay cases are compared to each other. In the second part of this chapter, the conclusions drawn from the simulations are presented, analyzed and suggestions for further research are discussed. The results are viewed in the scope of the research questions presented in the introduction of this thesis.

In addition, the reliability of the results is also reviewed throughout this section, and an initial review on the correct designed behavior of the simulations is presented.

Figure 18 shows the PMU measurements and how they are taken every 20 ms (50 Hz) as they should be when the sampling is done every 4 timesteps with a timestep of 0.005 as described in Subsection 4.2.1. This is a confirmation of the PMUs working as intended.

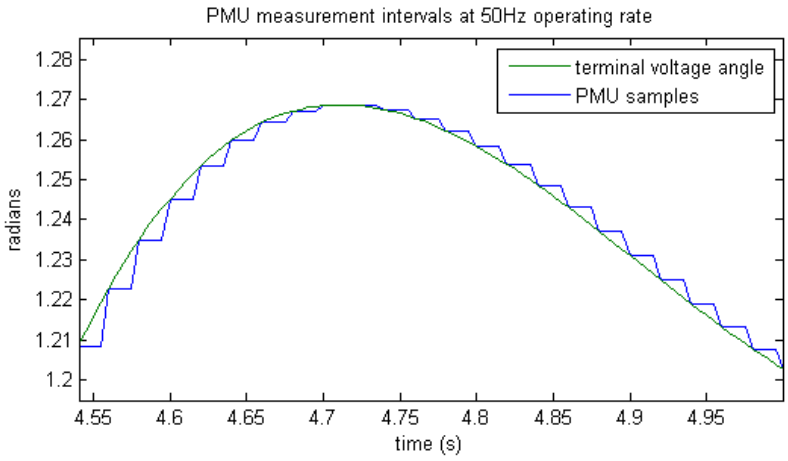

Figure 18: Phasor measurement samples taken at 50 Hz, or every 20 ms, in the simulation.

In Figure 19, a comparison is presented between real and measured values from power system B under delay. The figure shows the difference between the actual terminal voltages of a bus and the measured terminal voltage angles at PDC output. The phase lag is a well-known effect observed in systems with delayed inputs or outputs. Additionally, the phase lag is not a constant but varies slightly based on the properties of the components. These phenomena happen across all simulation components described in Section 4.2, and is thus another confirmation of the simulation and delay implementation working correctly.

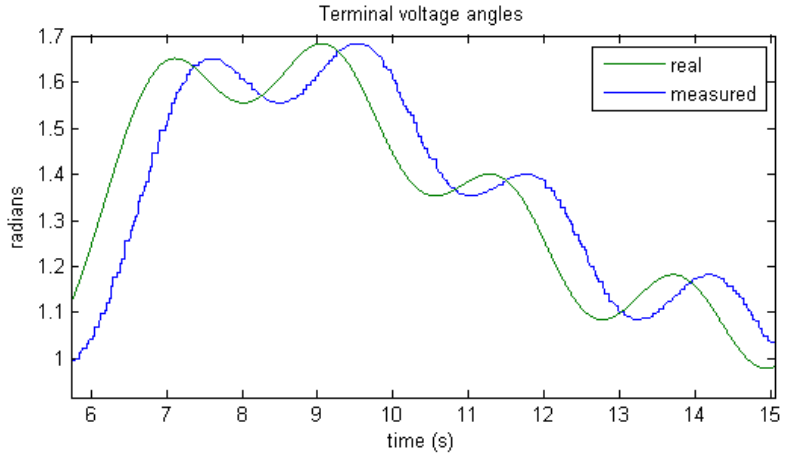

Figure 19: An example of the real terminal voltage angle values and its corresponding delayed measurements at PDC output.

Next, the results from each of the three simulated power systems A, B and C are examined individually. Some of their results are looked in more detail, compared among each other and finally conclusions are made. The generator 3 was chosen as a reference generator for further examination shown later.

5.1 System A

This section presents the results obtained from the simulations for the power system A. In this section, some simulation cases are presented on their own, and then later some comparisons between the varying delays are shown. The power system A was able to stand a maximum end-to-end delay of less than 280 ms, and the first mode to become unstable was the local mode for Area 2, see Table 19. However, the interarea mode damping while under 3% is able to withstand a longer delay.

Table 19: Power system A tolerance for delays.

Maximum delay tolerance	**Unstable mode**
Under 280 ms	Local mode for Area 2

The ITSE values for power system A with a given end-to-end mean delay are presented in Figure 20. It shows that the overall damping performance is better under delays of about 160 ms compared to a case with no delay. With larger delays the ITSE value experiences a significant increase, and the system becomes unstable quickly.

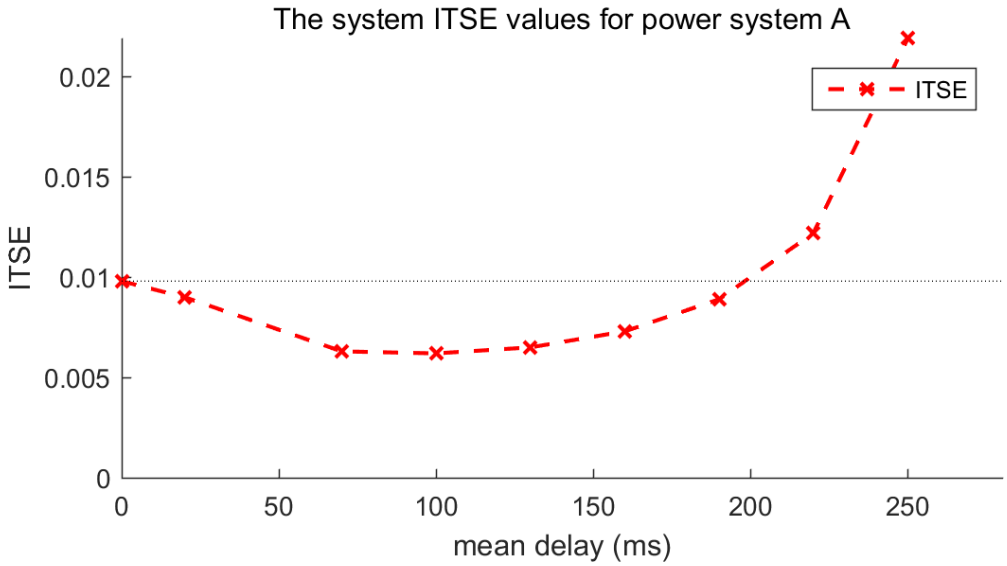

Figure 20: The system ITSE values for power system A.

The simulations show that the oscillation frequency of the interarea mode increases as more delay is introduced into the system. The damping improves initially but gets worse after a certain delay margin is exceeded. The real and absolute imaginary values of the generator interarea modes with different delays are shown in Figure 21, the delays increase clockwise along the spiral. The cluster of points near $-0.2 + 4.5i$ is the case with a mean end-to-end delay of 220 ms seen in Figure 20. It is the first delayed case performing worse than the case without delay.

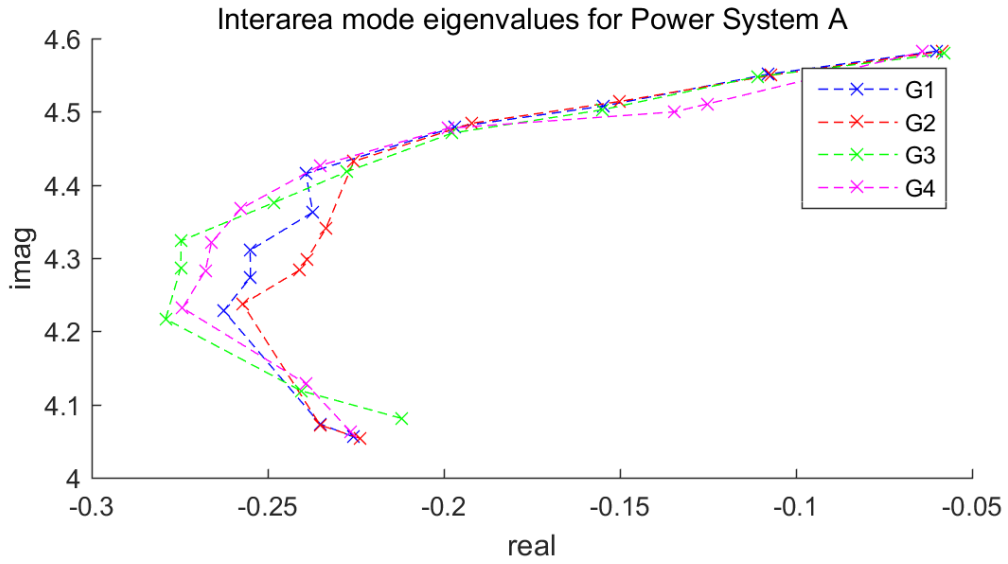

Figure 21: The real and absolute imaginary values of the generator interarea oscillation modes with different delays. The delay increases clockwise along the spiral curve.

In the next subsections several simulation cases are shown in more detail. The

first one is the reference case with no delays, the second is the so-called fiber-optics case, the third is the first case performing worse than the case with no delays and the last case is the first unstable one.

5.1.1 No Delay Case A

The generator speed deviations of power system A in the case of no delays are shown in Figure 22, the values are displayed as per-unit (pu) values. As can be seen from the speed deviation figure, after the transient is introduced to the system at t = 4.0s the decaying oscillations decay in about 20 s almost completely. Generator pairs in both areas, Area 1 and Area 2, oscillate in synchronized phase, and the areas oscillate against each other at the interarea mode with a phase difference of about 180 degrees.

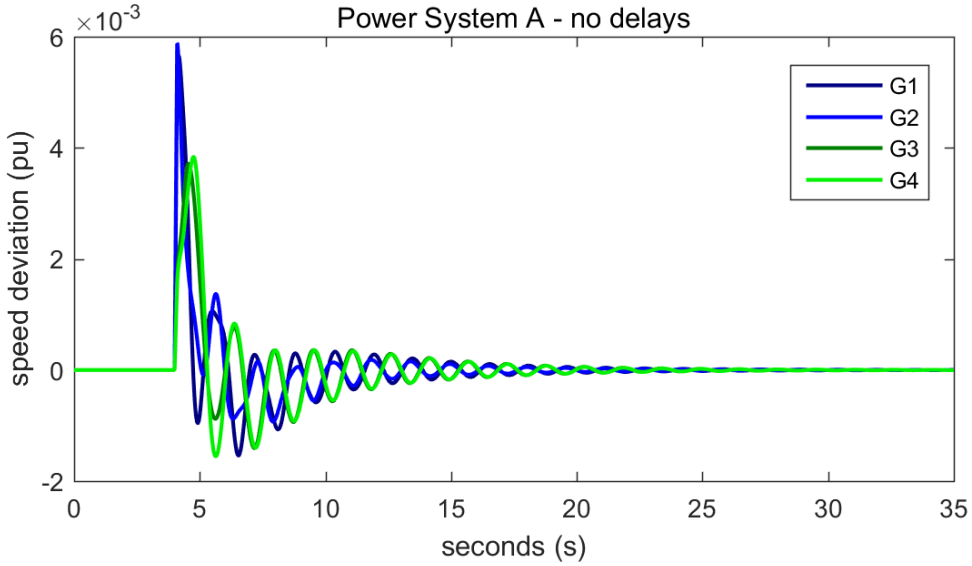

Figure 22: Generator speed deviation without delays in the power system A.

The dominant modes obtained using the Prony analysis are shown in Table 20, and the values confirm the results shown in Figure 22 presenting the speed deviations. The interarea mode's frequency is about 0.65 Hz which is slightly lower than the initial numeric eigenvalue analysis, results shown in Table 11, done using the PST-Toolbox suggested. The damping for the interarea mode with no delays is in the range of 5.2% to 5.6% across all generators which is an acceptable value for damping. The phases are about the same for each area and the phase difference between the areas is about 180 degrees with Area 1 leading the oscillation.

Table 20: Interarea mode for system A without any delays.

	Mode	**Freq (Hz)**	**Damping ratio** $\zeta(\%)$	**Phase** (°)
G1	$-0.226 \pm 4.056i$	0.646	5.56%	-56.14
G2	$-0.224 \pm 4.054i$	0.645	5.52%	-42.59
G3	$-0.212 \pm 4.081i$	0.650	5.19%	136.35
G4	$-0.226 \pm 4.063i$	0.647	5.57%	137.30

Local mode is also strongly present in the oscillation for each area and the values are displayed in Table 21. Generators 1 and 2 in Area 1 oscillate against each other with generator 2 leading, and the frequency for local mode is in the range of 1.17 to 1.18 Hz. The damping for this local mode is better than the damping ratio for the interarea mode. The local mode for the second area is around 1.07 to 1.25 Hz, and the damping is very good above 10% for both generators. Generators 3 and 4 in Area 2 are also oscillating against each other with generator 3 leading, as seen from the phase of the oscillation.

Table 21: Local modes for system A without any delays.

	Mode	**Freq (Hz)**	**Damping ratio** $\zeta(\%)$	**Phase** (°)
G1	$-0.432 \pm 7.397i$	1.177	5.83%	112.42
G2	$-0.456 \pm 7.364i$	1.172	6.18%	-84.25
G3	$-0.977 \pm 6.758i$	1.076	14.30%	-107.28
G4	$-0.846 \pm 7.910i$	1.259	10.63%	86.54

The ITSE values are shown in Table 22, and while they offer little insight it can be seen that the values in Area 2 are greater than the values for Area 1. Additionally, the frequency spectrum of generator speed oscillations shows that in the case of no delays the dominant modes are the ones observed with the initial power system eigenvalues analysis. The main oscillation mode frequencies are around 0.65 Hz and 1.10 to 1.20 Hz, and there are no other frequencies with significant magnitude at this point. The frequency spectrum is presented in Figure 23.

Table 22: The ITSE values for system A without any delays.

The generator, area and system ITSE values				
G1	0.0023	Area 1	0.0038	System 0.0098
G2	0.0015			
G3	0.0027	Area 2	0.0060	
G4	0.0033			

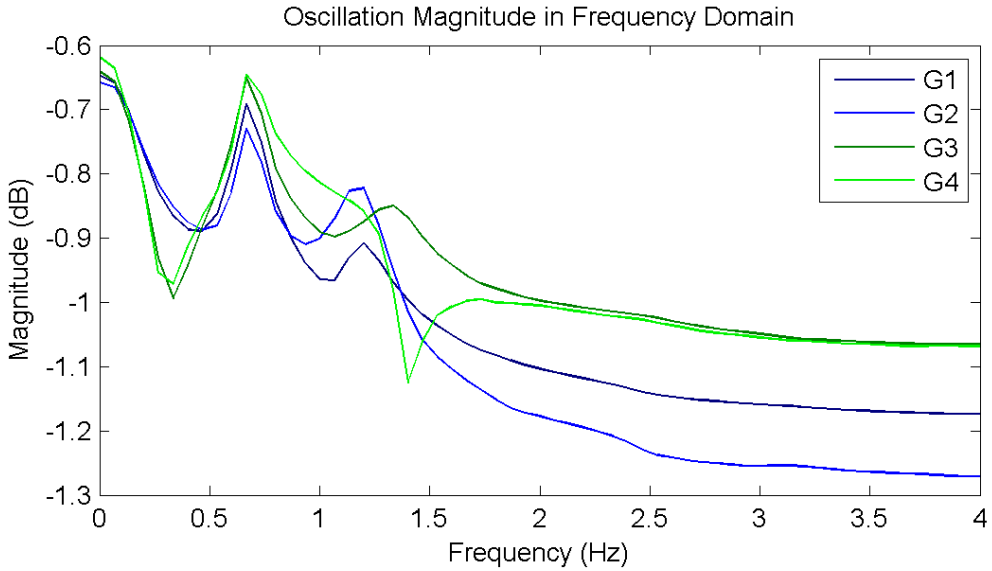

Figure 23: The frequency spectrum for power system A with no delays.

The speed, prediction and control signals for generator 3, are shown in Figure 24. It can be noticed how closely the controller predictions correspond to the real generator speeds. The greatest difference is at the start when the transient appears in the linear system. Otherwise the prediction is close to the actual generator speed values. The control signal lags behind the generator oscillations at about 45 degrees.

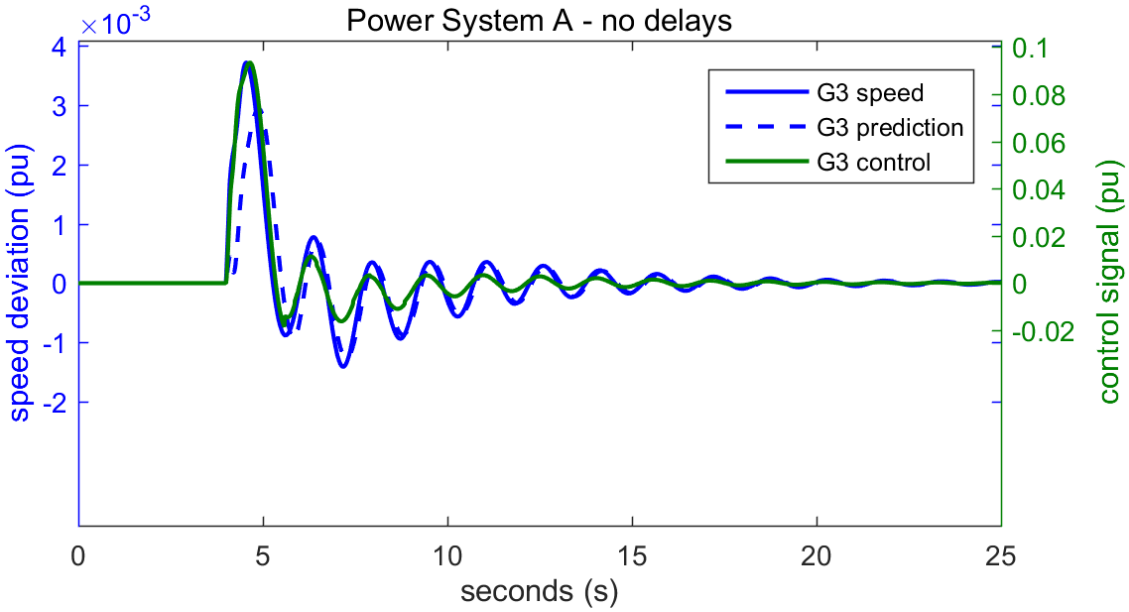

Figure 24: Power system A generator 3 speed deviation, controller speed prediction and the control signal with no delays.

The results for the case with no delays will be the base for comparing the results with delays. In summary, in the case with no delays the interarea mode is the most

dominant and the local mode is quite strong in Area 1 but not in Area 2.

5.1.2 Fiber-Optic Case A

The second case examined closely for power system A has a mean end-to-end delay of about 100 ms, and it emulates the real life delay of a dedicated fiber-optic wide-area network. The generator speed deviation is presented in Figure 25 and it shows that the oscillations decay faster than in the case with no delay. The first few peaks following the transient in all generators are significantly lower than the ones compared to the case with no delay, see Figure 22. Furthermore, the presence of some other oscillation mode in generator 2 is clearly visible, as can be seen from the double peaks around t = 7.0 seconds.

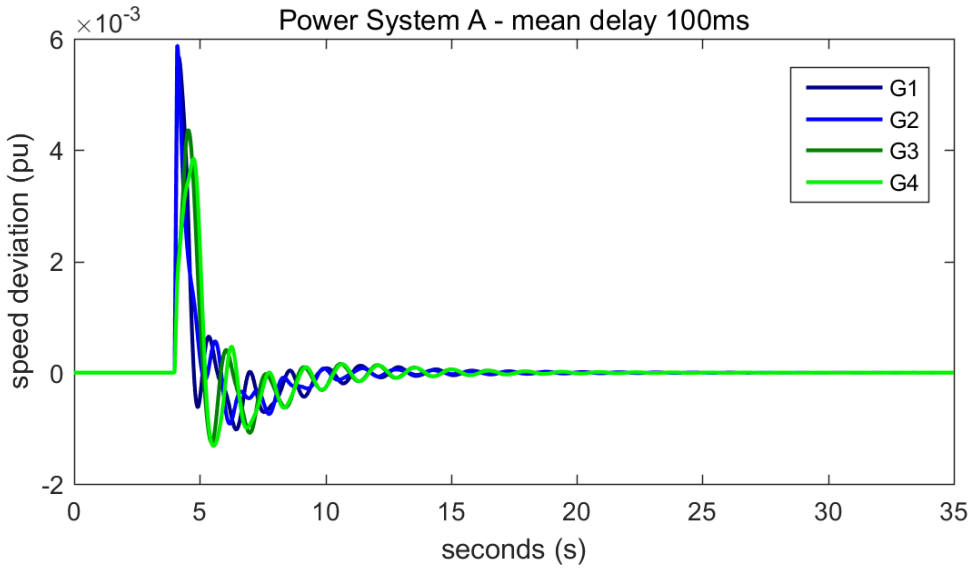

Figure 25: Generator speed deviation with a mean delay of 100 ms in the system.

The interarea mode in this case is around 0.68 Hz which an increase to the previous case. The damping for the interarea mode is also better than previously. The phase difference between the two areas is still around 180 degrees with Area 1 in the lead. The results for the interarea mode are shown in Table 23.

Table 23: Interarea mode for system A with a mean delay of 100 ms.

	Mode	**Freq (Hz)**	**Damping ratio** $\zeta(\%)$	**Phase (°)**
G1	$-0.255 \pm 4.274i$	0.680	5.96%	-15.99
G2	$-0.241 \pm 4.284i$	0.682	5.62%	-6.37
G3	$-0.275 \pm 4.287i$	0.682	6.40%	176.81
G4	$-0.268 \pm 4.283i$	0.682	6.24%	176.54

The results for the local modes are shown in Table 24. When compared to the previous case, it can be seen that there are changes in damping and frequencies.

The damping for both modes remains about the same for each generator with slight changes, but the phase leads are reversed for Area 2. However, it should also be noted that the frequency of the local mode for Area 2 had a significant jump to 1.32 Hz.

Table 24: Local modes for system A with a mean delay of 100 ms.

	Mode	**Freq (Hz)**	**Damping ratio** $\zeta(\%)$	**Phase (°)**
G1	$-0.523 \pm 7.409i$	1.179	7.04%	94.01
G2	$-0.445 \pm 7.480i$	1.190	5.94%	-92.02
G3	$-0.900 \pm 8.293i$	1.320	10.78%	137.31
G4	$-0.796 \pm 8.298i$	1.321	9.54%	-30.70

The ITSE values show are similar as previously, and confirm the better performance in comparison to the case without any delay. This was also observed from the speed deviation plots. The ITSE values for this case are shown in Table 25.

Table 25: The ITSE values for System A with a mean delay of 100 ms.

The generator, area and system ITSE values					
G1	0.0013	Area 1	0.0023	System	0.0062
G2	0.0010				
G3	0.0018	Area 2	0.0039		
G4	0.0021				

The frequency spectrum in Figure 26 shows that no significant additional new modes are present. The seemingly new oscillation observed in generator 2 is quite certainly just the local mode oscillation.

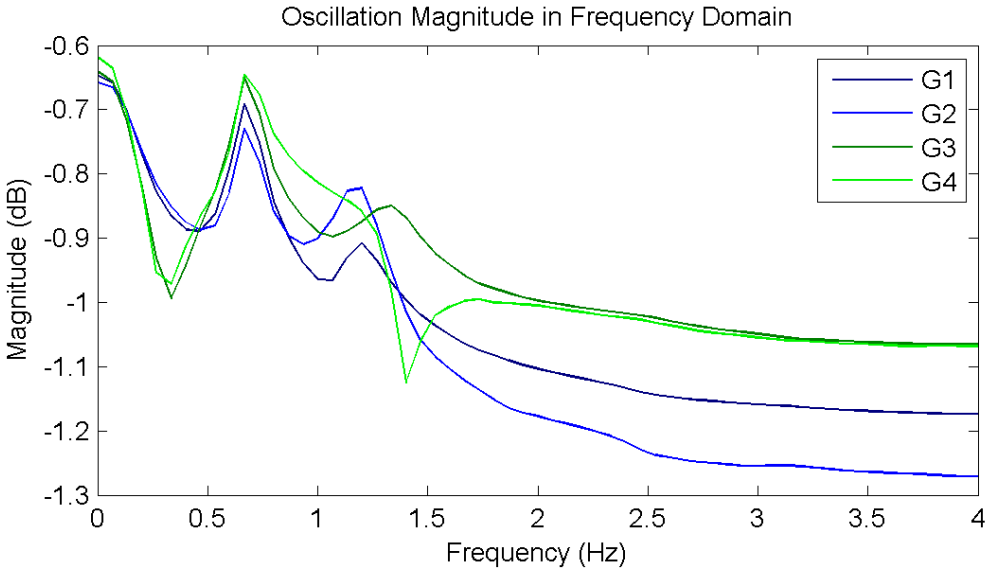

Figure 26: The frequency spectrum for power system A with a mean delay 100 ms.

The speed, prediction and control signals for generator 3, are shown in Figure 27. It shows how closely the controller predictions correspond to the real generator speeds. The greatest difference is at the start of the transient. In comparison to the case with no delay, a stronger control is applied after the transient which causes the first negative peak to become smaller than with no delay. Despite a small phase shift between prediction and real state the controller is able to damp the oscillations in a short time.

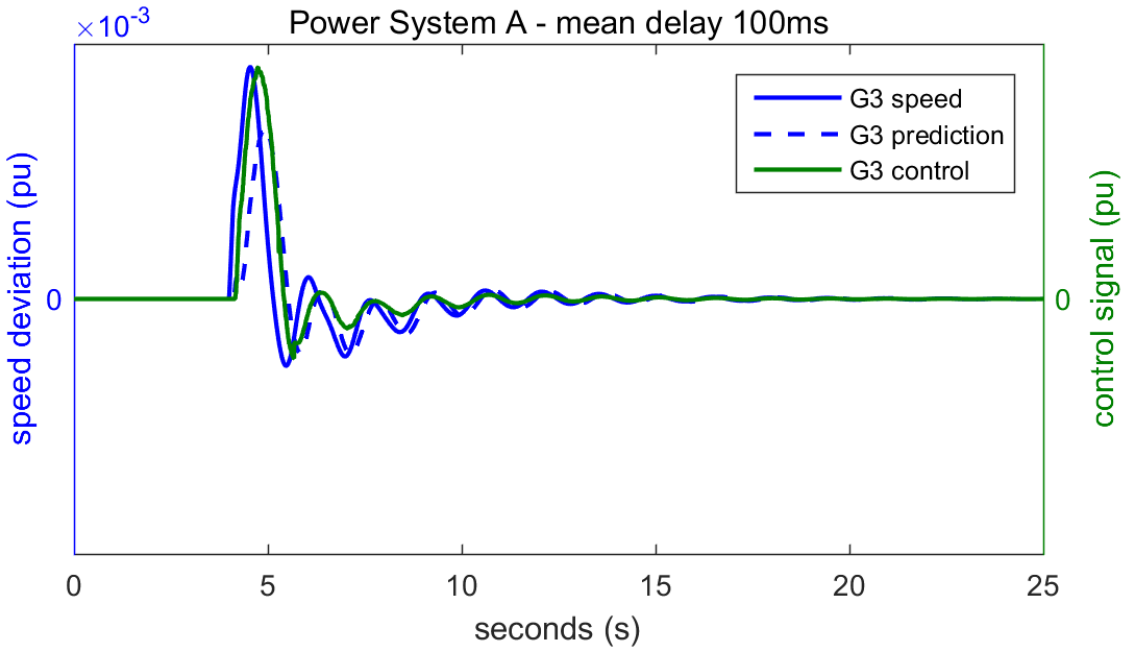

Figure 27: Power system A generator 3 speed deviation, controller speed prediction and the control signal with a mean delay of 100 ms.

5.1.3 Border Case A

The simulation case with a mean end-to-end delay of 220 ms is the first simulation case where the wide-area damping controller performs worse than in the case with no delay based on the ITSE value. The damping is worse and the peaks following the transient are larger than previously. The presence of some other mode is clearly visible in generator 4 while no longer so clearly in generator 2 as previously. This is shown in Figure 28.

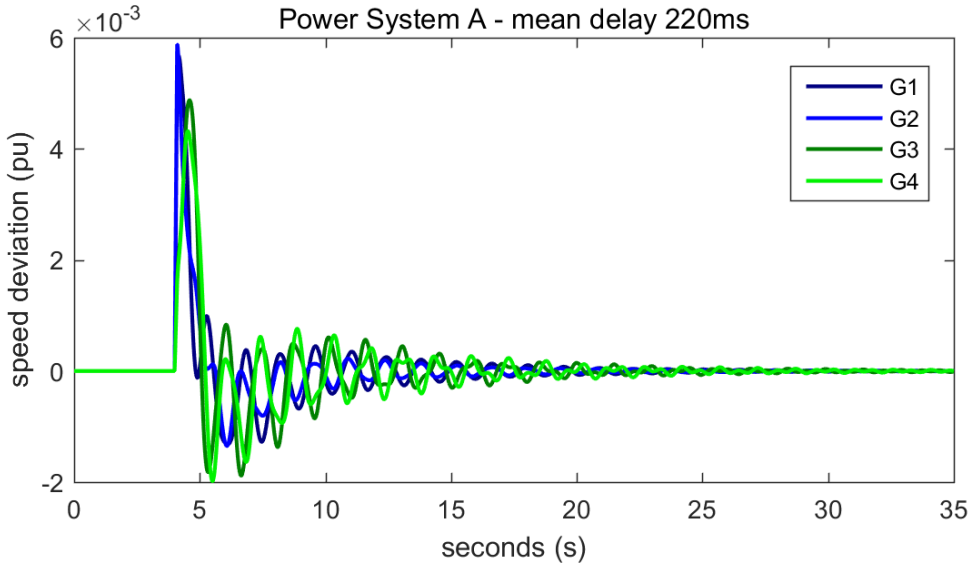

Figure 28: Generator speed deviation with a mean delay of 220 ms.

The trend of rising frequency for the interarea mode continues, and interarea mode oscillates at 0.71 Hz for the mean end-to-end delay of 220 ms. The damping is above 4% for every generator and it does not satisfy the requirements for sufficient damping. The phases of the oscillation remain in synchronization against each other, but Area 2 is now in the lead.

Table 26: Interarea mode for system A with a mean delay of 220 ms.

	Mode	**Freq (Hz)**	**Damping ratio $\zeta(\%)$**	**Phase (°)**
G1	$-0.197 \pm 4.480i$	0.713	4.39%	22.84
G2	$-0.192 \pm 4.484i$	0.714	4.28%	33.29
G3	$-0.198 \pm 4.471i$	0.712	4.42%	-128.76
G4	$-0.199 \pm 4.477i$	0.713	4.44%	-146.57

The local mode damping for Area 1 continues to be above performance requirements but the damping for the local mode of Area 2 is already very poor. The effects of local mode oscillation in Area 2 can be best observed from the speed deviation of generator 4. The presence of more than one oscillation mode is clearly visible, as shown in Figure 28. The local mode frequencies for both areas continue to vary

slightly but stay mostly the same, likely a result of the Prony analysis rather than a sign of any real change due to delays.

Table 27: Local modes for system A with a mean delay of 220 ms.

	Mode	**Freq (Hz)**	**Damping ratio $\zeta(\%)$**	**Phase (°)**
G1	$-0.566 \pm 7.331i$	1.167	7.69%	109.03
G2	$-0.457 \pm 7.437i$	1.184	6.13%	-89.06
G3	$-0.114 \pm 8.238i$	1.311	1.38%	11.85
G4	$-0.086 \pm 8.213i$	1.307	1.05%	-145.98

The ITSE values are now larger than they were previously. The system ITSE value with the mean delay of 220 ms is now 0.0122, as shown in Table 28. The frequency spectrum, shown in Figure 29, shows the dominance of the interarea mode. In addition, it shows also the poor damping performance for Area 2. This was also observed from the results of Prony analysis. Furthermore, the high frequencies for generator 1 start to show some new and interesting behavior not previously present.

Table 28: The ITSE values for System A with a mean delay of 220 ms.

The generator, area and system ITSE values					
G1	0.0024	Area 1	0.0039	System	0.0122
G2	0.0015				
G3	0.0043	Area 2	0.0083		
G4	0.0040				

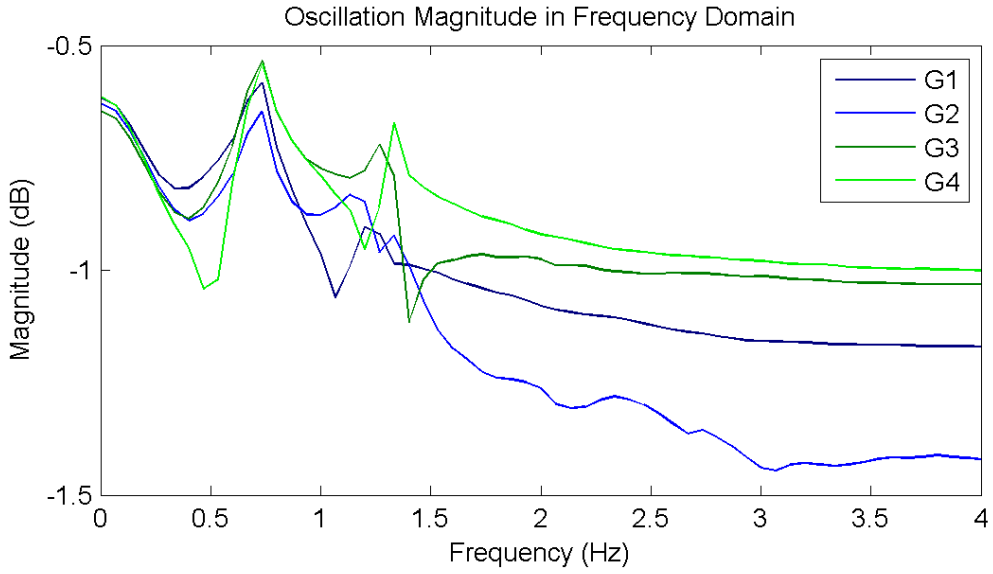

Figure 29: The frequency spectrum for Power System A with a mean delay 220 ms.

For the speed and control signals for generator 4, see Figure 30. The control signal and speed deviation has a phase difference of about 45 degrees with control signal leading for the interarea mode. The phase difference is is closer to 90 degrees for the local mode and the presence of the local mode is clearly visible towards the end of the simulation.

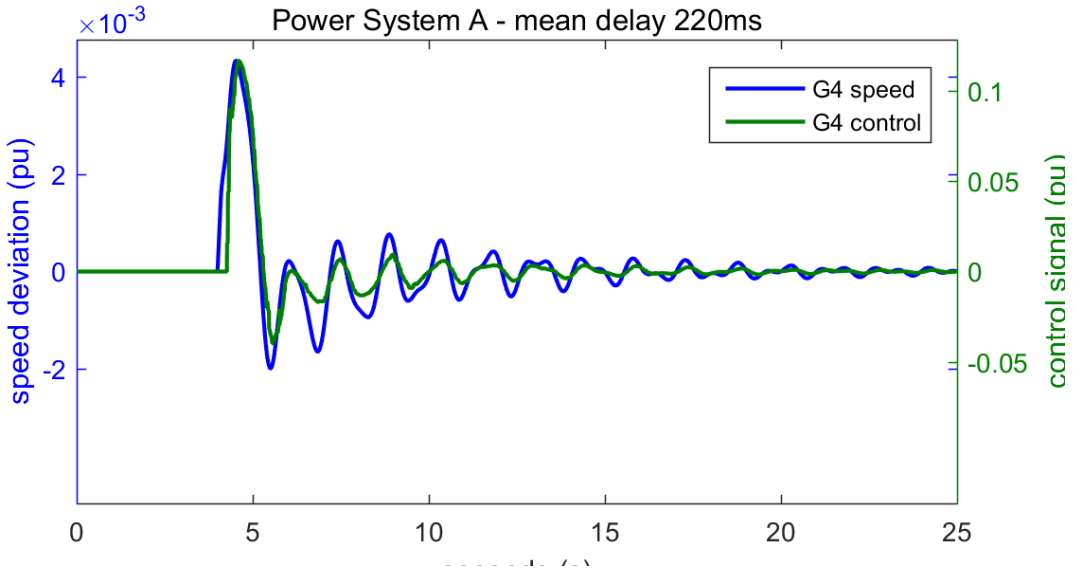

Figure 30: Power System A generator 4 speed deviation and the control signal with a mean delay of 220 ms.

5.1.4 Unstable Case A

The simulation case with a mean end-to-end delay with 280 ms is the first simulation case to become unstable for power system A. The local mode in Area 2 becomes unstable first, as can be seen from Figure 31. The interarea mode is damped successfully but with poor damping values less than 3%. The generators in Area 1 start to oscillate in an uncontrollable way towards the end of the simulation.

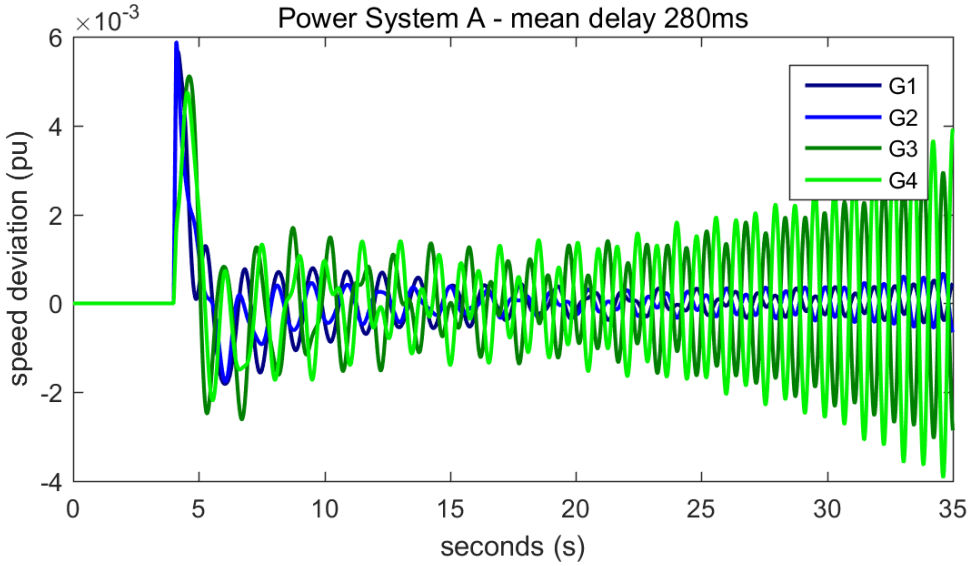

Figure 31: Generator speed deviation with a mean delay of 280 ms.

The trend of rising frequency for the interarea mode continues, and interarea mode oscillates at 0.724 Hz for the mean end-to-end delay of 280 ms. The damping is slightly above 2% for every generator, and it does not satisfy the requirements for sufficient interarea damping. The phases of the oscillation remain in synchronization against each other with Area 2 leading.

Table 29: Interarea mode for system A with a mean delay of 280 ms.

	Mode	**Freq (Hz)**	**Damping ratio** $\zeta(\%)$	**Phase** (°)
G1	$-0.108 \pm 4.551i$	0.724	2.37%	24.53
G2	$-0.107 \pm 4.550i$	0.724	2.36%	39.99
G3	$-0.111 \pm 4.548i$	0.724	2.44%	-128.86
G4	$-0.112 \pm 4.551i$	0.724	2.47%	-149.16

The local mode damping for Area 1 continues to be above performance requirements but the damping for the local mode of Area 2 is now negative confirming the observation of local mode being unstable. Additionally, a new previously unseen local mode appears in Area 1, see Table 31. The new mode has the same frequency as the unstable local oscillation mode for Area 2. The new mode is either unstable control mode, or the local mode of Area 2 is starting to affect Area 1.

Table 30: Local modes for system A with a mean delay of 280 ms.

	Mode	**Freq (Hz)**	**Damping ratio** $\zeta(\%)$	**Phase** (°)
G1	$-0.556 \pm 7.429i$	1.182	7.47%	91.60
G2	$-0.593 \pm 7.368i$	1.173	8.02%	-74.04
G3	$0.067 \pm 8.013i$	1.275	-0.84%	-43.42
G4	$0.068 \pm 8.013i$	1.275	-0.84%	140.77

Table 31: Additional unstable mode in Area 1 for system A with a mean delay of 280 ms.

	Mode	**Freq (Hz)**	**Damping ratio** $\zeta(\%)$	**Phase** (°)
G1	$0.053 \pm 8.018i$	1.276	-0.66%	124.78
G2	0.0738 ± 8.010	1.275	-0.92%	-41.33

The ITSE values are now much larger than they were previously. The system ITSE value with the mean delay of 280 ms is now 0.3610, as shown in Table 32. The ITSE values grow rapidly as the system becomes unstable. The frequency spectrum, shown in Figure 32, shows the dominance of the interarea mode for both areas, but also the poor damping performance for Area 2. In addition, the high frequencies for the generators have some small magnitude spikes indicating a presence of new oscillation modes.

Table 32: The ITSE values for System A with a mean delay of 280 ms.

<table>
<tr><td colspan="5">The generator, area and system ITSE values</td></tr>
<tr><td>G1</td><td>0.0085</td><td rowspan="2">Area 1</td><td>0.0153</td><td rowspan="4">System 0.3610</td></tr>
<tr><td>G2</td><td>0.0068</td><td></td></tr>
<tr><td>G3</td><td>0.1412</td><td rowspan="2">Area 2</td><td>0.3456</td></tr>
<tr><td>G4</td><td>0.2044</td><td></td></tr>
</table>

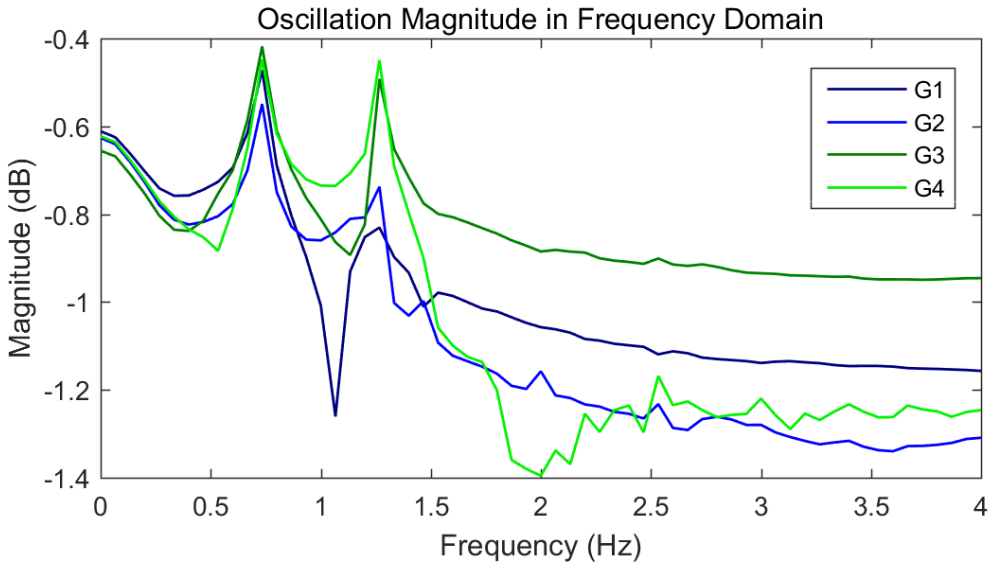

Figure 32: The frequency spectrum for power system A with a mean delay 280 ms.

In the first unstable case, the generator 4 speed deviation and the control signal have a phase difference of about 45 degrees before the system becomes unstable. The presence of multiple interfering modes is clearly visible.

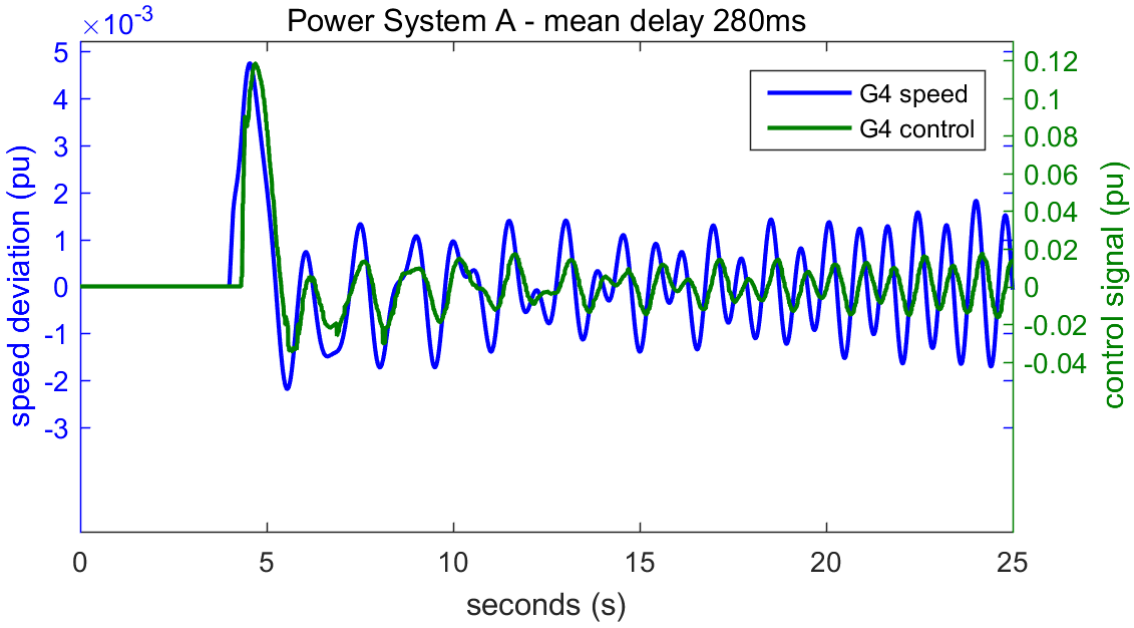

Figure 33: Power system A generator 4 speed deviation and the control signal with a mean delay of 280 ms.

5.2 System B

This section presents the results obtained from the simulations for the power system B. The general structure of this section is similar as was for power system A. The power system B was able to stand a maximum end-to-end delay of slightly less than 700 ms, and the first mode to become unstable was the local mode for Area 2, as shown in Table 33. The dynamics of the power system B are very different from power system A, as shown by its ability to tolerate delays over twice the length.

Table 33: Power system B tolerance for delays.

Maximum delay tolerance	**Unstable mode**
Under 700 ms	Interarea mode and Area 2 local mode

The ITSE values for power system B with a given end-to-end mean delay are presented in Table 34. It shows that the overall damping performance is better under delays of about 190 ms compared to the case with no delay. After that point it experiences a significant increase but the system is able tolerate delays until 700 ms.

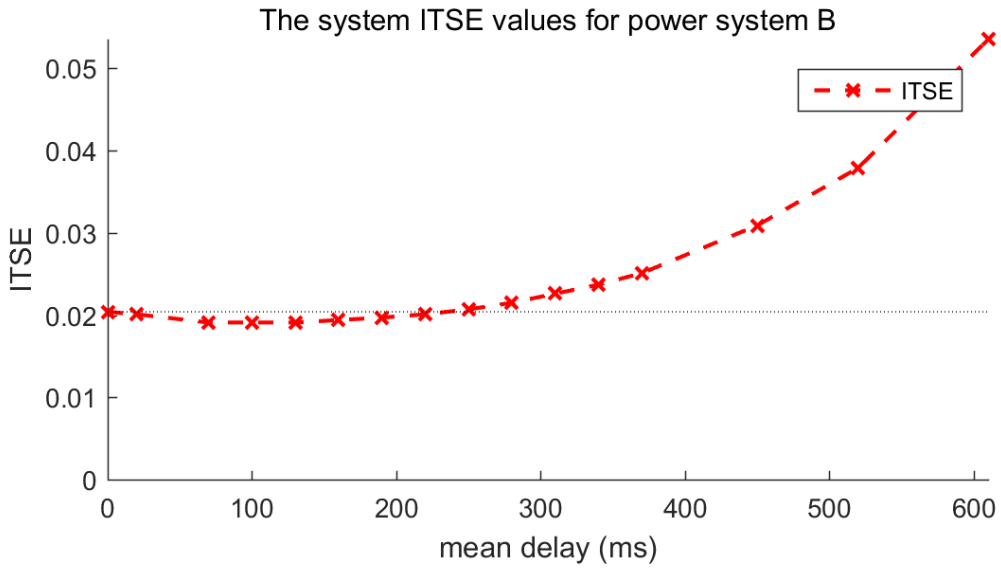

Figure 34: The system ITSE values for power system B.

The real and absolute imaginary values of the generator interarea modes with different delays are shown in Figure 35, the delays increase clockwise along the spiral. The simulations show that the oscillation frequency of the interarea mode increases as more delay is introduced into the system. The damping improves initially but gets worse after a certain delay margin is exceeded. The margin is the cluster of points near $-0.6 + 2.7i$, where the mean end-to-end delay is 250 ms, as also seen in Figure 34. It is the first delay case performing worse than the case without any delay.

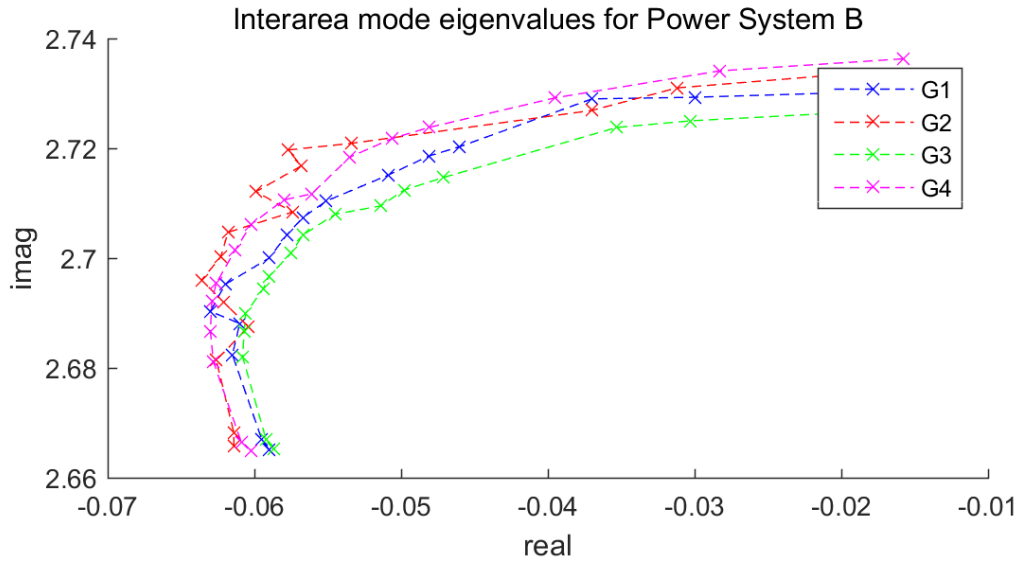

Figure 35: The real and absolute imaginary values of generator interarea oscillation modes with different delays. The delay increases clockwise along the spiral curve.

In the next subsections several simulation cases are shown in more detail. The first one is the reference case with no delay, the second is the so-called fiber-optics case, the third is the first case performing worse than the case with no delay and the last case is the first unstable one.

5.2.1 No Delay Case B

The generator speed deviations of power system B in the case of no delays are shown in Figure 36, the values are displayed as per-unit (pu) values. As can be seen from the speed deviation figure, after the transient is introduced to the system at t = 4.0 seconds, the damping is not very good. Generator pairs in both areas oscillate in synchronization, and the areas oscillate against each other at the interarea mode with a phase difference of about 180 degrees.

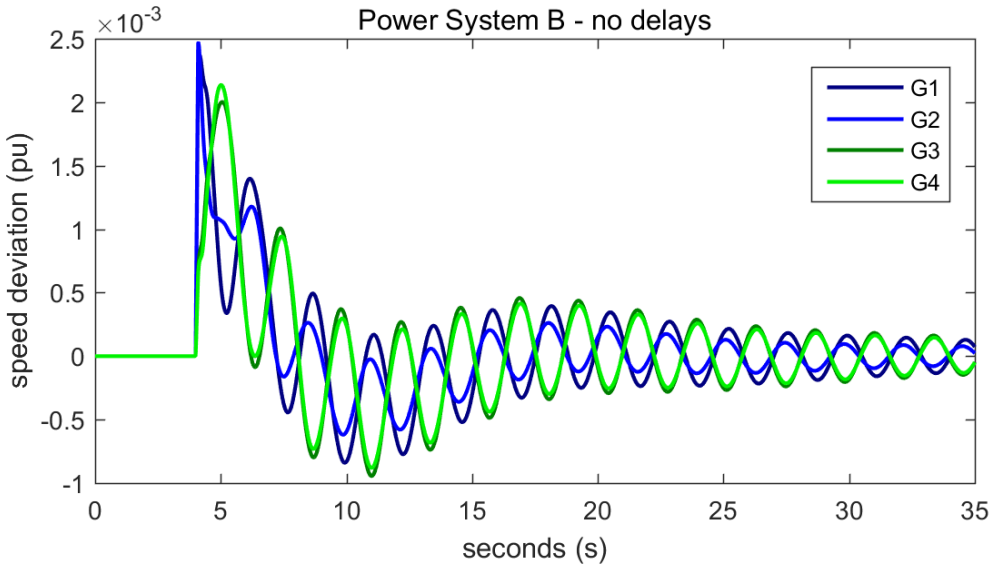

Figure 36: Generator speed deviation with no delays.

The dominant modes obtained using the Prony analysis are shown in Table 34, and the values confirm the results of the generation speed deviation. The interarea mode has a frequency of about 0.42 Hz which is slightly lower than the initial numeric eigenvalue analysis. The damping for the interarea mode with no delays is above 2.2% which is quite poor value for damping. The phases are about the same for each area and the phase difference between the areas is about 180 degrees with Area 1 leading the oscillations.

Table 34: Interarea mode for system B with no delays.

	Mode	**Freq (Hz)**	**Damping ratio** $\zeta(\%)$	**Phase** (°)
G1	$-0.059 \pm 2.665i$	0.424	2.21%	-134.01
G2	$-0.061 \pm 2.666i$	0.424	2.31%	-116.00
G3	$-0.059 \pm 2.665i$	0.424	2.20%	60.64
G4	$-0.060 \pm 2.665i$	0.424	2.26%	57.14

Local modes can not be observed from the speed deviation graph since the interarea mode is so dominant. Generators 1 and 2 in Area 1 oscillate against each other with generator 1 leading, and the frequency for local mode is in the range of 0.72 Hz which is low value for local mode. The damping for this local mode is excellent and better than the damping ratio for the interarea mode. The local mode for the Area 2 is around 0.82 Hz, a low value, and the damping is barely adequate for generator 3 at 3% and better for generator 4 at almost 5%. The generators 3 and 4 in Area 2 also oscillate against each other with generator 3 leading, as can be seen from the phase of the oscillation.

Table 35: Local modes for system B with no delays.

	Mode	Freq (Hz)	Damping ratio $\zeta(\%)$	Phase (°)
G1	$-0.784 \pm 4.506i$	0.717	17.13%	-89.13
G2	$-0.702 \pm 4.510i$	0.718	15.38%	85.25
G3	$-0.250 \pm 5.170i$	0.823	4.83%	-101.33
G4	$-0.163 \pm 5.277i$	0.840	3.09%	36.82

The ITSE values can be seen from Table 36, and the values in Area 2 are greater than the values for Area 1. Additionally, the frequency spectrum of generator speed oscillations shows that in the case with no delays the dominant modes are the ones observed with the initial power system eigenvalues analysis. The frequency spectrum is presented in Figure 37.

Table 36: The ITSE values for System B with no delays.

The generator, area and system ITSE values				
G1	0.0051	Area 1	0.0079	System 0.0204
G2	0.0028			
G3	0.0067	Area 2	0.0124	
G4	0.0057			

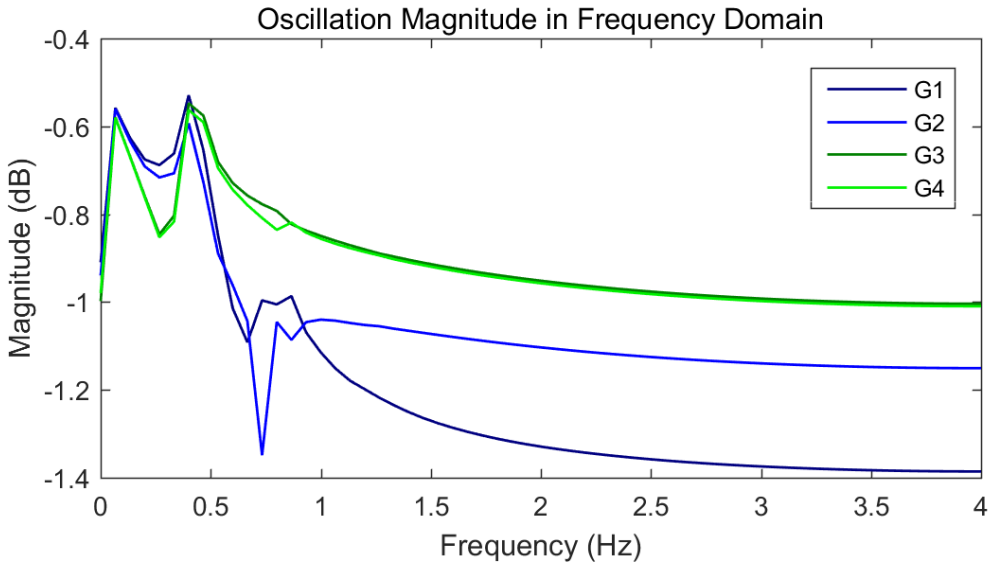

Figure 37: The frequency spectrum for power system B with no delays.

In the case with no delays, the generator 3 speed deviation and the control signal have a phase difference of about 45 degrees, control trailing behind, and the controller predictions, excluding the initial transient behavior, is very close to the real generator speed.

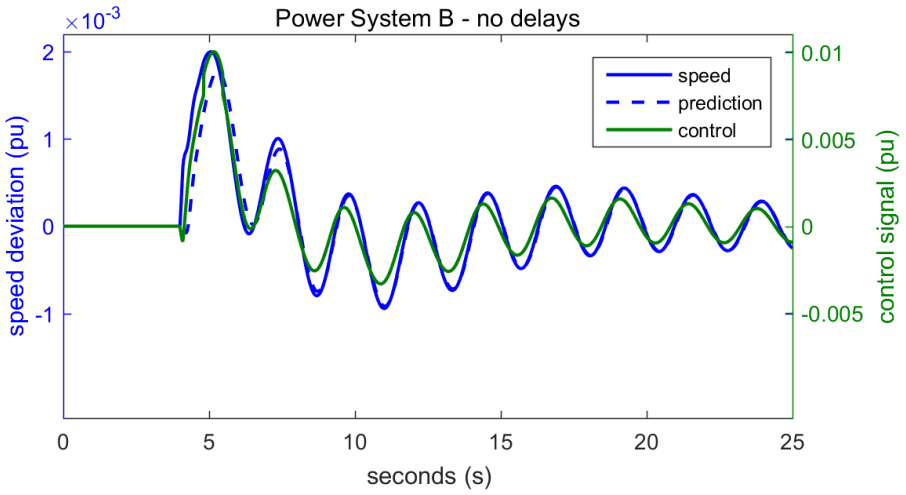

Figure 38: Power system B generator 3 speed deviation, controller speed prediction and the control signal with no delays.

5.2.2 Fiber-Optic Case B

The second case examined closely for power system B has a mean end-to-end delay of about 100 ms, and it emulates the real life delay of fiber-optic wide-area network similarly as was with the power system A. The generator speed deviation is presented in Figure 39 and it shows that the oscillations decay faster than in the case with no delay.

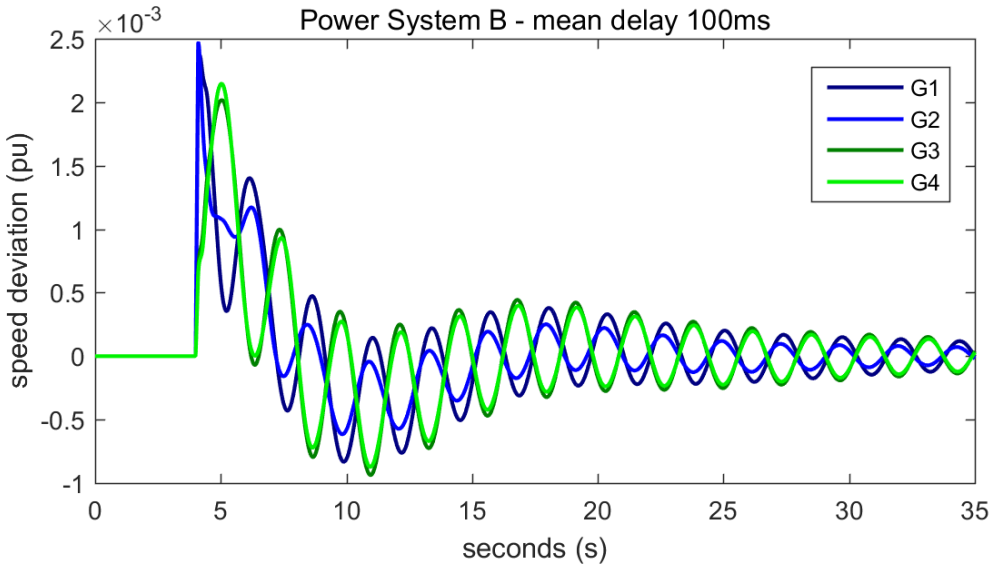

Figure 39: Generator speed deviation with a mean delay of 100 ms.

The interarea mode in this case is around 0.428 Hz which is an increase compared to the previous case with no delays. The damping for the interarea mode is also better than previously but not by a large margin. The phase difference between the

two areas is still around 180 degrees with Area 1 in the lead. The results for the interarea mode are shown in Table 37.

Table 37: Interarea mode for system B with a mean delay of 100 ms.

	Mode	**Freq (Hz)**	**Damping ratio** $\zeta(\%)$	**Phase** (°)
G1	$-0.061 \pm 2.688i$	0.428	2.27%	-134.32
G2	$-0.0604 \pm 2.688i$	0.428	2.25%	-116.30
G3	$-0.061 \pm 2.687i$	0.428	2.26%	60.78
G4	$-0.063 \pm 2.687i$	0.428	2.34%	57.36

Thee local mode damping is excellent for Area 1 and inadequate for Area 2. The local mode oscillation modes are shown in Table 38.

Table 38: Local modes for system B with a mean delay of 100 ms.

	Mode	**Freq (Hz)**	**Damping ratio** $\zeta(\%)$	**Phase** (°)
G1	$-0.947 \pm 4.722i$	0.752	19.65%	-99.33
G2	$-0.702 \pm 4.401i$	0.700	15.74%	95.11
G3	$-0.226 \pm 5.191i$	0.826	4.35%	-93.16
G4	$-0.112 \pm 5.272i$	0.839	2.13%	61.94

The ITSE values for power system B are lower with this case than with no delays, and Area 2 continues to contribute more to the total ITSE than Area 1. In other words, the damping in Area 2 is worse, as the damping ratios also showed earlier. The ITSE values are displayed in Table 39. The frequency spectrum of oscillation modes confirms the observations and results presented in Figure40.

Table 39: The ITSE values for System B with a mean delay of 100 ms.

The generator, area and system ITSE values					
G1	0.0048	Area 1	0.0074	System	0.0191
G2	0.0026				
G3	0.0063	Area 2	0.0116		
G4	0.0054				

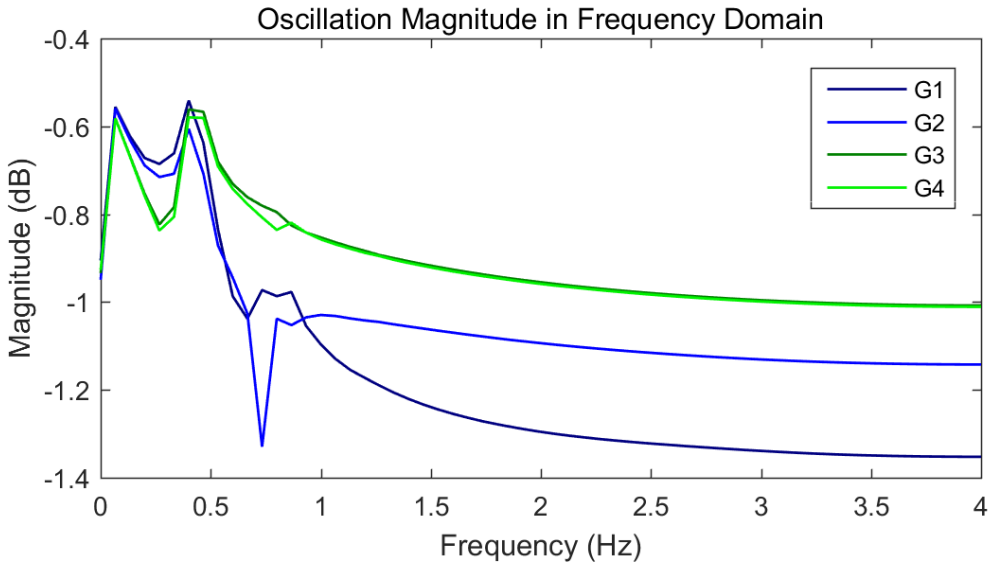

Figure 40: The frequency spectrum for power system B with a mean delay of 100 ms.

Figure 41 shows how strong control action during the transient helps to achieve a good overall damping as the prediction lines up with the real generator speeds after the first oscillation peak.

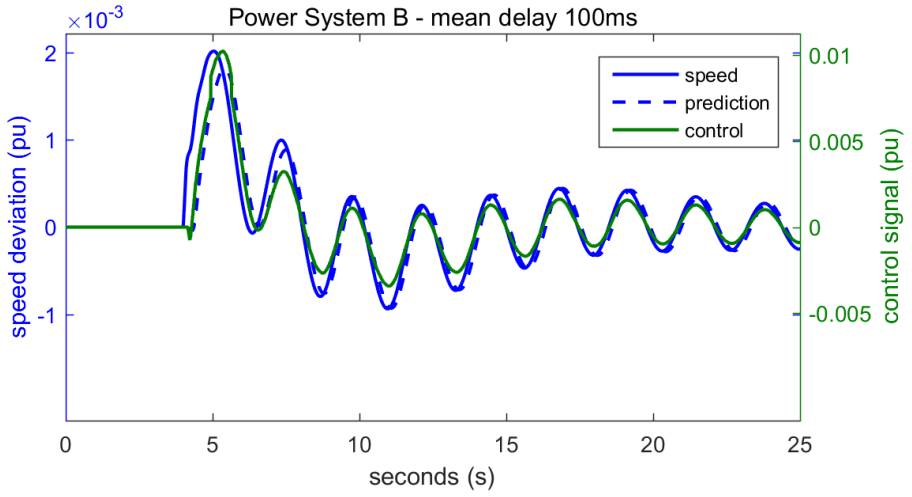

Figure 41: Power system B generator 3 speed deviation, controller speed prediction and the control signal with a mean delay of 100 ms.

5.2.3 Border Case B

The simulation case with a mean end-to-end delay of 310 ms is one of the first simulation cases for power system B where the wide-area damping controller performs worse based on ITSE value than in the case with no delays. The damping is worse than in the case with no delays and the peaks following the transient are larger than previously. Figure 42 shows the generator speed deviations for this case.

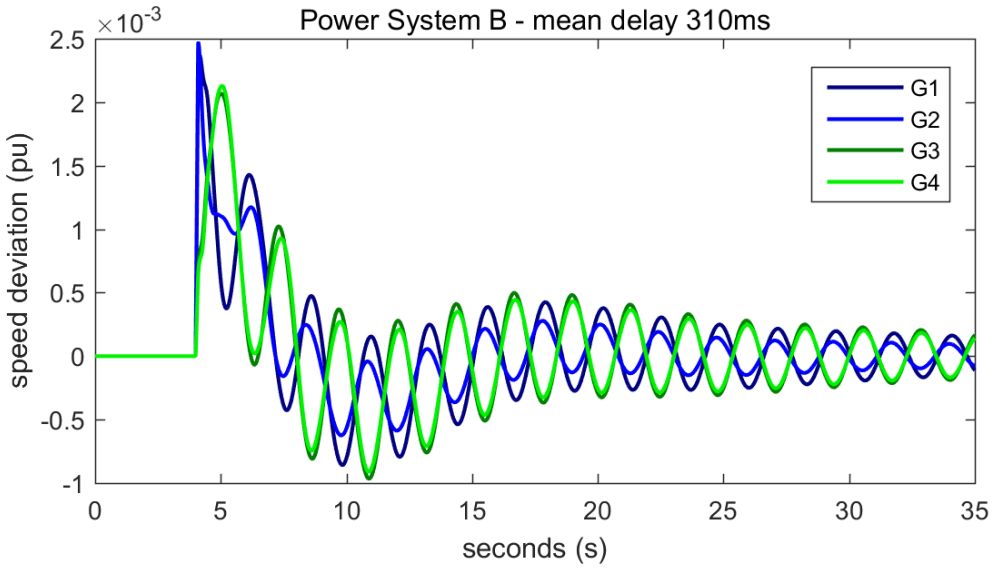

Figure 42: Generator speed deviation with a mean delay of 310 ms.

The frequency for the interarea mode continues to rise, and the interarea mode oscillates now at 0.432 Hz with a mean end-to-end delay of 310 ms. The damping is around 2% for every generator, and it does not satisfy the requirements for sufficient interarea damping. The phases of the oscillation remain in synchronization against each other with Area 1 leading the oscillations.

Table 40: Interarea mode for system B with a mean delay of 310 ms.

	Mode	**Freq (Hz)**	**Damping ratio** $\zeta(\%)$	**Phase** (°)
G1	$-0.051 \pm 2.715i$	0.432	1.87%	-132.56
G2	$-0.057 \pm 2.717i$	0.432	2.09%	-115.77
G3	$-0.051 \pm 2.710i$	0.431	1.90%	64.09
G4	$-0.054 \pm 2.718i$	0.433	1.97%	56.50

The local mode damping for Area 1 continues to be above performance requirements but damping for the local mode of Area 2 remains inadequate.

Table 41: Local modes for system B with a mean delay of 310 ms.

	Mode	**Freq (Hz)**	**Damping ratio** $\zeta(\%)$	**Phase** (°)
G1	$-0.795 \pm 4.614i$	0.734	16.98%	-103.55
G2	$-0.761 \pm 4.589i$	0.730	16.36%	81.80
G3	$-0.212 \pm 5.185i$	0.825	4.08%	-106.31
G4	$-0.129 \pm 5.274i$	0.839	2.44%	58.01

The ITSE values are now larger than they were with case with no delays for power system B, and Area 2 has greater oscillations as seen from the ITSE values,

or alternatively from the poor damping of Area 2 local mode. The ITSE values are displayed in Table 42 and the frequency spectrum in Figure 43.

Table 42: The ITSE values for System B with a mean delay of 310 ms.

The generator, area and system ITSE values					
G1	0.0057	Area 1	0.0086	System	0.0226
G2	0.0029				
G3	0.0076	Area 2	0.0140		
G4	0.0064				

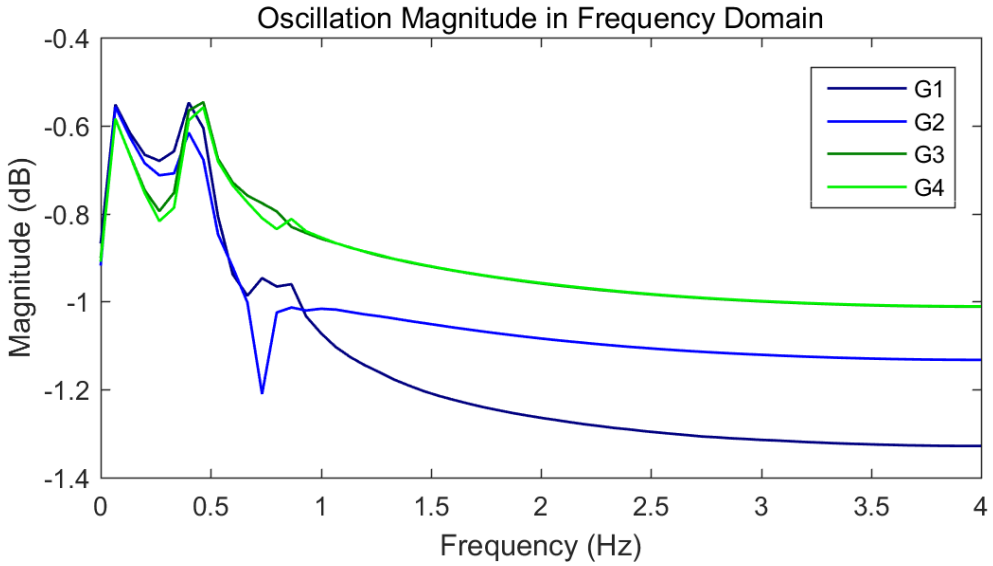

Figure 43: The frequency spectrum for power system B with a mean delay of 310 ms.

The generator 3 speed deviation and the control signal have a phase difference of about 45 degrees excluding the transient behavior where phase difference is almost 90 degrees. Additionally, the controller is never exactly right about the state of the generator but the damping control is still successful in damping the oscillations. Generator 3 speed, prediction and control signals are shown in Figure 44.

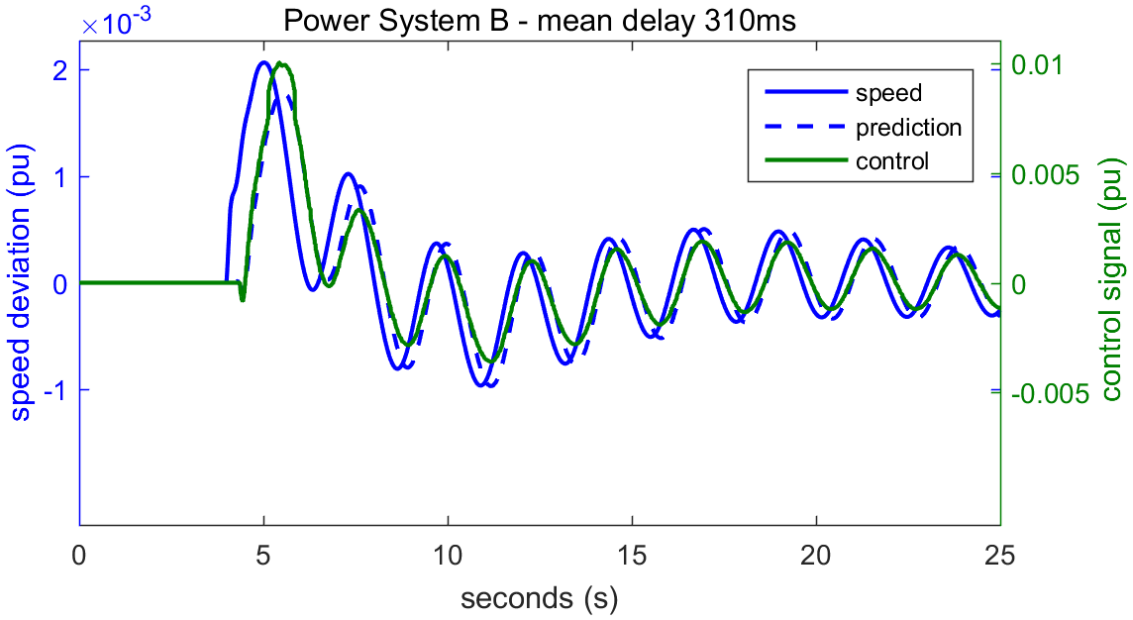

Figure 44: Power system B generator 3 speed deviation, controller speed prediction and the control signal with a mean delay of 310 ms.

5.2.4 Unstable Case B

The simulation case with a mean end-to-end delay of 700 ms is the first simulation case to become unstable for power system B. The local mode in Area 2 and interarea mode becomes unstable first. The areas oscillate against each other at 180 degrees and the local mode for Area 1 remains well damped. The speed deviation for the generators is shown in Figure 45.

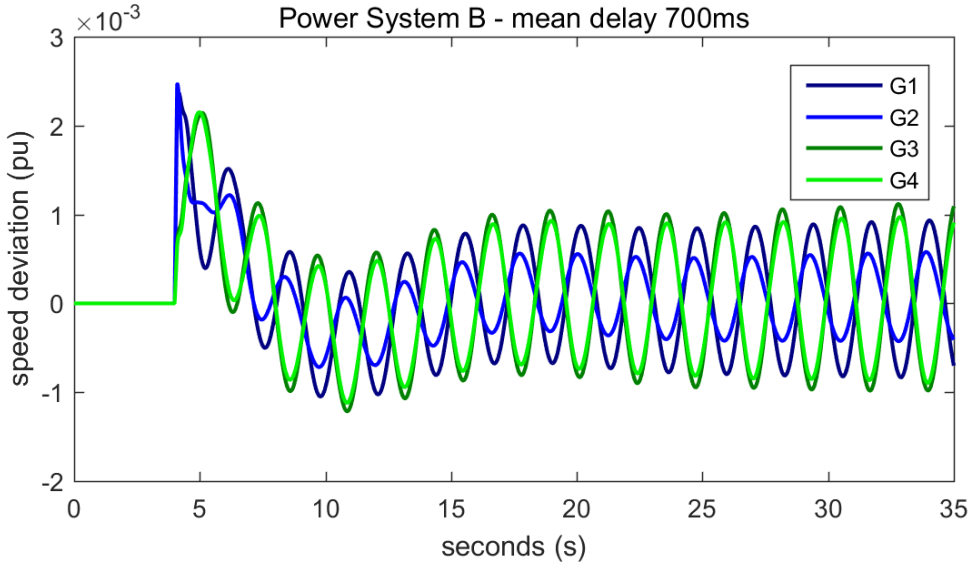

Figure 45: Generator speed deviation with a mean delay of 700ms.

The interarea mode oscillates at 0.433 Hz, an increase to the previous case. This continues the familiar trend observed earlier. Table 43 shows the properties of interarea oscillation mode.

Table 43: Interarea mode for system B with a mean delay of 700 ms.

	Mode	**Freq (Hz)**	**Damping ratio** $\zeta(\%)$	**Phase** (°)
G1	$0.009 \pm 2.721i$	0.433	-0.33%	128.51
G2	$0.010 \pm 2.72i$	0.433	-0.35%	110.02
G3	$0.009 \pm 2.721i$	0.433	-0.32%	-64.17
G4	$0.010 \pm 2.722i$	0.433	-0.38%	-60.69

The local mode damping for Area 1 continues to be above the performance requirements but damping for the local mode of Area 2 is now negative confirming the observation of local mode being unstable. Additionally, a new previously unseen local mode appears in Area 1, see Table 31. The new mode has the same frequency as the unstable local oscillation mode for Area 2. The new mode is either unstable control mode, or the local mode of Area 2 is starting to affect Area 1. These aforementioned oscillation modes are shown in Tables 44 and 45, respectively.

Table 44: Local modes for system B with a mean delay of 700 ms.

	Mode	**Freq (Hz)**	**Damping ratio** $\zeta(\%)$	**Phase** (°)
G1	$-0.542 \pm 4.516i$	0.719	11.91%	-100.50
G2	$-0.661 \pm 4.529i$	0.721	14.45%	78.63
G3	$0.003 \pm 5.415i$	0.862	-0.06%	-119.4882
G4	$0.033 \pm 5.410i$	0.861	-0.61%	33.4767

Table 45: Additional unstable mode in Area 1 for system B with a mean delay of 700 ms.

	Mode	**Freq (Hz)**	**Damping ratio** $\zeta(\%)$	**Phase** (°)
G1	$0.015 \pm 5.446i$	0.867	-0.28%	-121.03
G2	$0.013 \pm 5.438i$	0.865	-0.23%	-154.23

The ITSE values grow rapidly as the system becomes unstable, and are much larger than previously. The frequency spectrum, shown in Figure 46, shows the dominance of the interarea mode for both areas, but also the poor damping performance for Area 2.

Table 46: The ITSE values for System B with a mean delay of 700 ms.

The generator, area and system ITSE values					
G1	0.0364	Area 1	0.0495	System	0.1413
G2	0.0131				
G3	0.0517	Area 2	0.0917		
G4	0.0401				

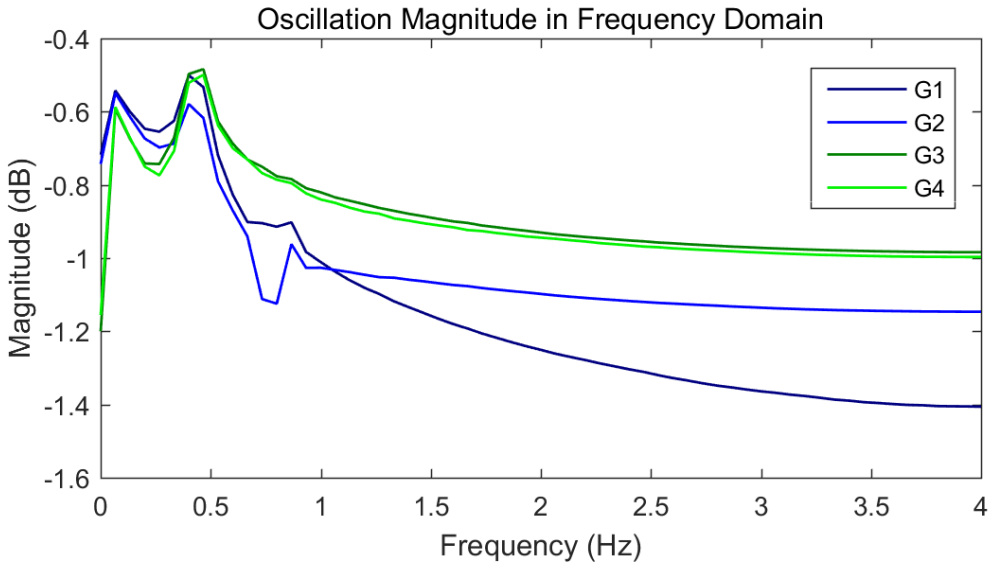

Figure 46: The frequency spectrum for power system B with a mean delay of 700 ms.

In the first unstable case, the generator 3 speed deviation and control signal have a phase difference of over 90 degrees when the system becomes unstable. Additionally, the controller is never right about the state of the generator, and the phase difference of the delay is too great for the damping control to overcome. Generator 3 speed, prediction and control signals are shown in Figure 47.

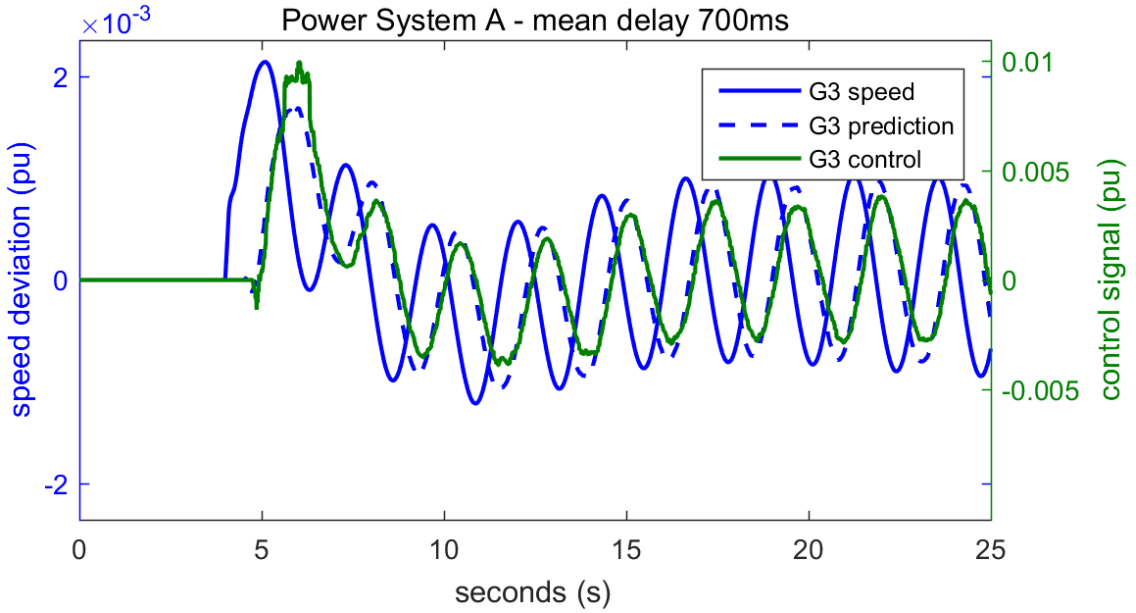

Figure 47: Power system B generator 3 speed deviation, controller speed prediction and the control signal with a mean delay of 700 ms.

5.3 System C

This section presents the results obtained from the simulations for power system C. The structure of this section is similar to the other power system sections. The power system C was able to stand a maximum end-to-end delay of less than 400 ms, and the first mode to become unstable was the interarea mode along with several other modes, as shown in Table 47. The dynamics of the power system C are very different from the power system B but resemble more closely those of the power system A.

Table 47: Power system C tolerance for delays.

Maximum delay tolerance	**Unstable mode**
Under 400 ms	Interarea mode and several others

The ITSE values for power system C with a given end-to-end mean delay are shown in Figure 48. It shows that the overall damping performance is better under delays of about 220 ms compared to the case with no delay. After this point the ITSE value experiences a significant increase and the system becomes unstable soon after.

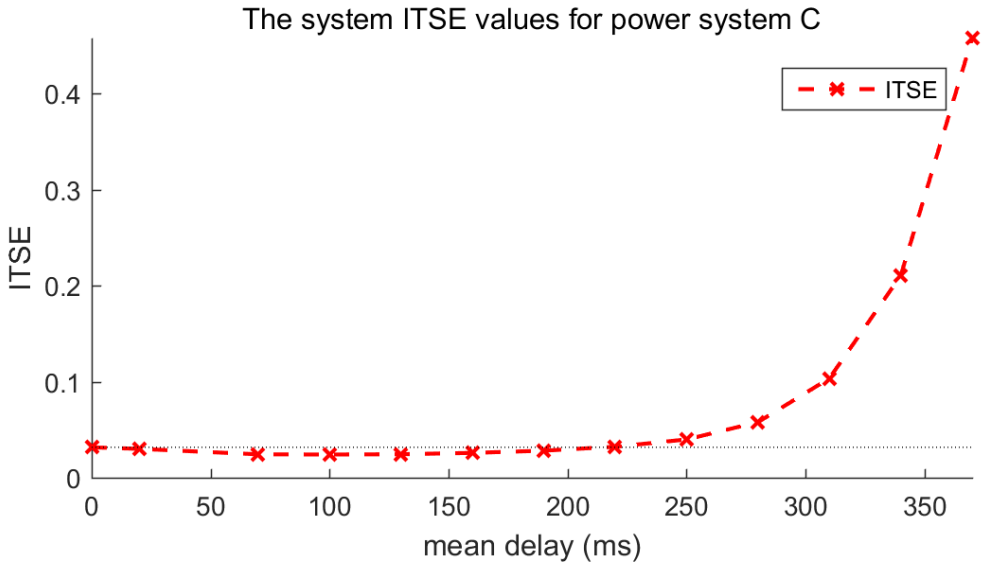

Figure 48: The system ITSE values for power system C.

The simulations show that the oscillation frequency of the interarea mode increases as more delay is introduced into the system. The damping improves initially but gets worse after a certain delay margin is exceeded. The real and absolute imaginary values of the generator interarea modes with different delays are shown in Figure 49, the delays increase clockwise along the spiral. The cluster of points near $-0.15 + 4.0i$ is the case with a mean end-to-end delay of 220 ms mentioned earlier. It is the first simulation case performing worse than the one with no delays.

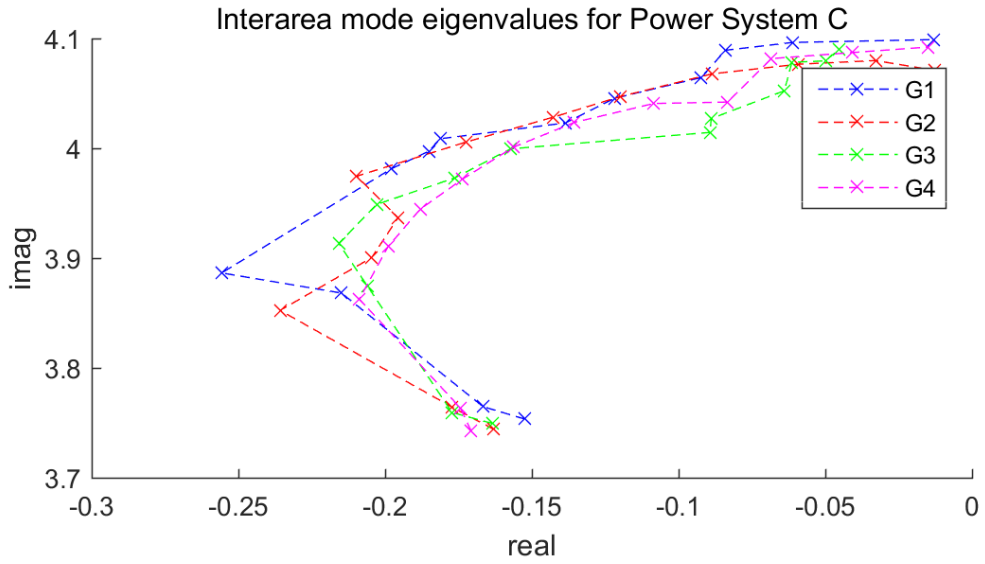

Figure 49: The real and absolute imaginary values of generator interarea oscillation modes with different delays. The delay increases clockwise along the spiral curve.

In the next subsections several simulation cases are shown in more detail. The

first one is the reference case with no delays, the second is the so-called fiber-optics case, the third is a border case performing worse than the case with no delays and the last one is the first unstable case.

5.3.1 No Delay Case C

The generator speed deviations of power system C in the case of no delays are shown in Figure 50, the values are displayed as per-unit (pu) values. Generator pairs in both areas oscillate in synchronization, and the areas oscillate against each other at the interarea mode with a phase difference of about 180 degrees.

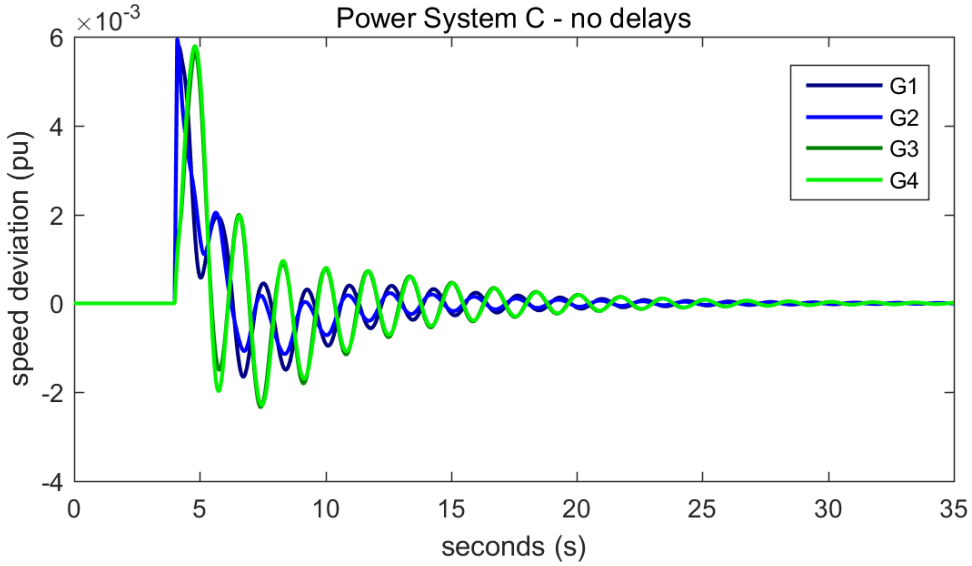

Figure 50: Generator speed deviation without any delays in the system.

The dominant modes obtained using the Prony analysis are shown in Table 48 and 49, and the values confirm the observed results of the generation speed deviation. The interarea mode has a frequency of about 0.597 Hz and the damping for the interarea mode with no delays is slightly above 4% which is not an adequate damping value. The phases are about the same for each area and the phase difference between the areas is about 180 degrees with Area 1 leading the oscillations.

Table 48: Interarea mode for system C with no delays.

	Mode	**Freq (Hz)**	**Damping ratio** $\zeta(\%)$	**Phase** (°)
G1	$-0.153 \pm 3.754i$	0.597	4.06%	-97.57
G2	$-0.163 \pm 3.744i$	0.596	4.35%	-79.08
G3	$-0.164 \pm 3.750i$	0.597	4.37%	110.64
G4	$-0.171 \pm 3.743i$	0.596	4.56%	109.27

Local modes can not be observed from the speed deviation graph since the interarea mode is so dominant and the damping for local modes is about the same

or better than damping of interarea mode.

Table 49: Local modes for system C with no delays.

	Mode	Freq (Hz)	Damping ratio $\zeta(\%)$	Phase (°)
G1	$-0.859 \pm 7.153i$	1.138	11.93%	55.40
G2	$-0.484 \pm 7.612i$	1.212	6.34%	-83.00
G3	$-0.339 \pm 7.340i$	1.168	4.61%	111.23
G4	$-0.163 \pm 7.230i$	1.151	2.28%	-69.12

The ITSE values can be seen from Table 50, and the values in Area 2 are greater than the values in Area 1. The frequency spectrum is presented in Figure 51 and it confirms the earlier oscillation mode observations.

Table 50: The ITSE values for System C with no delays.

The generator, area and system ITSE values					
G1	0.0053	Area 1	0.0088	System	0.0317
G2	0.0035				
G3	0.0113	Area 2	0.0229		
G4	0.0116				

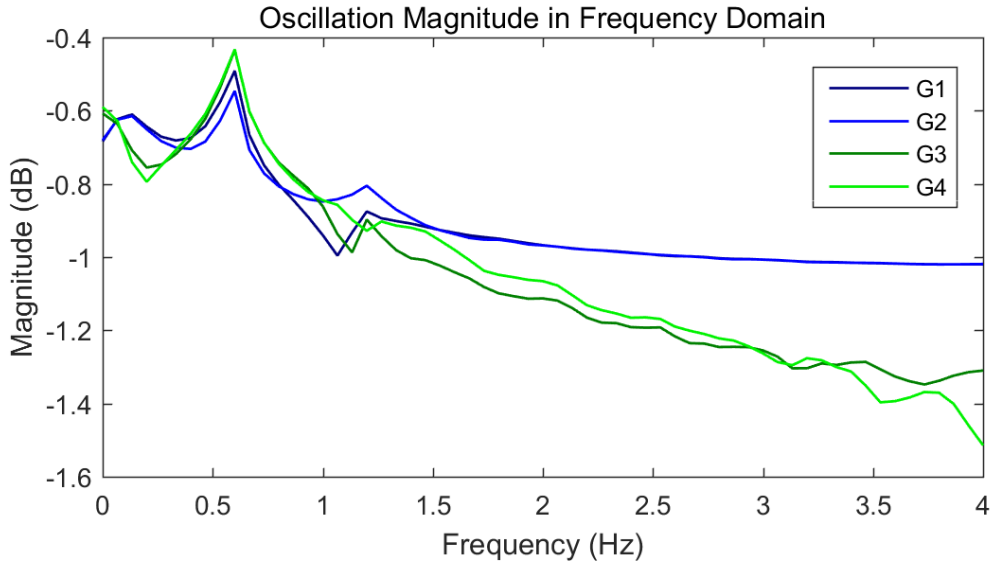

Figure 51: The frequency spectrum for power system C with no delays.

In the case with no delays, the generator 3 speed deviation and the control signal have a phase difference of about 45 degrees with the control trailing behind. The controller prediction lines up with the speed signal soon after the transient.

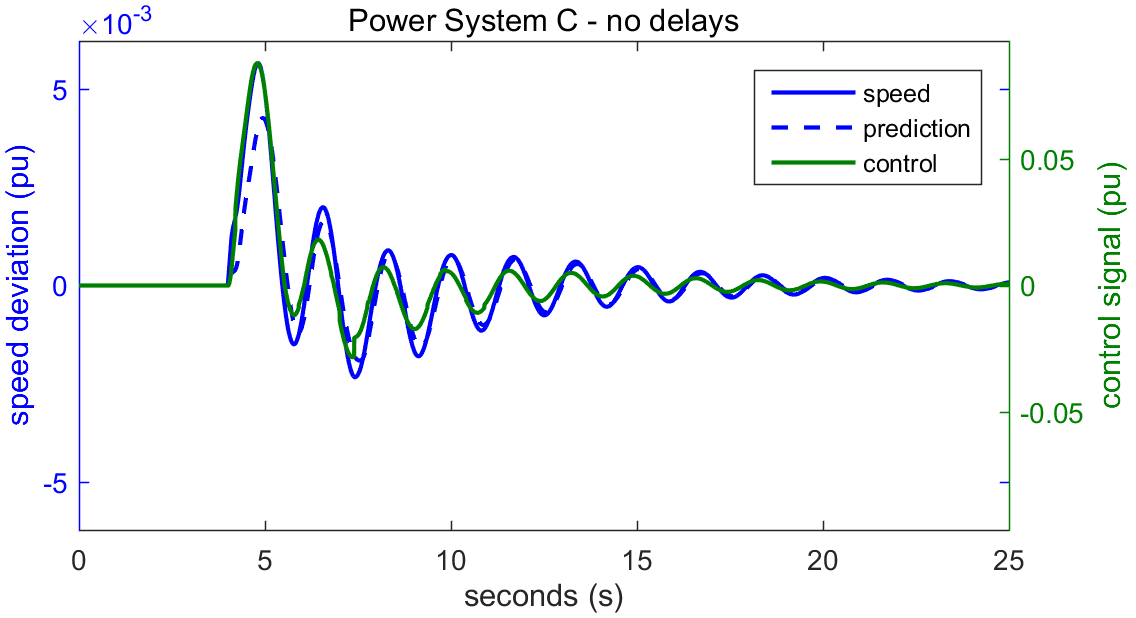

Figure 52: Power system C generator 3 speed deviation, controller speed prediction and the control signal with no delays.

5.3.2 Fiber-Optic Case C

The second case examined closely for power system C has a mean end-to-end delay of about 100 ms, and it emulates the real life delay of fiber-optic wide-area network similarly as was with power systems A and B. The generator speed deviation is presented in Figure 53 and it shows that the oscillations decay faster than in the case with no delay.

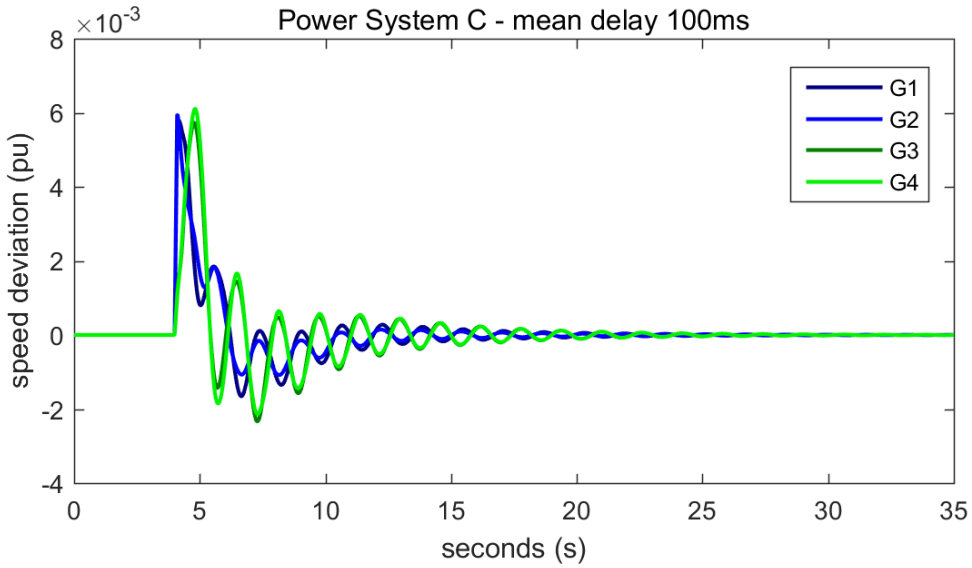

Figure 53: Generator speed deviation with a mean delay of 100 ms.

The interarea mode in this case is around 0.622 Hz which is an increase compared to the previous case with no delays. The damping for the interarea mode is also better and is above 5% for each of the generators unlike previously. The phase difference between the two areas is still around 180 degrees with Area 1 in the lead. The results for the interarea mode are shown in Table 51.

Table 51: Interarea mode for system C with a mean delay of 100 ms.

	Mode	**Freq (Hz)**	**Damping ratio** $\zeta(\%)$	**Phase** (°)
G1	$-0.211 \pm 3.908i$	0.622	5.38%	-77.60
G2	$-0.205 \pm 3.900i$	0.621	5.24%	-60.79
G3	$-0.216 \pm 3.913i$	0.623	5.51%	126.36
G4	$-0.199 \pm 3.911i$	0.622	5.08%	123.63

Thee local mode damping is sufficient for all generators except generator 4 which a local mode damping less than 5%. The local mode oscillation modes are shown in Table 52.

Table 52: Local modes for system C with a mean delay of 100 ms.

	Mode	**Freq (Hz)**	**Damping ratio** $\zeta(\%)$	**Phase** (°)
G1	$-0.490 \pm 7.426i$	1.182	6.58%	28.00
G2	$-0.376 \pm 7.190i$	1.144	5.22%	-104.62
G3	$-0.477 \pm 7.697i$	1.225	6.19%	73.07
G4	$-0.330 \pm 7.690i$	1.224	4.29%	-100.09

The ITSE values for power system C in this case are lower compared to the case with no delays, and Area 2 continues to contribute more to ITSE than Area 1. The ITSE values are displayed in Table 53 and the frequency spectrum in Figure 54.

Table 53: The ITSE values for System C with a mean delay of 100 ms.

The generator, area and system ITSE values					
G1	0.0041	Area 1	0.0072	System	0.0242
G2	0.0031				
G3	0.0082	Area 2	0.0170		
G4	0.0088				

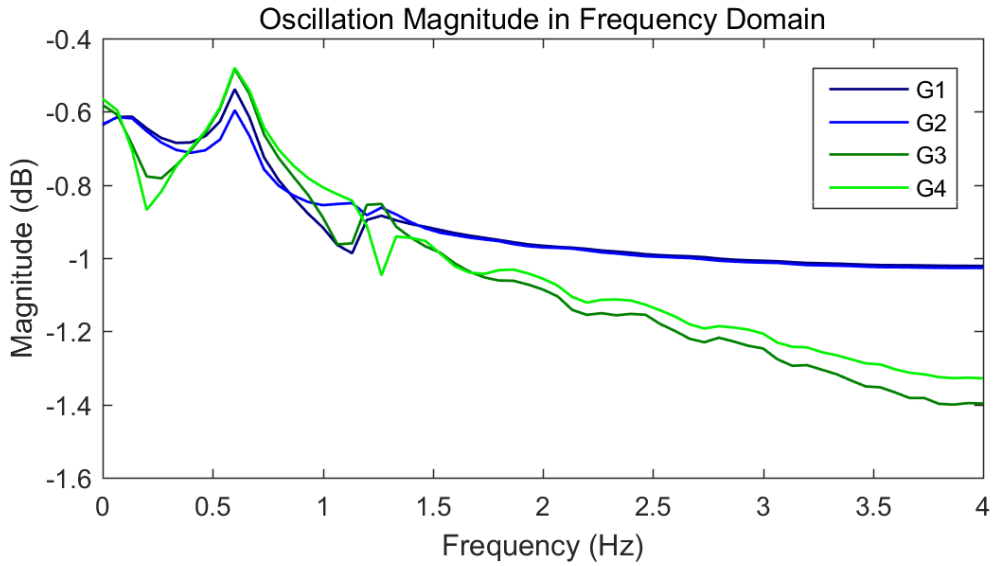

Figure 54: The frequency spectrum for power system C with a mean delay of 100 ms.

The generator 3 speed deviation and the control signal have about the same phase after the transient. Additionally, the controller is correct in its predictions on the generator speed soon after the transient and the control is able to damp the oscillations well. The generator 3 speed, prediction and control signals are shown in Figure 55.

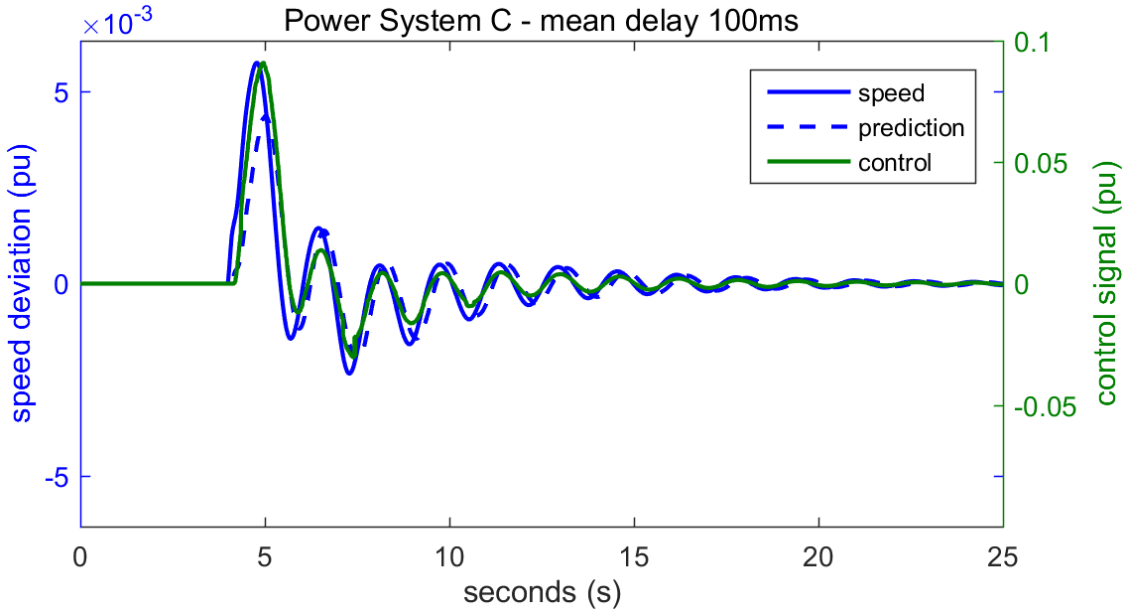

Figure 55: Power system C generator 3 speed deviation, controller speed prediction and the control signal with a mean delay of 100 ms.

5.3.3 Border Case C

The simulation case with a mean end-to-end delay of 220 ms is the first simulation case for power system C where the wide-area damping controller performs worse based on ITSE value than in the case with no delays. In addition, the speed deviation peaks following the transient are larger than previously. The generator speed deviations are shown in Figure 56.

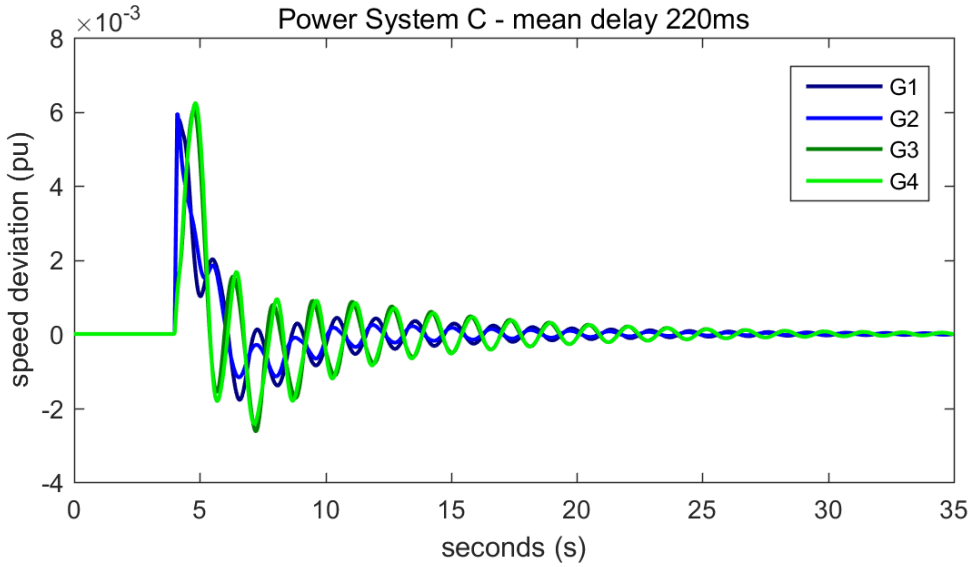

Figure 56: Generator speed deviation with a mean delay of 220 ms.

The frequency for the interarea mode continues to rise, and interarea mode oscillates now at 0.64 Hz with a mean end-to-end delay of 220 ms. The damping is around 3.5% for every generator, and it does not satisfy the requirements for sufficient interarea damping. The two areas oscillate against each other, and the generator pairs are in sync with each other.

Table 54: Interarea mode for system C with a mean delay of 220 ms..

	Mode	**Freq (Hz)**	**Damping ratio** $\zeta(\%)$	**Phase** (°)
G1	$-0.144 \pm 4.023i$	0.640	3.57%	-58.26
G2	$-0.157 \pm 4.035i$	0.642	3.88%	-49.41
G3	$-0.142 \pm 4.027i$	0.641	3.53%	145.03
G4	$-0.142 \pm 4.025i$	0.641	3.50%	140.82

The local mode damping for Area 2 continues to be above performance requirements but the damping for the local mode of Area 1 remains inadequate.

Table 55: Local modes for system C with a mean delay of 220 ms.

	Mode	Freq (Hz)	Damping ratio $\zeta(\%)$	Phase (°)
G1	$-0.314 \pm 7.501i$	1.195	4.18%	1.90
G2	$-0.546 \pm 7.188i$	1.144	7.58%	-106.48
G3	$-0.703 \pm 7.470i$	1.189	9.37%	170.79
G4	$-0.608 \pm 7.567i$	1.204	8.01%	4.91

The ITSE values are now larger than they were with case with no delays for power system C, and Area 2 has greater oscillations as seen from the ITSE values. The ITSE values are displayed in Table 56 and the frequency spectrum in Figure 57.

Table 56: The ITSE values for System C with a mean delay of 220 ms.

The generator, area and system ITSE values					
G1	0.0051	Area 1	0.0085	System	0.0323
G2	0.0034				
G3	0.0116	Area 2	0.0238		
G4	0.0122				

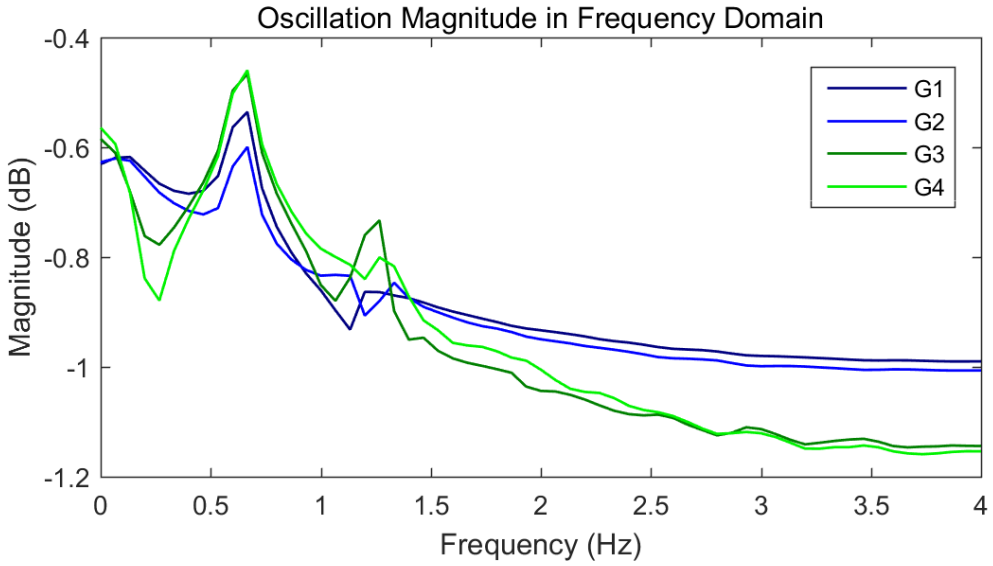

Figure 57: The frequency spectrum for power system C with a mean delay of 220 ms.

The generator 3 speed deviation and the control signal have a phase difference of about 45 degrees or more, excluding the initial transient behavior where phase difference is almost 90 degrees. Additionally, the controller is never exactly right about the state of the generator but the damping control is successful. The generator 3 speed, prediction and control signals are shown in Figure 58.

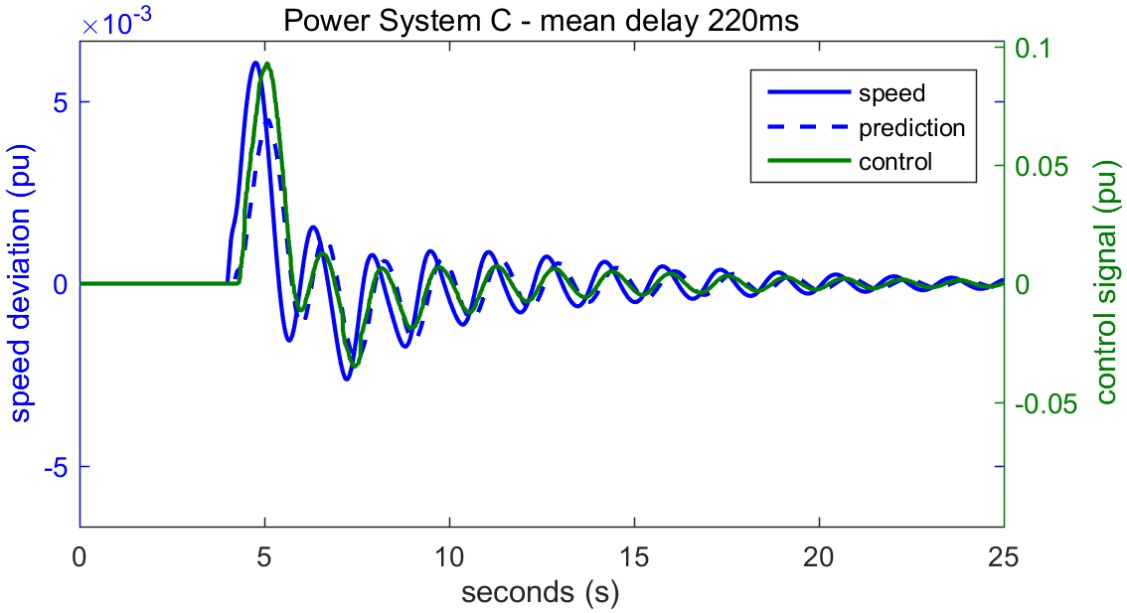

Figure 58: Power system C generator 3 speed deviation, controller speed prediction and the control signal with a mean delay of 220 ms.

5.3.4 Unstable Case C

The simulation case with a mean end-to-end delay of 400 ms is the first simulation case to become unstable for power system C. The local mode for generator 1 and the interarea mode for all generators become unstable. The areas oscillate against each other at 180 degrees. The generator speed deviations are shown in Figure 59.

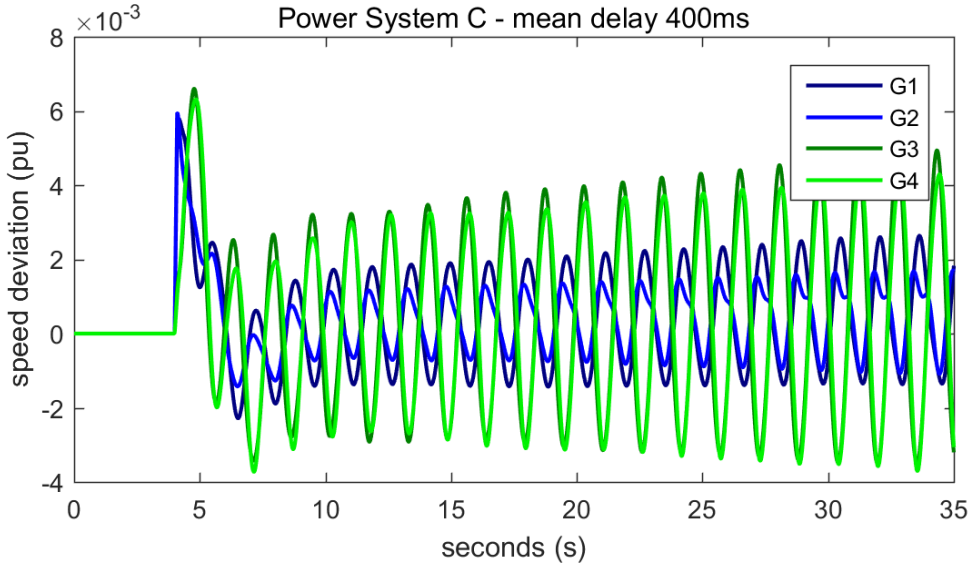

Figure 59: Generator speed deviation with a mean delay of 400 ms.

The interarea mode oscillates at 0.646 Hz with the mean end-to-end delay of 400

ms. This is an increase to the previous cases. The interarea modes are unstable with a negative damping of -0.6% to -0.4%, and the areas oscillate against each other. The interarea modes are shown in Table 57.

Table 57: Interarea mode for system C with a mean delay of 400 ms.

	Mode	**Freq (Hz)**	**Damping ratio** $\zeta(\%)$	**Phase** (°)
G1	$0.024 \pm 4.060i$	0.646	-0.60%	-45.99
G2	$0.016 \pm 4.059i$	0.646	-0.39%	-26.75
G3	$0.019 \pm 4.062i$	0.646	-0.46%	161.91
G4	$0.019 \pm 4.065i$	0.647	-0.48%	148.69

The local mode for generator 1 is unstable but generator 2 has a sufficient damping value. The unstable local mode of generator 1 can be observed from its speed deviation towards the later parts of the simulation. The generators 3 and 4 have poor damping but they do not become unstable. The local modes are shown in Table 58. In addition, a new mode is observed in Area 1 and its properties are shown in Table 59.

Table 58: Local modes for system C with a mean delay of 400 ms.

	Mode	**Freq (Hz)**	**Damping ratio** $\zeta(\%)$	**Phase** (°)
G1	$0.219 \pm 7.644i$	1.217	-2.87%	177.30
G2	$-0.445 \pm 7.694i$	1.224	5.78%	-142.15
G3	$-0.123 \pm 7.4521i$	1.186	1.65%	54.71
G4	$-0.209 \pm 7.547i$	1.201	2.77%	121.52

Table 59: Additional unstable mode in Area 1 for system C with a mean delay of 400 ms.

	Mode	**Freq (Hz)**	**Damping ratio** $\zeta(\%)$	**Phase** (°)
G1	$0.053 \pm 8.018i$	1.276	-0.66%	124.78
G2	0.0738 ± 8.010	1.275	-0.92%	-41.33

The ITSE values grow rapidly as the system becomes unstable. The frequency spectrum, shown in Figure 60, shows the dominance of the interarea mode for both areas and the presence of unstable local mode affects generator 1 ITSE value significantly. The frequency spectrums show that the system has a lot of unstable modes at high frequencies, as seen in Figure 60.

Table 60: The ITSE values for System C with a mean delay of 400 ms.

The generator, area and system ITSE values				
G1	0.1709	Area 1	0.2448	System 1.4511
G2	0.0740			
G3	0.6382	Area 2	1.2062	
G4	0.5681			

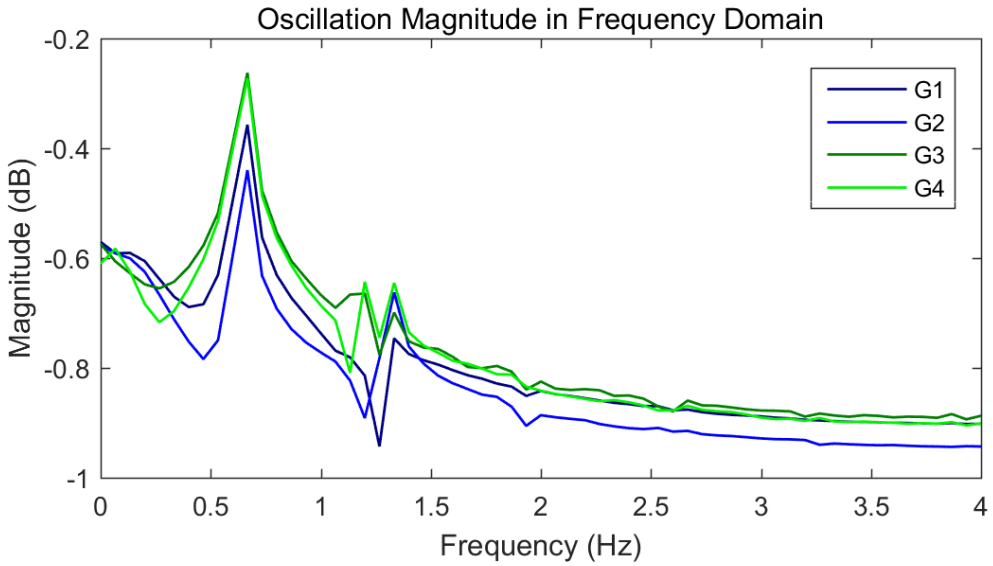

Figure 60: The frequency spectrum for power system C with a mean delay of 400 ms.

In the unstable case, the generator 3 speed deviation and the control signal have a phase difference of over 90 degrees when the system becomes unstable. Additionally, the controller is never right about the state of the generator, and the phase difference of the delay is too great for the damping control to overcome. The generator 3 speed, prediction and control signals are shown in Figure 61.

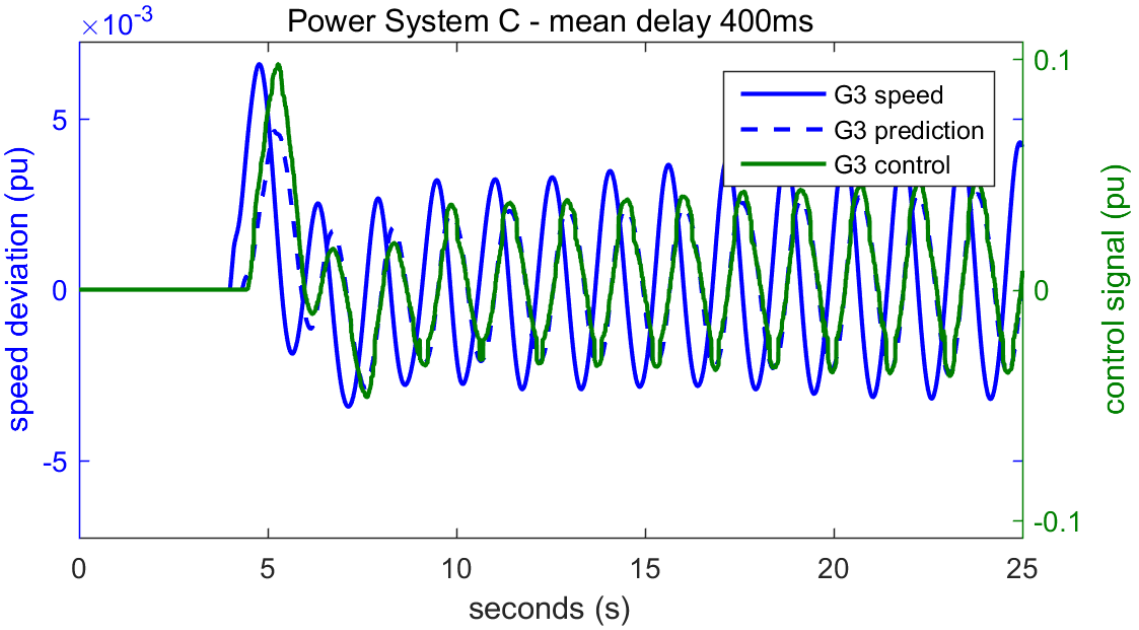

Figure 61: Power system C generator 3 speed deviation, controller speed prediction and the control signal with a mean delay of 400 ms.

6 Results

The results of the three different power system simulations show some similarities in some aspects but also differed from each other significantly. First of all, the properties of the simulation models were different. Power system B was the outlier, and power systems A and C were more similar to each other. Various delays were applied into the power systems, and each of the power system models was able to tolerate a different maximum delay under which the wide-area damping controller was able to damp the electromechanical oscillations. However, every system failed eventually and generally the local mode of Area 2 was the first to become unstable.

One particularly interesting observation was the similar behavior of the power systems under smaller latencies. Initially the power systems performed better with a small delay than without delay but after a certain delay threshold the performance decreased rapidly in all of them. This delay threshold was unique for each of the power systems. The delays ultimately manifest themselves at the end of the delay chain in the control signal. This time-shift builds in the delay chain at every component of the wide-area measurement system. The fact that delays add time lag to the signals was not unexpected but the effects had interesting unforeseen consequences.

The wide-area measurement system and the damping controller functioned properly, and the delay implementation performed as a real wide-area measurement and control system would work. In this sense the validity of the simulations seems reasonable. However, the largest the factor undermining the end results is the relative simplicity of the two-area four generator model. The system has only four generators on two areas with essentially one long transmission line through through the center bus. For this reason, it remains to be seen if the results obtained in these simulations would transfer to a more complicated power system model. Additionally, the values obtained using Prony analysis may contain some errors and inaccuracies, which are an inherent part of the method. Finally, the choice of disturbance is also critical since it may not provide excitation for all the critical modes [12].

Further development into the simulation should include configurations for other power system models and a lower execution rate for the damping controller. In addition, the next logical step in research into the effects of delays would the addition of different disturbance triggers, and finally the implement ion of some sort of delay compensation for the wide-area damping controller.

In the following sections the effects of delays as they were observed in the simulations are presented.

6.1 Latency Changes Interarea Oscillation Frequency

It was observed throughout every simulation that increase in delay resulted in the increase of the frequency of the most dominant oscillation mode, which in most cases was the interarea oscillation mode. In other words, the time-shift in the control signal results in it being applied at a later phase compared to the oscillation mode. A control which is applied with a time lag increases the frequency of the oscillations. Figures 21, 35 and 49 presented for each of the power systems at the beginning of

their sections illustrate well this described phenomenon. This is further demonstrated by an examples shown in Figures 62 and 63. In the former the control is applied early control with a smaller time lag than in the latter. The example with smaller time delay has a lower interarea mode frequency of 0.656 Hz compared to the 0.688 Hz of the other. This trend was clear in every power system simulation.

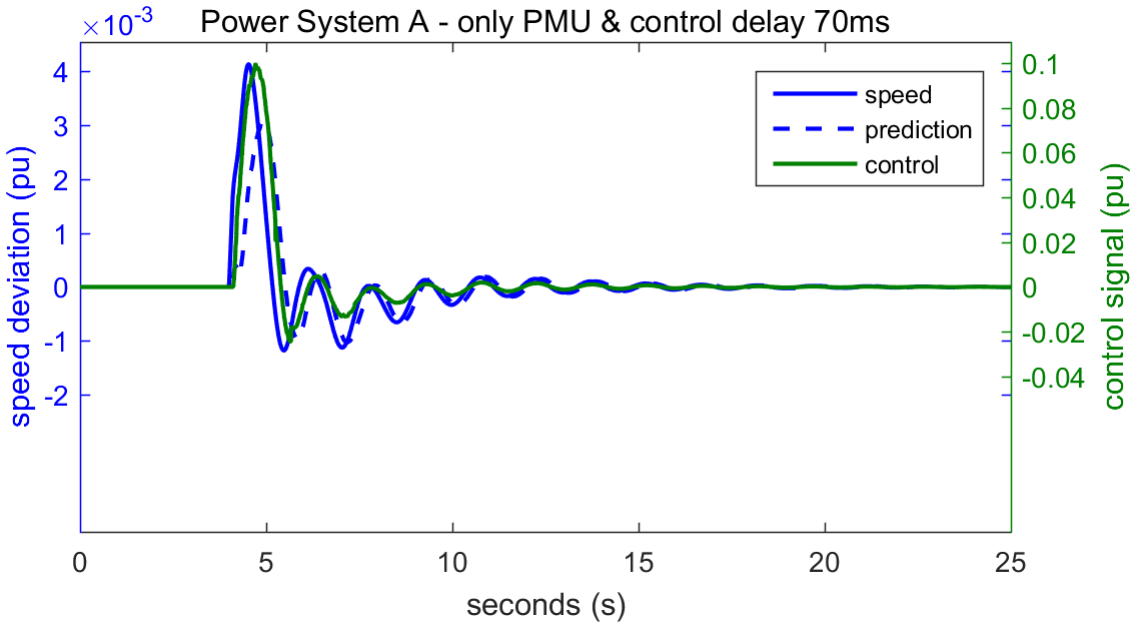

Figure 62: Power system A generator 3 speed deviation, controller speed prediction and the control signal with a mean delay of 70 ms.

This same phenomenon was observed with the cases with no delay but in reverse. It can be seen from the control signal timings that when there is no delay the signal affects the oscillation with a phase lead. This time lead in turn decreases the frequency, and this was observed without an exception in each of the no delay cases where their interarea oscillation frequency was lower than the values obtained using PST-Toolbox's numerical eigenvalue analysis.

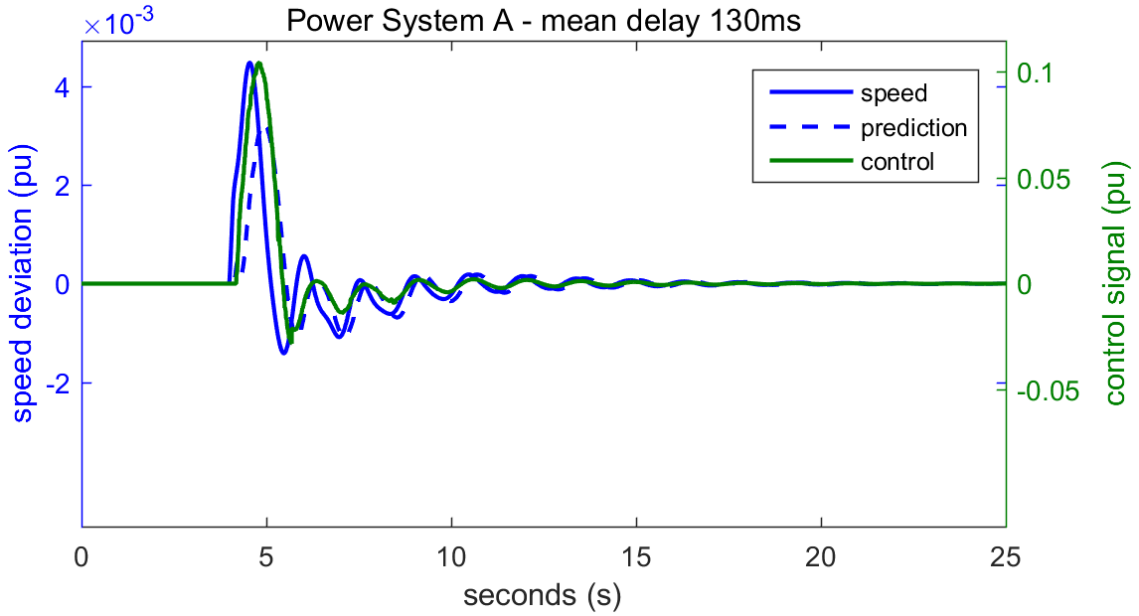

Figure 63: Power system A generator 3 speed deviation, controller speed prediction and the control signal with a mean delay of 110 ms.

6.2 Latency Changes Damping Ratio

Figures 21, 35 and 49, which show the plot of real and absolute eigenvalues of interarea mode oscillations, illustrate how the damping of the dominant interarea oscillation mode decreases as delay gets larger. The exception is the behavior when the delay is under a certain margin but this is explained in the next subsection covering the transient.

It should be noted that while the increased delay makes damping consequently worse, initial damping ratios are not an indication of the delay tolerance of the system. Power systems B and C with worse damping ratios than power system A were able to tolerate larger delays despite worse initial damping.

6.3 Size and Shape of the Transient

The strangest phenomenon was the improved damping performance for each system, while the delay was under a certain margin. The fact that the same value of about 170 to 250 ms applies for each of the power systems, despite power system B having very different behavior than the other two, suggests that it might be the result of the size and shape of the transient.

The initial peaks of the transient happen at about t = 4.17 – 4.25 seconds, or 170 – 250 ms after the transient is introduced into the system. It seems that a small delay causes the control signal to hit the transient at a better phase, and as a consequence the first negative peak of the oscillation is smaller. This results in a better overall damping as with small delays the system is able to correct itself after the transient is over.

If the delay is too large, the controller either gives the control response to the transient at an undesired phase, or alternatively applies undesired control for the subsequent peaks.

6.4 Systems Have Delay Tolerance Margin

Each of the power systems had its own maximum delay margin that it was able to tolerate before becoming unstable. The delay margins are tied into the system properties, and the most important property seems to be the frequencies of the oscillations. The power systems became unstable when the control signal had a phase difference of 90 degrees. This means that the delay is roughly equal or greater than the period time of the most dominant frequency. Lower interarea mode frequencies are able to withstand delays better than higher frequency modes.

However, when the wide-area damping control of electromechanical oscillations is considered the effects of local and control modes should be evaluated. Complementing the wide-area damping with a local power system stabilizer should be considered.

6.5 Review and Summary of Results

A summary for the results of the power system simulations in regards to the observed features is shown in Table 61. The importance of delays is significant for the wide-area measurement and control systems. The simulation properties change under real delays between 100 to 200 ms which have been observed in real world power systems. The oscillation frequencies and modes change. Control signal at wrong phase can excite undesired behavior in the power system. All of the system were able to tolerate a delay of at least a quarter of a second while remaining stable. However, the changes in damping and oscillation frequencies decrease the overall damping performance significantly.

Table 61: The results for maximum delay tolerance for each of the power systems are presented.

	Interarea mode	**Unstable modes**	**Maximum delay**
System A	0.64 – 0.72 Hz	Local mode for Area 2	$<$ 280 ms
System B	0.42 – 0.43 Hz	Interarea + other mode	$<$ 700 ms
System C	0.59 – 64 Hz	Interarea + several others	$<$ 400 ms

Therefore, in damping controller design the delays should be definitely be considered although even a delay unaware system is able to tolerate a relatively large amount of delay. If the delays are compensated then two different parameters have to considered. The parameters are the time lag and magnitude. The unstable simulations show that the damping controller is not able to damp out the oscillations with a too large time shift. The signals have to be compensated by shifting them in the time domain. The great thing about synchrophasors is that the time delay is known from PMU to PDC, and this delay before control calculation can be mitigated. The delay

after the control calculation is harder to determine but a time constant correction, or depending on the network properties, just leaving it as is could be sufficient. The other parameter to be compensated is the magnitude of the signal. The unstable cases show that the applied control and the controller prediction are too conservative. A simple compensator which might work and increase the delay tolerance margins for the systems, could a simple linear regression compensator. It would work extrapolate new values based on the previous values system measurement. The terminal voltage angles for example, excluding nonlinear behavior, follow sinusoid patterns as observed in the thesis.

7 Conclusion

In this thesis, the effects of delays on a wide-area damping control of electromechanical oscillations were studied. In the introduction the topic and the motivations were presented. The research goals and the scope of the thesis was outlined. The thesis presented a general introduction into electromechanical oscillations and wide-area power systems.

A part of the research goals was to study, identify and define the delay sources found in wide-area measurement systems. This part of the objective was achieved in Chapters 2 and 3, in the former the components of the wide-area measurement systems were presented. It was shown that the delays can be traced into the underlying system architecture. In the later sections the delay sources, their delay components and magnitudes were described, and the findings were presented. Additionally, a survey on reports and research in some known wide-area measurement system delays was presented.

It was observed that typical wide-area measurement systems have end-to-end delays in the magnitude of hundred milliseconds and more. The most important delay sources are the phasor measurement computation latency, and data transmission is a potential source for significant delay and impact on the system. The phasor data concentrator delay itself was shown to be insignificant but has an important role in managing the delay chain. The various control and actuator delays were analyzed, and the conclusion was that these delays are very case specific. Some applications have heavy computation requirements or slow instruments, and others use fast actuators or do not require complex real time calculations.

The second research goal was to study the effects of delays on the wide-area damping control of electromechanical oscillation using power system simulations. A part of this objective, was the delay implementation into the power system simulations. The rundown on the simulation implementation is given in Section 4.2. The simulation implementation was shown to work as intended when the results were reviewed.

The effects of delays were studied using three different simulation models with different properties. The simulations were run with different delays until a maximum tolerated delay was reached for each of the systems. Four simulation cases where presented for each of the simulation models. A no delay case, one so called fiber-optic case with good reasonable time delay, one border case and one unstable case. The simulations results were reviewed in Chapter 5 and the results were presented in Chapter 6.

The simulations showed that delay causes a time shift in the signals. The frequencies of interarea modes increase while the local modes are affected but in a less determinable manner. One interesting behavior was the initial better performance of the simulations under small delays. However, it was reasoned that the transient caused by the line fault disturbance might be the reason for this phenomenon. The conclusion from the simulation was that delays have to be considered in the wide-area damping control of electromechanical oscillations. Although every simulation was able to withstand more than reasonable delays which could be expected in dedicated

control systems, the damping of electromechanical oscillations is weaker even though the immediate system stability is not threatened.

Future work was also covered and the next step should be delay compensation, starting with a simple phase compensator. It was observed that phase lag and control magnitude have to be compensated. Additionally, the control was too conservative under most scenarios.

References

[1] L. Fan, "Synchronized Global Phasor Measurement Based Inter-Area Oscillation Control Considering Communication Delay," in *Power and Energy Society General Meeting*, 1 - 6, 2008.

[2] G. Chen, Y. Sun, V. Venkatasubramanian, L. Cheng, J. Lin, A. Bose, W. Zhaon, and C. Lin, "Wide Area Control Framework Design Considering Different Feedback Time Delays," in *Power and Energy Society General Meeting*, 2012.

[3] K. Praserrwong, M. Nadarajah, and D. Thakur, "Understanding Low-Frequency Oscillation in Power Systems," *International Journal of Electrical Engineering Education*, vol. 47, no. 3, pp. 248–262, July 2010.

[4] C. Lu, X. Wu, J. Wu, P. Li, Y. Han, and L. Li, "Implementations and Experiences of Wide-area HVDC Damping Control in China Southern Power Grid," in *Power and Energy Society General Meeting*, 2012.

[5] D. Dotta, A. S. e Silva, and I. C. Dexker, "Wide-Area Measurements-Based Two-Level Control Design Considering Signal Transmission Delay," *IEEE Transactions on Power Systems*, vol. 24, no. 1, pp. 208 – 216, February 2009.

[6] H. Jia, N. Guangyu, S. T. Lee, and P. Zhang, "Study on the Impact of Time Delay to Power System Small Signal Stability," in *Electrotechnical Conference. MELECON 2006. IEEE Mediterranean*, 2006.

[7] H. Wu, K. S. Tsakalis, and G. T. Heydt, "Evaluation of Time Delay Effects to Wide-Area Power System Stabilizer Design," *IEEE Transactions on Power Systems*, vol. 19, no. 4, pp. 1935 – 1941, November 2004.

[8] J. C. G. Rogers and L. Vanfretti, "Power System Toolbox." [Online]. Available: http://www.esce.rpi.edu/pst/PST.html

[9] P. Kundur, *Power System Stability and Control*. McGraw-Hill, New York, 1994.

[10] G. Gajjar and S. A. Soman, "Power System Oscillation Modes Identifications From Wide Area Frequency Measurement System," in *Power System Technology (POWERCON)*, October 2012.

[11] R. Lira, C. Mycock, D. Wilson, and H. Kang, "PMU Performance Requirements and Validation for Closed Loop Applications," in *IInnovative Smart Grid Technologies (ISGT Europe)*, 2011.

[12] P. system Dynamics and Stability, *The Electric Power Engineering Handbook*, L. Grigsby, Ed. CRC Press & IEEE Press, 2012.

[13] B. Pal and B. Chaudhuri, *Robust Control in Power Systems*, M. A. Pai and A. Stankovic, Eds. Springer, 2005.

[14] H. A. Sarde, R. M. Bandgar, and V. S. Dake, "Parameter Estimation of Low Frequency Oscillations using Prony," *International Journal of Engineering Research & Technology*, vol. 3, no. 5, pp. 1461–1464, May 2014.

[15] K. Narendra, D. R. Gurusinghe, and A. D. Rajapakse, "Dynamic Performance Evaluation and Testing of Phasor Measurement Unit (PMU) as per IEEE C37.118.1 Standard," in *IEEE General Meeting, Power Engineering Society*, 2012.

[16] B. Naduvathuparambil, M. C. Valenti, and A. Feliachi, "Communication delays in wide area measurement systems," in *Proceedings of the Thirty-Fourth Southeastern Symposium on System Theory*, 2002.

[17] A. Phadke and J. Thorp, *Synchronized Phasor Measurements and Their Applications*, M. A. Pai and A. Stankovic, Eds. Springer, 2008.

[18] A. Gomez-Exposito, A. Abur, P. Rousseaux, A. de la Villa Jaen, and C. Gomez-Quiles, "On the Use of PMUs in Power System State Estimation," in *17th Power Systems Computation Conference*, 2012.

[19] F. R. P. Safaei, S. G. Ghiocel, J. P. Hespanha, and J. H. Chow, "Stability of an adaptive switched controller for power system oscillation damping using remote synchrophasor signals," in *Decision and Control (CDC)*, 2014.

[20] K. Zhu, J. Song, M. Chenine, and L. Nordstrám, "Analysis of Phasor Data Latency in Wide Area Monitoring and Control Systems," in *Communications Workshops (ICC)*, 2010.

[21] M. Chenine and L. Nordström, "Investigation of Communication Delays and Data Incompleteness in Multi-PMU Wide Area Monitoring and Control Systems," in *Electric Power and Energy Conversion Systems, EPECS '09*, 2009.

[22] M. S. Thomas, N. Senroy, and A. S. Rana, "Analysis of Time Delay in a Wide-Area Communication Network," in *Power India International Conference (PIICON)*, 2014.

[23] M. Chenine, E. Karam, and L. Nordstrám, "Modeling and Simulation of Wide Area Monitoring and Control Systems in IP-based Networks," in *Power & Energy Society General Meeting*, 2009.

[24] K. Martin, "Synchrophasor Measurements Under IEEE Standard C37.118.1-2011 With Amendment C37.118.1a," *IEEE Transactions on Power Delivery*, vol. 30, no. 3, pp. 1514–1522, June 2015.

[25] K. Zhu, A. Al-Hammouri, and L. Nordström, "To Concentrate or not to Concentrate: Performance Analysis of ICT system with Data Concentrations for Wide-area Monitoring and Control Systems," in *Power and Energy Society General Meeting*, 2012.

[26] K. Zhu, M. Chenine, L. Nordström, S. Holmström, and G. Ericsson, "An Empirical Study of Synchrophasor Communication Delay in a Utility TCP/IP Network," *International Journal of Emerging Electric Power Systems*, vol. 14, no. 4, pp. 341 – 350, 2013.

[27] H. A. Retty, "Evaluation and Standard of Phasor Data Concentrators," Master's thesis, Virginia Polytechnic Institute, 2013.

[28] F. Ding and C. D. Booth, "Applications of PMUs in Power System Distribution Networks with Distributed Generation," in *UPEC 2011 - 46th International Universities' Power Engineering Conference*, 2011.

[29] G. Sánchez-Ayala, J. R. Agüero, D. Elizondo, and M. Lelic, "Current trends on applications of PMUs in distribution systems," in *Innovative Smart Grid Technologies (ISGT)*, 2013.

[30] S. Islam, P. X. Liu, and A. E. Saddik, "Wide-area Measurement-based Power System for Smart Transmission Grid With Communication Delay," in *Instrumentation and Measurement Technology Conference*, 2012.

[31] K. Zhu, M. Chenine, and L. Nordström, "ICT Architecture Impact on Wide Area Monitoring and Control Systems' Reliability," *IEEE Transaction on Power Delivery*, vol. 26, no. 4, pp. 2801 – 2808, October 2011.

[32] M. Asprou and E. Kyriakides, "The effect of time-delayed measurements on a PMU-based state estimator," in *IEEE PowerTech*, 2015.

[33] S. Fengjie, Q. Qi, and F. JieQing, "Real-Time Signal Time Delay Analysis of WAMS Based on MPLS VPN Technology," in *The International Conference on Advanced Power System Automation and Protection*, 2011.

[34] *Synchrophasor Measurement standard - IEEE C37.118.1*, WG H11 IEEE PSRC Std.

[35] S. Ayasun and A. Gelen, "Stability analysis of a generator excitation control system with time delays," *Electrical Engineering*, vol. 91, no. 6, pp. 347–355, January 2010.

[36] M. Kim, M. Damborg, J. Huang, and S. Venkata, "Wide-Area Adaptive Protection Using Distributed Control and High-Speed Communication," in *Proceedings of the 14th power system computation conference (PSCC)*, 2002.

[37] J. W. Stahlhut, T. J. Browne, G. T. Heydt, and V. Vittal, "Latency Viewed as a Stochastic Process and its Impact on Wide Area Power System Control Signals," *IEEE Transactions on Power Systems*, vol. 23, no. 1, pp. 84–91, February 2008.

[38] K. Zhu and L. Nordström, "Design of wide-area damping systems based on the capabilities of the supporting Information Communication Technology infrastructure," *IET Generation, Transmission & Distribution*, vol. 8, no. 4, pp. 640 – 650, April 2014.

[39] C. Cyr and I. Kamwa, "WACS design at Hydro-Quebec," in *Proc. of IEEE PES General Meeting*, 2010.

[40] O. Mäki, J. Turunen, J. Seppänen, K. Zenger, and L. Haarla, "Multi-objective Model Predictive Control for Damping Inter-area Power Oscillations," in *IEEE Eindhoven Powertech*, 2015.

[41] G. Rogers, *Power System Oscillations*, M. A. Pai, Ed. Kluwer Academic Publishers, 2000.

[42] E. Camacho and C. Bordons, *Model Predictive Control.* Berlin, Germany, Springer-Verlag, 2004.

[43] J. Maciejowski, *Predictive Control with Constraints.* Harlow, Englanf, Prentice Hall, 2002.

[44] D. R. Gurusinghe, A. D. Rajapakse, and D. Muthumuni, "Modeling of a Synchrophasor Measurement Unit in an Electromagnetic Transient Simulation Program," in *The International Conference on Power Systems Transients (IPST)*, 2013.

[45] Z. Liu, *Control Engineering and Information Systems.* CRC Press, 2014.

[46] H. Unbehauen, *Control Systems, Robotics and Automation.* EOLSS Publishers Co Ltd, 2009, vol. 2.

[47] S. Singh, "Application of Prony Analysis to Characterize Pulsed Corona Reactor Measurements," Master's thesis, Department of Electrical and Computer Engineering, The University of Wyoming, 2003.

[48] L. Qi, L. Qian, S. Woodruff, and D. Cartes, "Prony Analysis for Power System Transient Harmonics," *EURASIP Journal on Advances in Signal Processing*, 2007.

[49] J. Turunen, J. Thambirajah, M. Larsson, B. C. Pal, N. F. Thornhill, L. C. Haarla, W. W. Hung, A. M. Carter, and T. Rauhala, "Comparison of Three Electromechanical Oscillation Damping Estimation Methods," *IEEE Transaction on Power Systems*, vol. 26, no. 4, pp. 2398–2407, June 2011.

[50] Z. Gajic and M. Lelic, *Modern Control System Engineering*, ser. International Series in Systems and Control Engineering. Prentice Hall International, London, 1996.